INFORMATION TO USERS

This manuscript has been reproduced from the microfilm master. UMI films the text directly from the original or copy submitted. Thus, some thesis and dissertation copies are in typewriter face, while others may be from any type of computer printer.

The quality of this reproduction is dependent upon the quality of the copy submitted. Broken or indistinct print, colored or poor quality illustrations and photographs, print bleedthrough, substandard margins, and improper alignment can adversely affect reproduction.

In the unlikely event that the author did not send UMI a complete manuscript and there are missing pages, these will be noted. Also, if unauthorized copyright material had to be removed, a note will indicate the deletion.

Oversize materials (e.g., maps, drawings, charts) are reproduced by sectioning the original, beginning at the upper left-hand corner and continuing from left to right in equal sections with small overlaps.

ProQuest Information and Learning
300 North Zeeb Road, Ann Arbor, MI 48106-1346 USA
800-521-0600

DIFFUSION BONDING OF SILICON NITRIDE TO TITANIUM

José Lemus-Ruiz

Department of Mining and Metallurgical Engineering
McGill University, Montréal
August, 2000

A thesis submitted to the Faculty of Graduate Studies and Research in partial fulfilment of the requirement for the degree of Doctor of Philosophy

To my devoted parents and family…

ABSTRACT

The use of ceramic has gradually increased over the past few years. Si_3N_4 is one of the most important ceramics used as structural material for high temperature applications. The practical use of advanced ceramics depends on the reliability of ceramic/metal joining techniques and the properties of the resulting interfaces. This work focuses on various aspects of diffusion bonding of Si_3N_4 to Ti as well as on the use of Ti-foil interlayer during the self-joining of Si_3N_4. Si_3N_4/Ti and Si_3N_4/Ti-foil/Si_3N_4 combinations were diffusion joined by hot-uniaxial pressing and the microstructural characterization of the resulting interfaces was carried out by SEM, EPMA, and X-ray diffraction.

Diffusion bonding was carried out at temperatures ranging from 1200 to 1500°C using different holding times, pressures, and surface roughness of the joining materials. The results showed that Si_3N_4 could not be bonded to Ti at temperatures lower than 1400°C, however successful joining at higher temperatures. Joining occurred by the formation of a reactive interface on the Ti side of the joint. At temperatures greater than 1330°C, liquid formation occurred by the interaction of Ti with Si promoting bonding, as well as the high affinity of Ti for Si resulted in rapid interface formation of silicides, initially Ti_5Si_3. EPMA and X-ray diffraction confirmed the presence of Ti_5Si_3, TiSi, and TiN at the interface. The surface roughness of the joining materials plays an important role since thicker interfaces were obtained for polished samples compared to as-ground samples. The interfaces grew in a parabolic fashion with the formation of various Ti-silicides (Ti_5Si_3 and TiSi) as well as Ti-nitride (TiN) at the interface.

Evaluation of joint strengths as a function of the experimental parameters such as, joining temperature and time was obtained by four-point bending test performed on Si_3N_4/Ti/Si_3N_4 joints. Strong joints were produced at joining temperatures greater than 1450°C with average bend strength of more than 100 MPa. The maximum joint strength was obtained in samples hot-pressed at 1500°C and 120 minutes reaching a value of 147 MPa.

RÉSUMÉ

L'utilisation des matériaux céramiques a graduellement augmenté lors des dernières années. Le nitrure de silicium (Si_3N_4) est considéré comme l'une des plus importantes céramiques pour des applications structurales à haute température. L'utilisation dans un contexte pratique des céramiques techniques dépend de la fiabilité des méthodes de fabrication des joints métaux/céramiques ainsi que des propriétés des interfaces résultantes. Cette étude porte sur les différents aspects de l'adhésion par diffusion de Si_3N_4 à Ti ainsi que l'utilisation de feuille de titane lors de l'assemblage de Si_3N_4 à lui même. Les combinaisons Si_3N_4/Ti et Si_3N_4/feuille Ti/Si_3N_4 ont été fabriquées utilisant une presse uniaxe à chaud et les techniques de caractérisation tel MEB, EPMA et diffraction des rayons X ont été utilisées lors de l'analyse de la microstructure de l'interface.

L'assemblage par diffusion s'est effectué à des températures variant entre 1200 et 1500°C pour des temps de diffusion, des pressions et de rugosité de surface différentes. Les résultats démontrent que le titane ne peut être joint avec le nitrure de silicium à des températures inférieures à 1400°C mais que des joints peuvent être produit à des températures supérieures. Lorsque la température est supérieure à 1330°C, la formation de liquide se produit due a l'interaction du titane avec le silicium, favorisant ainsi la formation d'un joint. De plus, l'affinité du titane pour le silicium est observé par la formation rapide à l'interface de siliciure, initialement Ti_5Si_3. La microsonde électronique ainsi que la diffraction des rayons X confirme la présence à l'interface de Ti_5Si_3, TiSi et de TiN. La rugosité de surface des matériaux à joindre joue un rôle très important. Des distances de diffusion à l'interfaces plus importantes sont produites avec des échantillons polis comparé à des échantillons non polis. L'interface croit selon une loi parabolique avec la formation de divers siliciure de titane (Ti_5Si_3 et TiSi) ainsi que de nitrure de titane (TiN).

L'évaluation de la résistance mécanique des joints en fonction des paramètres expérimentaux comme la température d'assemblage, et du temps a été évaluée avec des tests de pliage à 4 points avec les échantillons Si_3N_4/Ti/Si_3N_4. Des joints résistants sont produits à des températures supérieures à 1450°C, avec des contraintes à la rupture supérieures en moyenne à 100 MPa. La résistance maximale de 147 MPa a été obtenu pour des échantillons joint à 1500°C durant 120 minutes.

ACKNOWLEDGEMENTS

I would like to express my gratitude to several persons and institutions whose support made this work possible.

Firstly, I would like to thank the "Consejo Nacional de Ciencia y Tecnologia" (CONACYT) of Mexico for the scholarship grant, and the Natural Science and Engineering Research Council of Canada (NSERC) for partially financing this research project.

I would like to express my gratitude to my supervisor, Professor Robin A.L. Drew, for his constant encouragement, guidance, constructive criticism and patience throughout the time of this work, and also for the opportunity to present this work to the Canadian, Mexican and International scientific communities.

Many thanks to the technical personnel of the Mining and Metallurgical Department at McGill for their indispensable contribution: Mrs. Helen Campbell for her assistance with the SEM imaging; Mr. Glenn Poirier (Department of Geological Science) for the use of the EPMA and AFM equipments; Mrs. Monique Riendeau for her aid with the X-Ray diffractometry; to all the workshop personnel for their assistance in the preparation of samples and maintenance of equipment.

I would also like to thank to all the members of the ceramics and composites materials group for the valuable discussions and for providing a stimulating environment. Special thanks go to Mr. Carlos Leon and Mrs. Ena Aguilar who assisted in many ways, especially when things were not progressing well, but, in particular, for their friendship.

Thanks also go to Dr. Rafael Quintana Puchol for his help and discussion with the X-Ray analysis and to Mr. Mathieu Brochu for the translation of the abstract into French.

Last, but not least, I would like to thank to my wife, Ana Maria, and my son, José Adolfo, for their continuous sacrifice and encouragement, and who were often neglected whilst I completed my research and thesis.

THANKS TO YOU ALL

TABLE OF CONTENTS

List of Figures

Chapter 1.

Chapter 2.

Chapter 4.

Chapter 5.

Chapter 7.

List of Tables

Chapter 7.

Chapter 1:

Introduction

Ceramics and metals are two of the oldest established classes of technologically useful materials. While metals dominate engineering applications, ceramics are used extensively to provide thermal and electrical insulation and are emerging as important structural materials. Properties of individual ceramics and metals can vary widely, but the characteristics of most materials in the two classes differ significantly. As shown in Table 1.1 ceramics are generally stronger, lighter and more refractory than metals, and have lower coefficients of thermal expansion [1, 2]. However, compared with metals, ceramics are poor thermal and electrical conductors and are brittle. The properties summarized in Table 1.1 reflect the different lattice binding characteristics of metals and ceramics. Ceramics are neither purely ionic nor purely covalent, and the relative degree of ionicity or covalency of ceramics can be related to the electronegativity of its components. From this it follows that in general ceramics become more ionic and less covalent in the sequence:

borides → *carbides* → *nitrides* → *oxides*

Ceramics are generally characterized by a crystalline structure and an ionic bond of the atoms. The difference in the atomic bonding distinguishes them from metals, and their inorganicity from organic materials.

Table 1.1. Physical and mechanical properties of some ceramics and metals [1,2].

Material	*Melting temperature (°C)*	*Theoretical density (g/cm^3)*	*Thermal Expansion ($10^{-6}/K$)*	*Strength (MPa)*	*Young's modulus (GPa)*
HfB_2	3200	11.2	7.6	100	....
B_4C	2350	2.5	5.6	350	470
SiC	2700*	3.2	4.5	650	430
TiC	3100	4.9	8.6	700	430
WC	2800	15.8	5.2	600	700
Si_3N_4	**1900***	**3.14**	**3.1**	**700-1000**	**310**
TiN	2900	5.4	8.1	....	250
Al_2O_3	2050	3.98	7.2 – 8.6	550	380
ZrO_2	2960	5.6	7.5	180	140
Al	660	2.7	22.4	200	70
Cu	1083	9.0	16.4	220	130
Fe	1536	7.9	12.6	260	210
Mo	2610	10.2	5.1	430	320
Nb	2468	8.6	7.1	340	100
Ti	**1668**	**4.5**	**8.6**	**470**	**120**
W	3387	19.3	4.66	550	410

Decompases

In general they are very stiff, hard but brittle, have low densities, high melting temperatures, high heat resistance, are electrical insulators. and chemical resistant. There are a

number of shaping processes for ceramics, but all ceramic materials need to be sintered. Metals are inorganic materials characterized by a metallic bonding of the atoms, a crystalline structure and a metallic sheen. They are generally very malleable, ductile, strong and tough. They have high densities and relatively low melting temperatures. Metals are good conductors of electricity and heat, and are easily attacked by corrosion and oxidation.

Modern ceramics are gradually becoming important in structural applications because of their high strength to weight ratio, high modulus, high corrosion resistance, excellent high temperature properties, and abundance. The manufacture of component shapes from monolithic engineering ceramics such as Si_3N_4 is difficult, and this has generated a continued interest in the use of joining technologies to produce complex configurations from assembles of simples shapes. Joining is also the only means to produce many of the ceramic/metal components of current interest to designers. In most applications, ceramic materials are used in combination with metals. This makes joining ceramics to metals a key technology in advanced engineering. Metal/ceramic joining is seen as important to widen the number of commercial uses for ceramic. The bulk of the component can be made of a metal that can be easily fabricated into complex shapes while the ceramic can be joined onto specific areas for use in corrosive, abrasive or hot environments.

Various techniques for joining ceramic to metal are available [3, 4], some need an intermediate liquid phase, brazing, thermal spraying, and others are produced by solid state bonding and co-sintering. In all cases some problems have to be overcome: (i) morphological adaptation of the surfaces in contact; (ii) formation of bonds: van der Waals bonds, chemical

bonds by simple recovery of the molecular orbital or by chemical reaction, where new phases are grown at the interface; (iii) strict control over the residual stresses developed in both materials; (iv) changes in mechanical properties of the alloy and ceramic close to the interface. Mechanical aspects are essential for the last two points and for the first one in the case of the solid state bonding [5].

All joining techniques must take into account the difference in coefficient of thermal expansion, CTE, between the metal and ceramic; metals can have a CTE up to five times larger than a ceramic as can be observed in Table 1.1. Upon subsequent cooling from the joining process, a region of high tensile stress develops at the intersection of the free edge and the interface as a result of CTE 'mismatch'. One of the most common techniques of reducing this stress in joint assemblies is to insert a strain accommodating interlayer between the metal and the ceramic. The interlayer deforms thus accommodating the mismatch in CTE. Generally, the method has been successful to a degree, since induced stresses have been lowered and joint strengths have been increased. However, the strength of metal/ceramic joints, so far, has never approached the strength of the parent materials.

Silicon-based ceramics, particularly Si_3N_4 and SiC, because of their hardness, high strength at elevated temperatures, and resistance to corrosive environments, are promising structural ceramics for a variety of high temperature applications. However, practical applications often require these ceramics to be joined to themselves and to metals, and consequently the development of appropriate joining techniques is required. Many techniques could be used to join ceramics to metal, however, because the joining processes

exhibit different features, the best process must be selected for the intended application, brazing for example, has attracted particular interest and is being used in the automobile industry to fabricate Si_3N_4/metal components [6]. Joining ceramic/ceramic and ceramic/metal structures by brazing is attractive because of the flexibility of design that can be accommodated, the wide availability of the processing equipment, and the established use of brazing technique for high-integrity metal/metal structures such as aero-engine components. However, new and specially developed braze alloys are generally required to join ceramics because they are not wetted by conventional brazes based on Ag, Au, or Cu. These alloys, called "active brazes", contain components that react with the ceramics to change the chemistry of their surfaces to promote wetting and bonding. Most commercially available active-metal brazes employ Ti additions to eutectic or near-eutectic Ag-Cu alloys, which melt at about 800°C.

In the absence of a liquid phase, ceramic/metal joining can only be accomplished with temperature, pressure, and time sufficient to promote mobility and interdiffusion of reacting species, producing adequate interfacial contact between the ceramic and the metal. Diffusion bonding is a relatively simple technique suitable for joining ceramics to ceramics and ceramics to metals. During diffusion bonding, the components to be joined are brought into contact under a relatively small compressive force at an elevated temperature, typically, 0.6 to 0.95 of the absolute melting temperature of the component having the lowest melting point. Initially, the two components contact only at their asperities. In the first stage of the bonding process, more intimate contact is achieved by plastic deformation, which results in two partly joined surfaces with residual voids in between. When ceramic/metal bonds are being formed, and

deformation of the metal is permissible, plastic flow generally occurs within the metal, and in the second stage of the bonding process, creep and diffusion eliminate the voids. The key step in the formation of a ceramic/metal interface is to achieve adequate contact between the two materials at the interface. The driving force for the formation of a ceramic/metal interface is the reduction in free energy when intimate contact is established between the ceramic and metal surfaces. In order for this to occur, both surfaces have to be brought into intimate contact, which is usually accomplished by controlling the temperature and atmosphere during interface formation. The application of pressure results in displacement of impurities and adjustment of irregularities due to localized deformation.

The advantages of solid-state pressure bonding include a simple fabrication procedure, a one-step process, and potentially very high joint strength. However, there are also several limitations and disadvantages: high cost, shape of the specimen, a vacuum/inert atmosphere is required, and pressure must be applied. The need to apply pressure during diffusion bonding imposes restrictions on the joint geometry; most joints are of the face seal type, and are not well suited for accommodating thermal expansion mismatch. As a result, the bonded components must either be small, one component must be thin, or the thermal expansion coefficient of the components must be well matched. The use of graded thermal expansion laminates for bonding materials with highly dissimilar thermal expansion coefficients is one method of overcoming this limitation.

The successful application of ceramics depends greatly on the ability of the design engineer to develop structures and components in ways that properly utilize the advantageous properties of ceramics and minimize the impact of their poor toughness. The choice of a

ceramic/metal combination is based on the design required for the joint; for example, SiC/Mo joints have been studied for applications in fusion reactor technology and for electrical contacts. The electronics industry relies heavily on advanced ceramic materials such as Al_2O_3 and AlN for substrates, and a variety of glassy materials for a host of devices and packaging. The area of structural or load-bearing applications require materials which have high strength at elevated temperatures and/or retain high strength at elevated temperatures, resist deformation, and are resistant to corrosion and oxidation. Advanced ceramics, such as SiC and Si_3N_4, have generated a great deal of interest for various applications in internal combustion engines because of their excellent high-temperature strength and resistance to wear and oxidation. Most internal combustion engines are required to adjust rapidly from one set of operating conditions, engine speed and load, to another.

One application for which ceramics, such as Si_3N_4 and SiC, are particularly attractive is turbocharger turbine wheels [7, 8]. These components must operate for long periods of time under conditions of high temperature and stress, which can result in creep-rupture failures in metallic materials. However, the primary advantage of using ceramics for turbine wheels is their low density. A historic limitation of the automotive turbocharger is the time required to accelerate from the worst case, low-idle, no-load condition to some desired speed and load condition. The low density of ceramics offers a technological alternative that can significantly improve on this limitation by reducing the polar moment of inertia of the turbocharger rotating parts. Depending on the specific application, turbine wheel temperatures can exceed 1000°C and centrifugal force produced by the rotational speeds can result in peak stresses of 26 MPa [9, 10].

Because automobile manufacturers have required the use of ceramics as high temperature structural components, Si_3N_4 has been used for several components, rocker arm with Si_3N_4 tip, and glow plug with Si_3N_4 head. Two typical products that utilize Si_3N_4/metal joining are rocker arms with a ceramic pad and Si_3N_4 turbocharger rotor. The geometry of the Si_3N_4 insert in a rocker arm is shown in Figure 1.1.

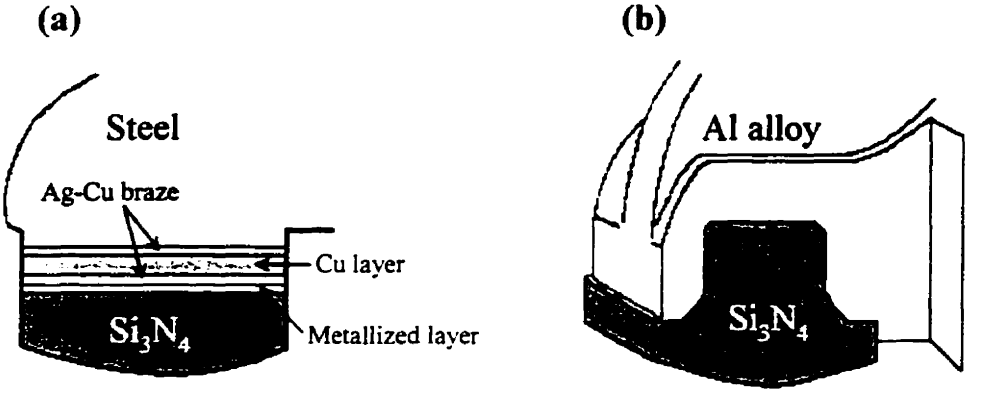

Figure 1.1. Schematic representation of Si_3N_4 rocker arm. (a) Active metal brazing with soft metal interlayer and (b) Al die cast insert [9].

The main advantage in replacing the sintered alloy tip with Si_3N_4 is to reduce stress concentration on the tip by rounding the tip edge. Figure 1.1 also shows the interlayer structure for a rocker arm fabricated by active metal brazing. In the case of Si_3N_4 turbocharger the joint region is exposed to more severe heat conditions than the rocker arm. Two joining techniques, direct active metal brazing and shrunk-in insert, have been

applied, Figure 1.2. In brazing the Si_3N_4 rotor, a three interlayer structure has been used to reduce thermal stress. The shrunk-in insert technique utilizes mechanical joining.

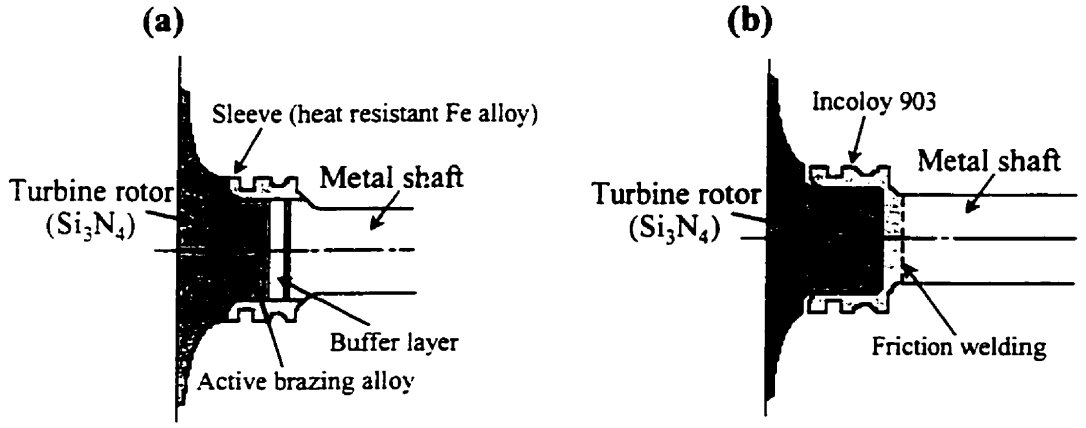

Figure 1.2. Schematic representation of Si_3N_4 turbocharger rotor. (a) Active metal brazed with triple-laminated interlayers and (b) shrunk-in inserted rotor [10].

The development of joining techniques to produce high-quality attachments of the ceramic components to the metal partners is critical to the continued growth of ceramic applications.

Chapter 2:

Ceramic/Metal Joining, Interfaces, and Mechanical Evaluation

2.1. Materials Properties

In recent years, significant progress has been made in the development of engineering ceramic materials. The use of ceramics in high technology applications depends strongly on the supply of materials. Although the basic ceramic raw materials occur abundantly in nature, they must be refined or processed before use in a manufacturing process. Silicon-based non-oxide ceramics, SiC, Si_3N_4, do not occur naturally; and they must be synthesized from precursor materials. Raw materials are generally processed into powders and fabricated into composite parts. Monolithic structural ceramic materials are currently based on silicon nitride (Si_3N_4) or silicon carbide (SiC) systems. Processing and microstructural advances have made significant strides in improving mechanical properties and reliability. It is clear that each type of material has its own range of applications in which it is the most suitable product. The newer materials and development of enhanced properties in existing ones, offer a scope for widening the range

of applications. Direct comparisons between the strengths of metals and ceramics for engineering design purposes have little value. When one is dealing with ceramics, allowances have to be made for stress concentrations, thermal mismatch or gradient stresses, and probabilities of failure. So, in addition to material development, there is also currently a great interest in understanding mechanical properties and fracture mechanisms, in improving stress analysis and risk estimation, and on the manufacturing side, in identifying and eliminating the sources of failure.

Ceramic materials are generally processed at high temperatures before use. Ceramics materials have many characteristics, which distinguish them from metals [11, 12]. Ceramics are generally more stable chemically and thermally and are better insulators than metals. They are much stronger in compression than in tension and do not exhibit any ductility prior to fracture. On the other hand, ceramics are harder, more rigid and more stable at high temperatures than either metals or polymers. The tightly held electrons also account for ceramics' low electrical conductivity at ordinary temperatures; by contrast, the mobile bonding electrons in metals make them good conductors.

2.1.1. Silicon Nitride

A new generation of ceramics has been developed which are expected to find wide use in structural applications at high temperatures. Because of the good combination of mechanical, thermal and thermo-mechanical properties, silicon nitride (Si_3N_4) is one of the

most promising materials in this class. In particular, Si_3N_4 has high strength at high temperatures, good thermal stress resistance due to low coefficient of thermal expansion $3.5x10^{-6}$ $°C^{-1}$, and relatively good resistance to oxidation compared to other high-temperature structural materials. This combination of properties can be used to increase operating temperatures. Moreover, the low density of Si_3N_4 of 3.14 $g\ cm^{-3}$ (about 40% of the density of high temperature superalloys) offer components of lower weight and is therefore an important advantage over other high temperature materials [13, 14].

Si_3N_4 has recently been at the forefront of developments in high-strength, high temperature materials, as it has been the focus of an international effort to develop more efficient, ceramic-based gas turbine and diesel engines which would operate at temperatures above the useful range for metal superalloys. In addition, this material is being used, or proposed for employment, in a multitude of other energy conversion or energy transfer devices, which would be employed at high temperatures. As such, deformation of these materials as a function of stress, temperature and time is of concern for the prolonged utilization of these devices. Si_3N_4 crystallizes in the two hexagonal modifications α and β [15], which differ in their lattice parameters in that for α-Si_3N_4 (a-axis 0.775 Å, c-axis 0.516 Å, c/a 0.7) is about twice the unit cell size compared to the β-modification (a-axis 0.759 Å, c-axis 0.271 Å, c/a 0.37). The two structures of Si_3N_4 are shown in Figure 2.1; α-Si_3N_4 is a defect structure where one nitrogen atom in 30 is replaced by oxygen, and β-Si_3N_4 is the stoichiometric form.

The Si atoms are located in the center of irregular N tetrahedral, each N atom belonging to three tetraheda. The Si_6N_8 unit cell of the β-phase is derived from the

phenacite type (Be_2SiO_4) with the beryllium atoms being replaced by silicon and the oxygen atoms by nitrogen [16].

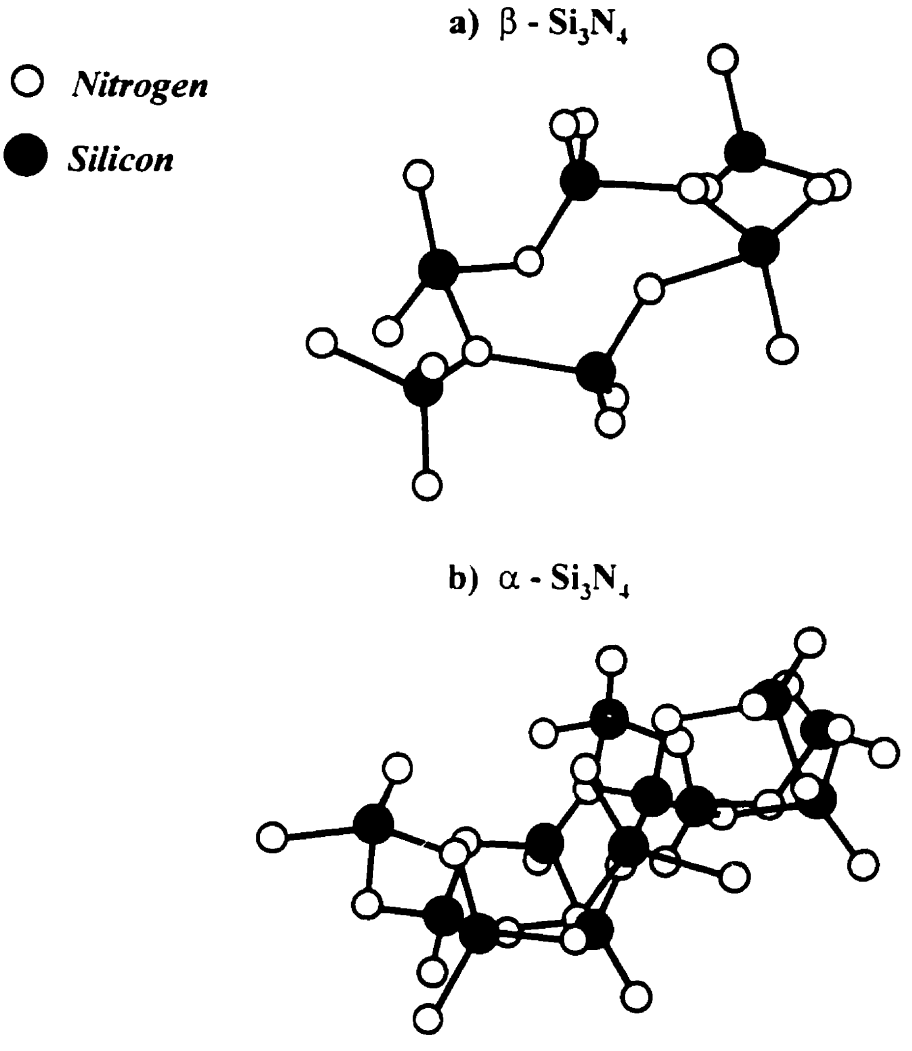

Figure 2.1. The two polymorphs forms of Si_3N_4 [15].

The structure consists of Si_3N_4 layers which alternate in the sequence *AB*, forming hexagonal tunnels in the direction of the crystallographic c-axis. In the $Si_{12}N_{16}$ unit cell of the α-phase, the layers known from the *β*-structure alternate with mirror-inverted layers in the sequence *ABCD*, resulting in a c-direction lattice distance which is about twice as large as for the *β*-modification. The hexagonal tunnels in the c-direction are not present in the α-phase. According to older views, the α-Si_3N_4 phase is stabilized by the presence of oxygen [17, 18]. However, current opinion is that α-Si_3N_4 is a metastable form. The formation of α-phase seems to be associated with certain reaction routes during nitridation of Si, like gas-phase reaction of silicon vapour or SiO with N [19]. With increasing temperature, the α-phase becomes increasingly unstable with respect to β-Si_3N_4. Silicon nitride does not have a real melting point but decomposes under 0.1 MPa N_2 at 1900°C. The reaction during decomposition is according to:

$$Si_3N_4\,(s) \Leftrightarrow 3\,Si\,(s) + 2\,N_2\,(g) \qquad (2.1)$$

and becomes increasing important above 1500°C. Extensive covalent bonding means a high bond strength and hence low self-diffusion coefficients and very high sintering temperatures must be selected. Diffusion of nitrogen in α and β-Si_3N_4 (activation energy of *235 kJ/mol* and *778 kJ/mol* respectively), which is assumed to be the slowest and rate controlling step during sintering of Si_3N_4 for reasons of steric arrangement and electron neutrality, is about four orders of magnitude below the self-diffusion coefficients of oxygen and aluminum in polycrystalline Al_2O_3 (activation energy of *460 kJ* mol^{-1} and *440 kJ* mol^{-1} *respectively*) [20]. As a consequence, Si_3N_4 cannot be fully densified without any

additional measures. The difficulties and problems outlined above have led to the development of different approaches for the production of components from Si_3N_4.

Because of the high degree of covalent bonding, classical sintering is not applicable to produce pure density Si_3N_4 ceramics. As a consequence, alternative techniques have been developed and supplementary means have been used, such as nitridation of silicon compacts or the addition of sintering aids to Si_3N_4 powders to create liquid-phase sintering with or without the application of pressure to assist the sintering process. These techniques comprise of: reaction–bonding, hot-pressing, sintering and hot-isostatic pressing. Figure 2.2 shows a schematic representation of the different processing routes in the hot-isostatic pressing of Si_3N_4.

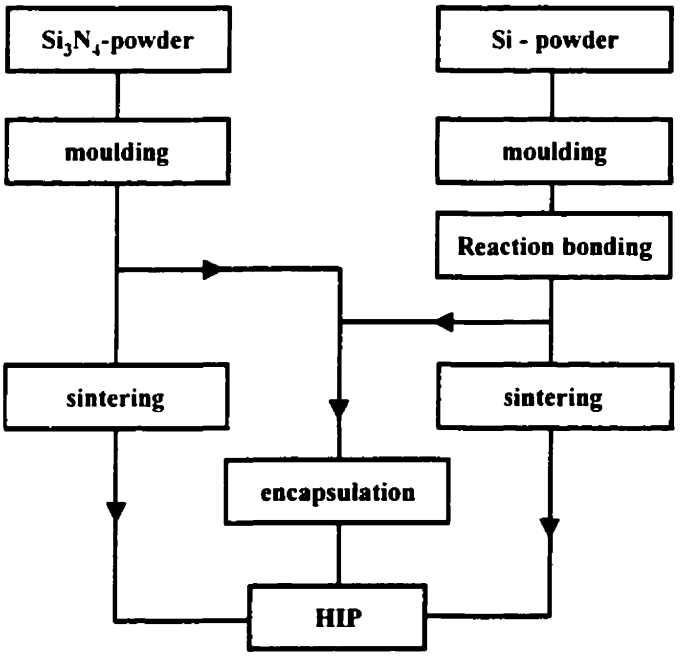

Figure 2.2. Different processing routes for hot-isostatic pressing Si_3N_4.

Reaction-bonding results in still porous material and dense Si_3N_4. However, dense Si_3N_4 can only be manufactured on a production scale by hot-pressing, sintering and hot-isostatic pressing, with the use of different oxide or non-oxide sintering additives. The usual additives are Y_2O_3, Al_2O_3 and MgO although CeO_2, ZrO_2, BeO, and BaO have been used as successful sintering aids. SiO_2 is usually present on the surface of the Si_3N_4 and some other minor impurities such as Fe, Ca, Si and C are present in the Si_3N_4 as a result of powder manufacturing techniques. At high temperatures during sintering a liquid forms by reaction of the additive with SiO_2 and Si_3N_4 to give an oxynitride liquid which promotes liquid-phase sintering and "shrinkage" to a dense body. The liquid, when it cools, forms a glassy phase and/or crystalline phases. Densification takes place by solution and precipitation of Si_3N_4 in the oxynitride liquid. In these cases, a liquid-phase sintering process controls densification and microstructure. Nearly complete densification of Si_3N_4 is only possible by utilizing the following steps, in most cases in combination: *(i)* use ultrafine powders, *(ii)* apply external pressure, *(iii)* increase the sintering temperature (simultaneously an increase of nitrogen pressure is necessary), *(iv)* establish the equilibrium partial pressures of the various silicon compounds by using a Si_3N_4 bed, and *(v)* particularly add sintering aids to form a liquid phase.

As the first four steps do not result in a sufficient densification, the addition of sintering aids, forming a suitable liquid, is the most important step in the densification of Si_3N_4 [21]. If the liquid phase fulfils the conditions of good wettability and solubility of Si_3N_4, densification can be described according to the mechanisms of liquid-phase sintering formulated by Kingery: rearrangement, solution-diffusion-precipitation, and

coalescence [22]. On basis of these mechanisms the formation of dense Si_3N_4 can be described in the following way shown in Figure 2.3. Usually the powder selected for sintering is *>70% α-Si_3N_4* so that during densification the transformation from *α to β-Si_3N_4* occurs and a fibrous microstructure is obtained. The crystalline or glassy phases often form a continuous network around the grains of Si_3N_4.

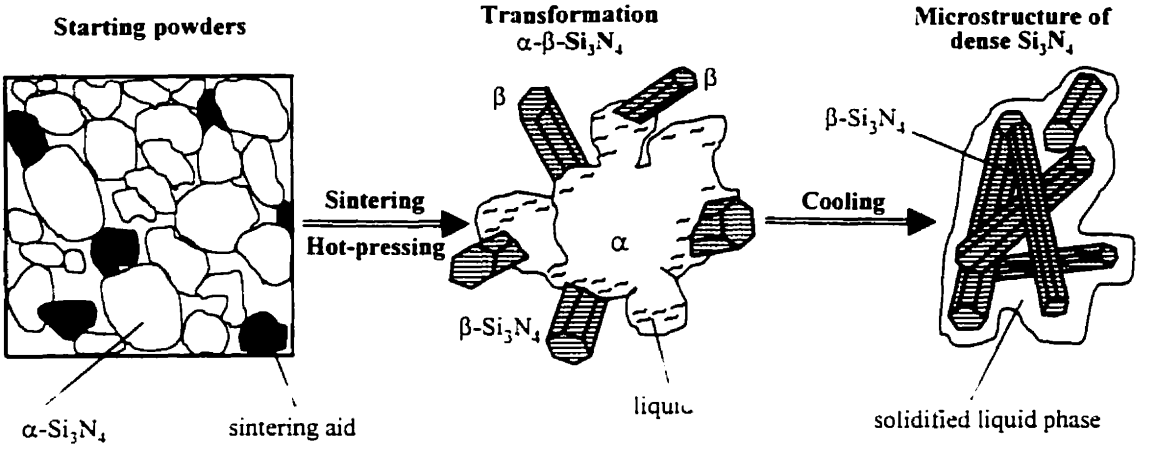

Figure 2.3. Solution-precipitation model for the liquid phase sintering of Si_3N_4 (schematic drawing) [21, 22].

2.1.2. Titanium

Ti is the ninth most abundant element on the planet; it makes up approximately 0.6% of the earth's crust. Ti occurs in nature only in chemical combination, usually with

oxygen and iron. The mineral sources of Ti are rutile (TiO_2), ilmenite (Fe, Mg, Mn)TiO_3, and leucoxene, an alteration product of ilmenite. Rutile is 93-96% titanium dioxide; ilmenite contains 44-70% titanium dioxide. Leucoxene concentrates contain up to 90% titanium dioxide. Ti is a low-density element, approximately 60% of the density of steel, which can be strengthened greatly by alloying and deformation processing. Some characteristic properties of elemental Ti are given in Table 1.1. Ti is nonmagnetic and has good heat-transfer properties. Its coefficient of thermal expansion is somewhat lower than that of steel's and less than half that of Al. Ti and its alloys have melting points higher than those of steel's, but maximum useful temperatures for structural applications generally range from 425° to 550°C. Ti has the ability to passivate and thereby to exhibit a high degree of immunity against attack by most mineral acids and chlorides. The excellent corrosion resistance and good strengths make Ti and its alloys useful in chemical and petrochemical applications, marine environments, and biomaterials applications. Ti is an allotropic element; that is, it exists in more than one crystallographic form. At room temperature, Ti has a hexagonal close-packed *(hcp)* crystal structure, which is referred to as "alpha", (α), phase. This structure transforms to a body-centered cubic *(bcc)* crystal structure, called "beta", (β), phase, at 883°C [23].

Alloying elements generally can be classified as α or β stabilizers. Alpha stabilizers, such aluminum and oxygen, increase the temperature at which the α phase is stable. Beta stabilizers, such as vanadium and molybdenum, result in stability of the β phase at lower temperatures. The lowest equilibrium temperature at which the material is

100% β is known as the β transus temperature, and below this temperature, Ti will be a mixture of $\alpha + \beta$ if the material contains some β stabilizers, otherwise it will be all α if it contains limited, or no β, stabilizers. The β transus is important, because processing and heat treatment are often carried out with reference to some incremental temperature above or below the β transus. Two groups of elements stabilize the β crystal structure by lowering the transformation temperature. The β isomorphous group consists of elements that are miscible in the β phase, including molybdenum, vanadium, tantalum, and niobium. The other group forms eutectoid systems with Ti, having eutectoid temperatures as much as 333°C below the transformation temperature of unalloyed Ti. The eutectoid group includes manganese, iron, chromium, cobalt, nickel, copper, and silicon. Two other elements that often are alloyed in Ti are tin and zirconium. These elements have extensive solid solubilities in α and β phases, although they do not strongly promote phase stability, they retard the rates of transformation and are useful as strengthening agents.

The effects and ranges of some alloying elements used in Ti are indicated in Table 2.1 [24]. Ti and its alloys are used primarily in two areas of application where the unique characteristics of these metals justify their selection: corrosion-resistant service and strength efficient structures. Ti has the ability to passivate, and thereby exhibit a high degree of immunity to attack by most mineral acids and chloride. The commercially pure Ti generally demonstrates the best corrosion-resistance qualities. Pure Ti usually has some amount of oxygen alloyed with it. The strength of commercial Ti is affected by the interstitial (oxygen and nitrogen) element content [23, 25].

Table 2.1. Ranges and effects of some alloying elements used in Ti [24].

Alloying Element	Range (approx.) wt%	Effect on Structure
Aluminum	2 to 7	Alpha stabilizer
Tin	2 to 6	Alpha stabilizer
Vanadium	2 to 20	Beta stabilizer
Molybdenum	2 to 20	Beta stabilizer
Chromium	2 to 12	Beta stabilizer
Copper	2 to 6	Beta stabilizer
Zirconium	2 to 8	Alpha and beta strengthener
Silicon	0.2 to 1	Improves creep resistance

The raw materials commonly used in producing Ti and its alloys include Ti in the form of sponge metal. This sponge must not contain hard, brittle, and refractory TiO_2 or TiN that, if retained through subsequent melting operations, could act as crack-initiation sites in the final product. Carbon, nitrogen, oxygen, silicon, and iron commonly are found as residual elements in sponge. These elements must be held to acceptably low levels because they raise the strength and lower the ductility of the final product as can be observed in Figure 2.4. Basically, oxygen and iron contents determine strength levels of commercial pure Ti and the differences in mechanical properties between extra-low interstitial grades and standard grades of Ti alloys. In higher strength grades, oxygen and iron are intentionally added to the residual amounts already in the sponge to provide extra strength. On the other hand, carbon and nitrogen usually are held to minimum residual levels to avoid embrittlement.

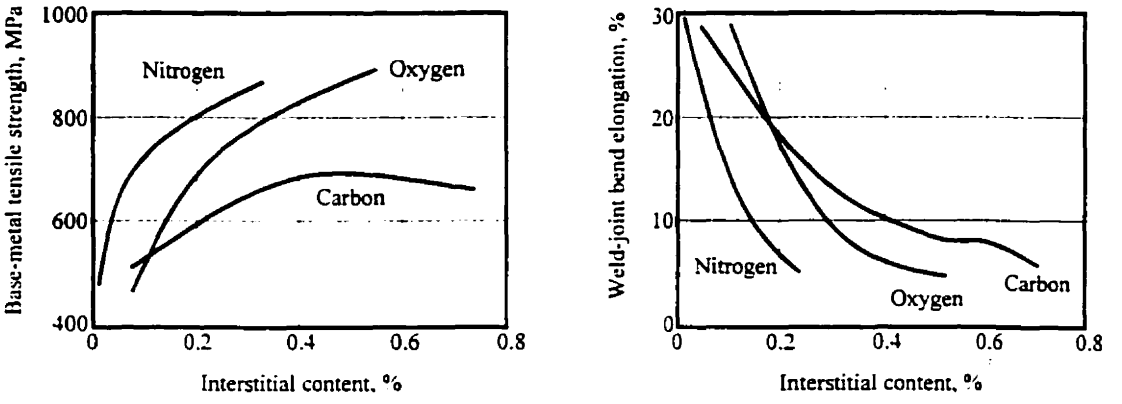

Figure 2.4. Effect of interstitial-element content on strength and ductility of unalloyed Ti [23, 25].

2.1.3. Techniques for Joining Ceramics to Metals

With the development of new ceramic materials, including those for structural applications, the demand to join ceramic components to metal structures has increased. Successful application of ceramics in many devices and structures requires some type of ceramic-metal joining. Using joining processes as part of a manufacturing route can offer considerable technical and economic advantages to the designer, provided careful and informed decisions are made about the processes to be applied, materials to be selected, joint configurations and the process parameters to be employed. There are many reasons for wishing to join particular ceramic and metal components, but the motives can usually be related to design, manufacturing, or economic factors. Two factors drive the need of improved joining technologies [26]. *First*, it is difficult to fabricate large ceramic structures

with complex shapes. Although small individual pieces of complex shape, such as a turbine rotor, can be fabricated, the path of least technological resistance to developing larger structures will often entail joining assemblies of more easily fabricated small components. If the joints are sufficiently strong, this may also provide indirect benefits, since quality control and nondestructive testing of small components may be simpler. *Second*, although ceramics may possess a unique and desirable set of properties, there will be applications in which these properties are needed and desirable, not for an entire structure, but only in one portion of a structure. For these applications, it will be necessary to joint the ceramic to another ceramic or to a metal.

The development of viable joining techniques will facilitate the assimilation of advanced ceramics into complex multimaterial structures. Several methods have been developed over the years to produce hardy and reliable joints between ceramics or to metals. The choice of appropriate joining method depends on the materials to be joined, joint design, and the anticipated service conditions. The classification of joining techniques is somewhat arbitrary and can be done in different ways [27, 28].

There are three general categories or types of joining processes. In the first, attachment is *mechanical* and is achieved through the use of mechanical interlocking of components. The second approach is *direct joining*, in which components are bonded either by a solid-state process or by fusion. The third approach could be referred as *indirect joining* in the sense that an intermediate layer of material, such as an adhesive, cement, or braze, is used to bond two components.

i) Mechanical Joining Processes

Mechanical joining methods are often based on localized, point-attachment processes, in which the join is provided by: a nail, a rivet, a screw or a bolt. All such joints depend on residual tensile stresses in the attachment to hold the components in compression. The joint is usually formed by an ordered array of point-attachments, as in the equally spaced rivets at the edge of a ship's plate, or the uniformly spaced bolts around a pressure vessel flange.

Mechanical joining is used in both traditional and new applications such as tying-in of furnace roof refractories with metal hooks or dog bones and the clamping of space shuttle leading edges. Press and shrink fitting is another type of mechanical joining, which is widely employed in mass production processes. A common example of this type of attachment is provided by the carbon-carbon composite Space Shuttle leading edges, which are attached by fasteners to facilitate removal and replacements. Provided that the materials are refractory and chemically compatible, this approach should provide high strength at high temperatures. However, the lack of ductility in ceramics severely limits the temperature ranges over which this method is applicable because of the high local tensile stresses that can develop in systems with thermal expansion mismatches, causing failure in the ceramic [29].

Although mechanical joining provides low-cost products mechanical attachment is not a generally attractive process for joining structural ceramics because of the frequent necessity for introducing intrusive stress-raising features such as threads or bolt holes, and the low strengths and lack of hermeticity of the joints.

ii) Indirect Joining Processes

The use of a liquid, a glass, or a solid foil that flows readily under low applied stress to join materials can have advantages. Flow of a wetting liquid or glass or of the ductile solid can fill irregularities in the surface and therefore imposes less stringent demands on surface preparation and the degree or extent of surface mating required. Indirect joining is the most common method of achieving high integrity joints using a wide range of intermediate bonding materials. The major categories of joining using an intermediate layer include joining with adhesives, cements, glasses or glass-ceramics, and brazes. Joining with organic-based materials is simple and widely used. A broad range of materials can be joined by this method. Precise processing conditions have been specified for the preparation of aluminum and aluminum alloy surfaces for adhesive bonding, a consequence of the importance of this joining approach in the aerospace industry. The low elastic modulus of organic materials allows large strains to be accommodated without the development of significant stress, an attractive characteristic. However, the limited temperature capabilities of organics, and their susceptibility to chemical attack and degradation, limit their use.

Joining with cements has some of the same advantages as adhesive joining and provides a higher temperature capability. However, as the temperature range is increased, so too is the effect of thermal expansion mismatch. Chemical interactions between the cement and the ceramic, and decomposition of the cement, can limit the temperature range of application. Inorganic glasses and glass-ceramics generally wet, form an acute contact angle with, and bond to ceramics. As a result, they can be used to coat one or both mating

surfaces, and in principle, can form strong joints. The thermal expansion coefficients of glasses can be varied to match, or at worst decrease the mismatch with, a particular material. When two articles of the same material are to be joined, glasses or crystallized glasses provide an attractive joining route. However, in comparison to metals, glasses are less tolerant of thermal expansion mismatch. Thus, for applications in which materials with different thermal expansion characteristics are to be joined, glass-ceramics may be more desirable. Glasses and glass-ceramics often provide good environmental compatibility, although it may not equal that of the components to be joined. Difficulties may also arise from excessive chemical reaction between the glass and the ceramic or metal [30]. Softening of the glass and decomposition of certain glasses are additional concerns, particularly for high temperature applications.

The indirect bonding of ceramics includes those techniques in which a liquid medium is responsible for bonding. Liquid phase bonding using molten metals has been widely used to create ceramic/ceramic and ceramic/metal joints. In cases where ceramics are being introduced into predominantly metal structures, brazes provide a more familiar joining material. Brazing is commonly used in the manufacture of high-integrity joints with good mechanical properties. However, brazing requires wetting of the ceramic into contact angles less than 90°C, which is often difficult to achieve because of the high stability of ceramic compounds. One way to promote wetting is to metallize the ceramic surface. Another alternative is to add small percentages of a reactive metal, e.g. Ti, which reacts with the ceramic and generally facilitates wetting via the formation of a more metallically bonded reaction product at the interface [31], in order to promote wetting of the

surface by the braze. The Figure 2.5 shows the effect of time at temperature on the contact angles of several reactive liquid metal/solid ceramic systems [32]. The criteria for selection of brazing alloys are that they must wet or coat the ceramic, form a chemical bond at the interfaces resulting in a strong joint, and they should cause minimal degradation of the base material or materials. Successful brazing alloys produce bonds that are, strong, reliable, and relatively inexpensive to manufacture. As is the case for any joining process, there are also some important constraints and concerns, many of which are the direct consequence of the presence and action of the reactive metal.

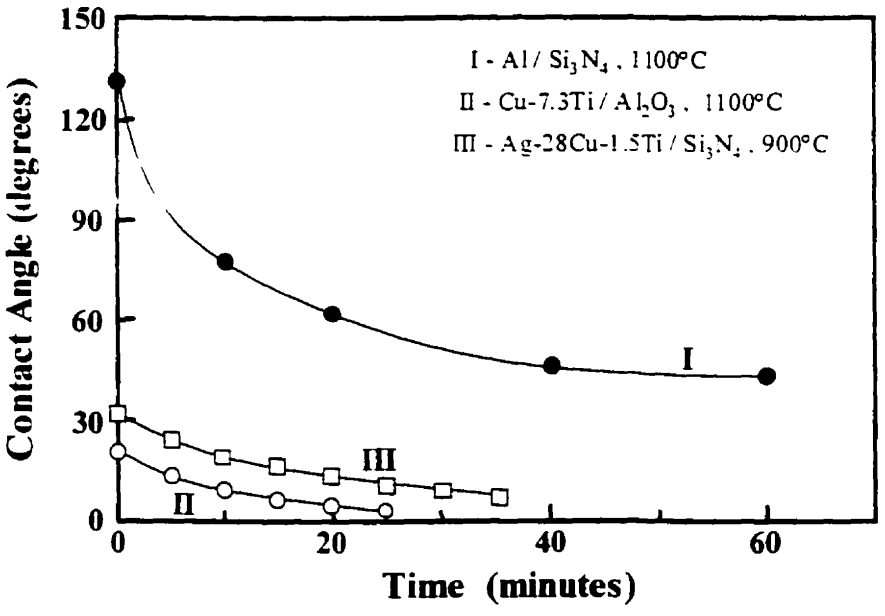

Figure 2.5. Effect of time and temperature on the contact angle [32].

iii) Direct Joining Processes

Direct joining includes processes where the ceramic is joined to the metal without an interlayer. Successful direct pressure joining relies upon the achievement of adequate interfacial contact and subsequent diffusion or plastic flow to eliminate interfacial porosity. When both materials undergo limited plastic flow, e.g. ceramic-ceramic bonding, or when deformation of the workpiece must be avoided, e.g. the Al_2O_3 to niobium bond during the fabrication of high-pressure sodium lamps, special care must be taken to assure smooth mating surfaces [33]. When ceramic-metal bonds are being formed, and deformation of the metal is permissible, plastic flow generally occurs within the metal. The advantages of direct pressure bonding include a simple fabrication procedure, a one-step process, and potentially very high joint strength. However, there are also several limitations and disadvantages: high cost; only relatively planar specimens can be joined; a vacuum/inert atmosphere is required; and pressure must be applied. The need to apply pressure during diffusion bonding imposes restrictions on the joint geometry; most joints are of the face seal type and are not well-suited for accommodating thermal expansion mismatch.

Experimental work on fusion welding using electron beam, laser, and arc imaging techniques has also met with some success with high melting point systems. Welding involves fusion of one of the components at the interfacial region to promote joining. In solid-state diffusion, bonding occurs with or without mass transfer across the interface. Physical bonding is a result of charge transport across the interface with the establishment of van der Waals forces between the materials. Mass transfer occurs when the atomic species of the original materials diffuse across the interface, and leads to chemical

bonding. In this case the resulting interface can have a diffusion layer or a reaction layer, depending on the thermodynamics of the system and the joining conditions [34].

Whatever process is used, the formation of successful joints depends on the achievement of intimate contact between the workpieces, the conversion of these contacting surfaces into an atomically bonded interface, and the ability of this interface to accommodate thermal expansion mismatch stresses generated during cooling process after fabrication or temperature changes during operational conditions. Successful fabrication of metal ceramic interfaces is not easy, and the difficulties are often inherent rather than matters of engineering design or economics.

2.1.4. Solid-State Diffusion Bonding

Diffusion bonding is a solid-state process for the fabrication of metal-metal, ceramic-ceramic and ceramic-metal joints that is conceptually simple. The process requires no localized melting of components or introduction of foreign bonding materials, but merely that mating surfaces are brought into intimate, atomic scale contact so that an interface can be formed by interdiffusion to create a structural continuum. Such interfaces, whether between metals, ceramics or between a metal and a ceramic, can have good mechanical integrity even at high temperatures. The simplest form of diffusion bonding involves the application of a low pressure at a high temperature to achieve bonding of the components. It is important they have smooth and well-matched mating surfaces.

Understanding the relationship between processing, structure and properties of metal/ceramic interfaces is becoming increasingly important as performance requirements demand a combination of these different materials in applications ranging from electronic packaging to high temperature aircraft structures [35]. There are two possible mechanisms of the solid phase bonding of ceramics to metals without the intermediary of a liquid filler metal: when the solid-phase ceramic and metal are brought into contact, the metal may undergo plastic deformation, enter the surface irregularities of the ceramic, adhere and bond to the ceramic. In another possible mechanism, the metal may diffuse through the interface, react with the ceramic and form a continuous layer [34].

Diffusion bonding has attracted interest as a means of bonding Si_3N_4 and successes have been achieved by controlling the microchemistry and microstructure of the interfaces formed. The first requirement for solid-state diffusion bonding is the creation of intimate contact between the surfaces to be bonded in order that the atomic species come into intimate contact. In addition to a good contact, there should be enough diffusion between the materials in a reasonable time. Pressure can be applied uniaxially (hot-press) or isostatically (hot-isostatic press) on a diffusion couple. Bonding of ceramics by uniaxial pressing has been achieved, but it is not yet an important and widely used industrial process.

There are several advantages of solid-state joining. Diffusion bonding is primarily employed in the joining of dissimilar materials, e.g. dissimilar metals, metal-glass, metal-ceramic and ceramic glass. When ceramic have to be bonded to metals, it is a common practice to introduce a metal interlayer between the components, producing a joint

structure similar to that created by brazing. The interlayer should be ductile so that it can deform readily to achieve intimate contact with both mating surfaces at various pressures and temperatures, that it should act as a stress relieving buffer layer if the thermal expansivities of the metal and ceramic components differ significantly, and of course that it should adhere strongly to both the metal and ceramic components [36]. The technique has been applied, so far, mainly for the joining of Al_2O_3 and SiO_2, but its utility has also been demonstrated for joining of Si_3N_4 and other new engineering ceramics. The technological advantages of diffusion bonding are low deformation which enables parts to be joined with little distortion, the ability to join large areas, the applicability of diffusion bonded joints at high service temperatures, and the possibilities for joining materials in a none conventional way [37].

The major disadvantages of diffusion bonding are high capital costs, and the restricted joint geometries that can be produced [38]. If the mating surfaces are not flat but wavy, there can also be regions where the mating surfaces arch away from each other, as illustrated schematically in Figure 2.6, and these substantial voids can be slow to close. While very idealized, this simple picture reflects some of the motivation that has led to the development of differing diffusion bonding techniques. In the figure, the marking of the mating surfaces is ended as contact area grows as a schematic imitation of dissolution of oxide or desorbtion of segregated impurities on the mating surfaces that is often necessary condition for successful diffusion bonding.

In addition, specific problems exist when applying diffusion bonding to Si_3N_4. The misfit in the coefficient of thermal expansion *(CTE)* of the joining materials can result in

areas of high residual stresses at the interface during the cooling process. This problem may be minimized by two different methods [39]. One method is to insert a metal with approximately the same thermal expansion coefficient as that of the ceramic to decrease the magnitude of thermal stress generated, while the other method involves thermal stress relief by using a ductile metal that easily develops plastic deformation under thermal stress. These two methods may also be employed in combination.

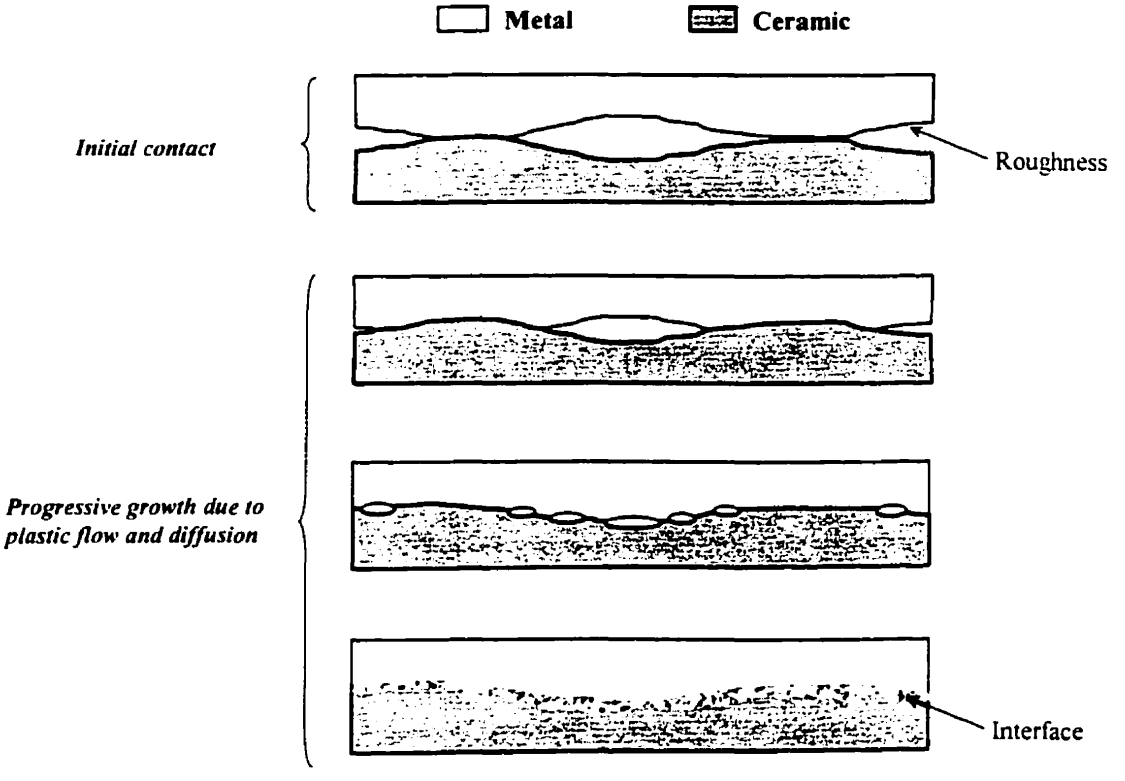

Figure 2.6. Schematic illustration of diffusion bonding induced growth of the contact area between two microscopically rough and wavy mating surfaces [32].

2.1.5. Modeling Joint Formation

Diffusion bonding can be defined as the creation of an intimate bond or joint between two materials by thermally assisted processes occurring in the solid state. In order to understand the mechanisms and driving forces of diffusion bonding, the evolution of the bond microstructure must be appreciated. The bonding process can be viewed as two steps operating in parallel [40]. The first is the transition from two surfaces contacting at their asperities to an intimate interfacial conformity, as illustrated in Figure 2.7. This must involve the elimination of a large volume of interfacial voids accommodated by mass transfer mechanisms, plastic flow and diffusion. In parallel with this, but sequential to each individual contact, there must be an adhesion process giving the interphase boundary strength. A third step, with possible destructive consequences, is a subsequent chemical reaction between the metal and ceramic in contact to form a third phase at the boundary. The driving force for the formation of an interface between materials is the energy decrease of the system resulting from its establishment. The interfacial energy should reach the lowest achievable value as the bond is formed, otherwise further changes that could degrade the stability of the bond may occur under operating conditions.

2.1.6. Bonding Mechanisms

The mechanisms of diffusion bonding two identical materials and similar surfaces have been studied since the 1960s, and it is now generally accepted that joint formation

occurs by collapse of interface voids produced by a number of diffusion and creep mechanisms.

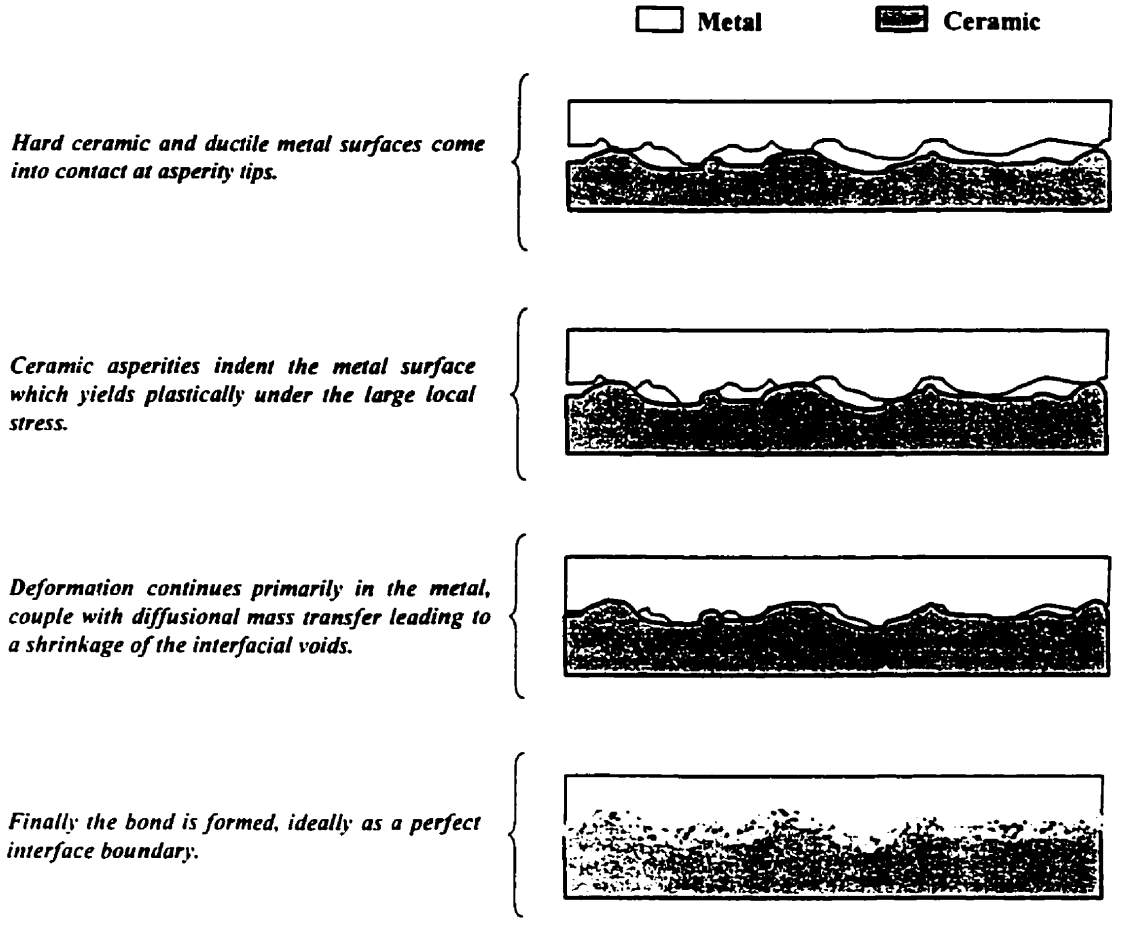

Figure 2.7. Sequence of events during metal-ceramic diffusion bonding [40].

The collapse of interfacial voids can be brought about by a number of mechanisms analogous to those occurring in pressure sintering, and these are best grouped in terms of sources and sink for matter and are [41, 42, 43].

A. Surface diffusion from a surface source to a neck.

B. Volume diffusion from a surface source to a neck.

B'. Evaporation from a surface source to condensation at a neck.

C. Grain boundary diffusion from an interfacial source to a neck.

D. Volume diffusion from an interfacial source to a neck.

E. Plastic yielding resulting in deformation of original surface asperities. ***(Figure 2.8)***

F. Power law creep.

An illustration of the various routes of material transfer is contained in Figure 2.9. These mechanisms are normally separated in two main stages.

Stage 1*: Plastic deformation.* The contact area of asperities, though initially small, will rapidly grow until the application load can be supported, which means that the local stress falls below the yield strength of the material.

Stage 2: *Diffusion and power law creep.* The driving force for mechanisms A, B, and B' is the difference in surface curvature. Matter is transferred from the point of least curvature (sharp neck of the void at the bond interface) to the point of greatest curvature. Thus, as the voids change from an elliptical to a circular cross section, the rates of these mechanisms will approach zero because the aspect ratio of the voids tends to unity.

In addition to these stages, recrystallization and grain growth may occur during bonding. Several attempts have been made to model the mechanisms and processes involved in diffusion bonding [44, 45, 46], however, these are all based on joining of similar materials parts. Bonds made between dissimilar materials will have a more complicated combination of bonding mechanisms [47]. The same void-closure mechanisms will operate

but many more diffusion pathways occur. Interface formation must be accompanied by the collapse and annihilation of voids created at first contact. The driving force for this collapse is identical to what drives diffusion bonding in metals. Void closure results in a net approach of the two surfaces being joined. This allows mechanical work to be done by the bonding pressure. The reduction in void volume is accompanied by a reduction of void surface energy, which is a further driving force. A number of additional competing mechanisms can occur during the bonding of dissimilar materials such as metals and ceramics.

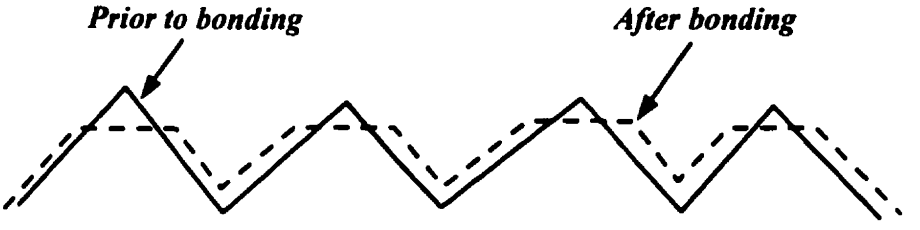

Figure 2.8. Reduction of surface roughness during initial stages of diffusion bonding [41].

These are all generated by the initial non-equilibrium nature of the interface. They may operate over a short period of time until a new equilibrium interface is formed, or if there is a chemical reaction between the two surfaces no equilibrium may be achieved and instead an extensive interfacial reaction may occur.

a) Transport from surface sources to an interfacial neck

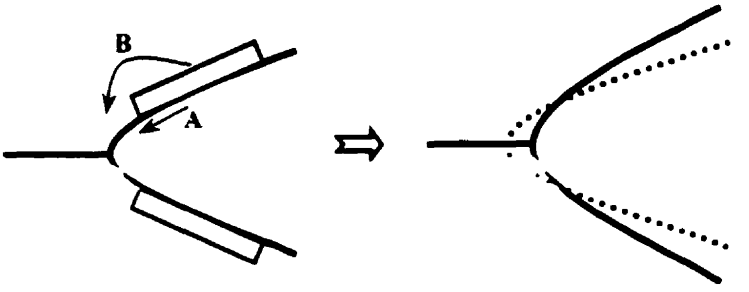

b) Transport from the bonding surface to a neck

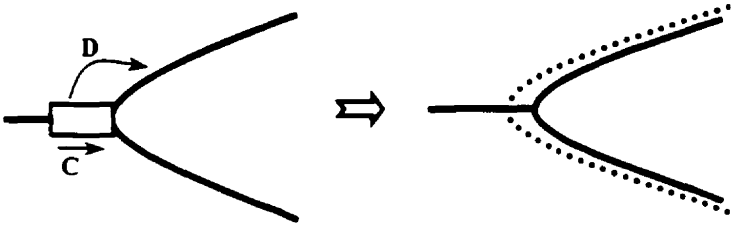

c) Bulk deformation by plastic flow after yield or during creep

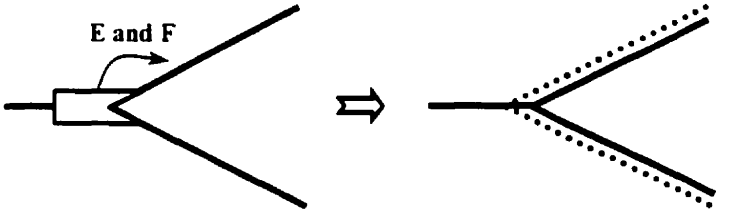

Figure 2.9. Schematic illustration of material transfers for various mechanisms involved in diffusion bonding [42, 43].

Several attempts have been made to model the mechanisms and process involved in diffusion bonding [48, 49, 50], however many of the models do not account for all mechanisms involved in the bonding process. Clearly the modeling of metal/ceramic diffusion bonding is intrinsically a highly complex operation and a complete model encircling all interactions may not be analytically possible. However, it is possible to apply simple models to certain metal/ceramic couples, which show a minimum of possible complication. One such system, Al-Al_2O_3, has been investigated [51] and simple void closure models are found to be applicable in this case, as shown in Figure 2.10. Much work needs to be done on this problem, and a major obstacle is to obtain good data on mass transfer in metal/ceramic systems.

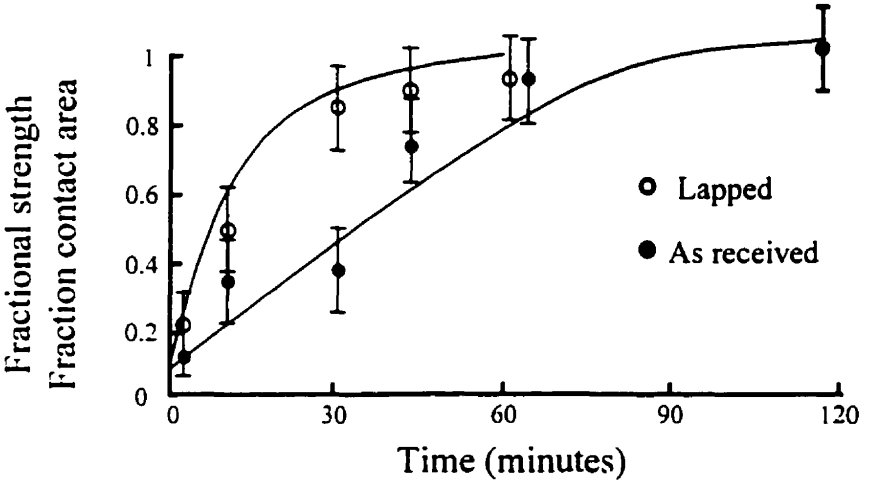

Figure 2.10. Predictions of diffusion bonding in Al-Al_2O_3 joints. The solid curves show the predicted area of bonding with time at 600°C and 50 MPa for two surfaces, the experimental points show the strength of the bond as a fraction of the maximum strength achieved after several hours at bonding temperature [51].

2.2. *Metal/Ceramic Interfaces*

Having selected suitable joining materials and decided upon a joint design, consideration can be given to the choosing of equipment and processing parameters that will ensure effective manufacture of the joints. While choices about materials and joint designs usually have to be made based on the nature of the components and the proposed service performance of the bonded assembly, those concerned with process parameters are numerous not only because of their variety but also because of the possibility of making incremental adjustments during trial runs to optimize joint quality by fine tuning.

2.2.1. *Experimental Parameters for Bonding*

The main variables that affect solid-state bonding are the pressure, temperature, time, surface roughness, and, in some cases environment [52]. These variables are not independent, but they are discussed separately below in order to emphasize the most important factors associated with each one.

a) Temperature. Temperature is the most important parameter in the bonding process due to the fact that: *(i)* in thermally activated processes, a small change in temperature will result in the greatest change in process kinetics, diffusion, creep, compared with other parameters; and *(ii)* virtually all mechanisms in diffusion bonding are sensitive to temperature, plastic deformation, diffusion, creep. Temperature increases

interaction across a metal/ceramic interface by increasing the mobility of atoms and also the mobility of dislocations in the metal during bonding. Since the mobility of dislocations increases with temperature and the flow stress correspondingly decreases, the pressure required for bonding decreases with increasing temperature. Therefore, an increase in bonding temperature should generally enhance bonding of a metal/ceramic interface for a given pressure and time, provided that the time is sufficiently short to prevent the development of detrimental reaction products at the metal/ceramic interface.

In general, the temperature required to obtain sufficient joint strength is typically within the range *0.6 and 0.95* T_m, where T_m is the absolute melting point of the base material. The effect of temperature on the penetration coefficient is shown for SiC/Nb and SiC/Mo joints in Figure 2.11 [53, 54]. It is seen that the coefficient varies within large limits, depending on the applied bonding temperature. The effect of the temperature on bond strength for specimens with failure at the alumina/steel (aluminum interlayer) interface is presented graphically in Figure 2.12 [55]. It is seen that the strength level increases with temperature, and that the calculated bond strength is in close agreement with the measured values. However, at higher bonding temperatures, it would be expected that the joint strength be reduced because of the high residual stresses formed as a result of thermal expansion mismatch between the joint members. The optimum bonding temperature occurs at a point where the strength reduction due to residual stresses starts to balance the strength enhancement as a result of void elimination. The presence of an optimum bonding temperature has been found in shear testing of Si_3N_4/Mo joints [56].

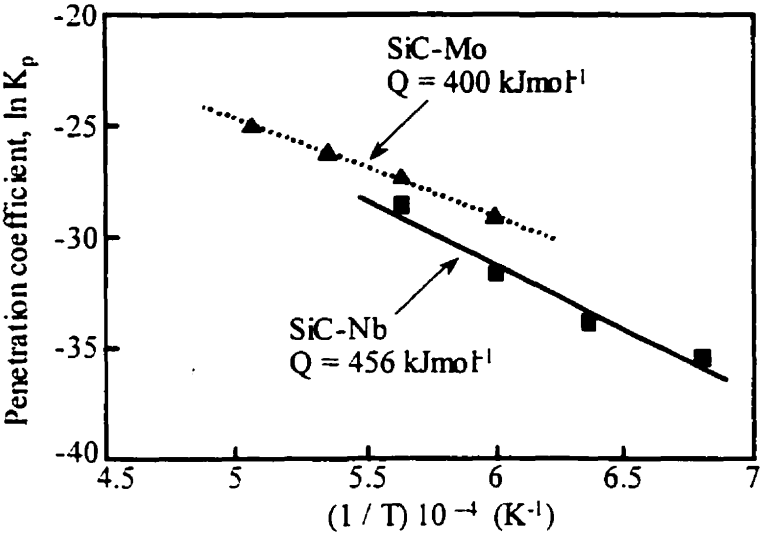

Figure 2.11. Penetration coefficient in function of temperature during diffusion bonding of SiC-Nb and SiC-Mo joints [53, 54].

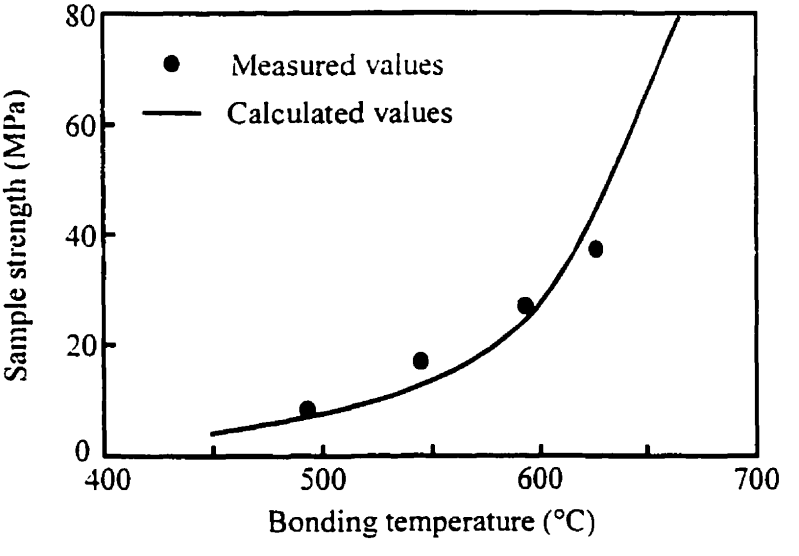

Figure 2.12. Effect of temperature on bond strength in joining of steel to alumina with 0.5 mm aluminum interlayer (vacuum, 30 min, 50 MPa) [55].

*b) **Pressure.*** The pressure applied in diffusion bonding is typically some small fraction of the room temperature yield stress of the base metal to avoid macroscopic deformation of the materials. Uniaxial pressure used in hot pressing of ceramics to metals ranges from 1 to 100 MPa [57]. In general, this is sufficient to reduce the size of surface asperities. In addition to establishing contact between the metal and ceramic, an important role of the pressure is to destroy the stable oxide film, through plastic deformation at the bonding temperature, present on the surface of most metals and this has a large effect on the integrity of the metal/ceramic bond. This, in turn, will increase the contact area subsequent to initial contact between the surfaces with a consequent reduction in the number of voids remaining from the initial stages of bonding. The exact pressure required depends on the metal/ceramic system, type and thickness of the oxide metal layer present at the surface and on the bonding temperature. As for temperature, the fracture strength increases with increasing bonding pressure up to a plateau corresponding to the maximum bonding area, but for high pressure and temperature, a decrease can be observed as in the case of Ni/ Al_2O_3 joints shown in Figure 2.13 [58].

*c) **Time.*** Process parameters as bonding temperature, time and pressure are strongly inter-related. In the case of diffusion bonding, variations in the bonding temperature also affect the yield strengths of the component and interlayer materials and hence the external pressure that must be applied to produce intimate contact by causing the surfaces to conform and dispersing oxide films that may be coating the bonding surfaces. Bonding times may vary from one second to several hours depending on the metal/ceramic combination and the joining temperature [57].

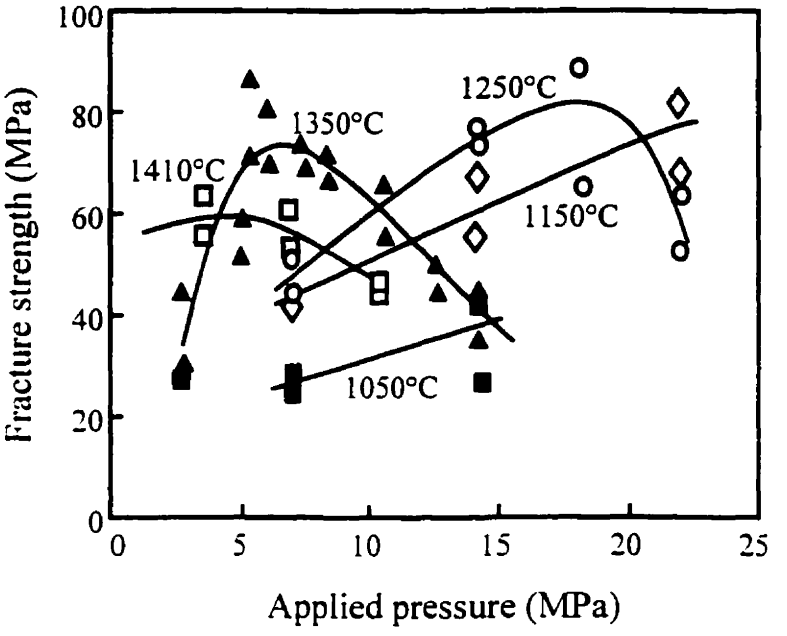

Figure 2.13. Tensile fracture strength of Ni/Al_2O_3 joints vs. bonding pressure for various temperatures; bonding time: 1 hour [58].

A relatively short bonding time is usually required to form a strong bond between a metal and ceramic under temperature and pressure conditions which are sufficiently high to cause rapid deformation of the metal. Time favors creep, diffusion and evaporation-condensation mechanisms. Therefore, fracture strength increases with bonding time to reach a plateau when the maximum bonding area is obtained. When prolonged times or higher temperatures are used, chemical reactions can progress at the interfaces of some systems and significantly influence bond quality. These reactions can initially enhance bonding, forming "chemical bridges", but often ultimately cause degradation because their growth progressively generates volume mismatch strains and stresses within the reaction

product or at the product/workpiece interfaces. Figure 2.14 shows results of shear strength as a function of time for SiC/Mo samples hot-pressed at 1400°C [59]. For each temperature, there is a corresponding minimum time required to promote complete bonding.

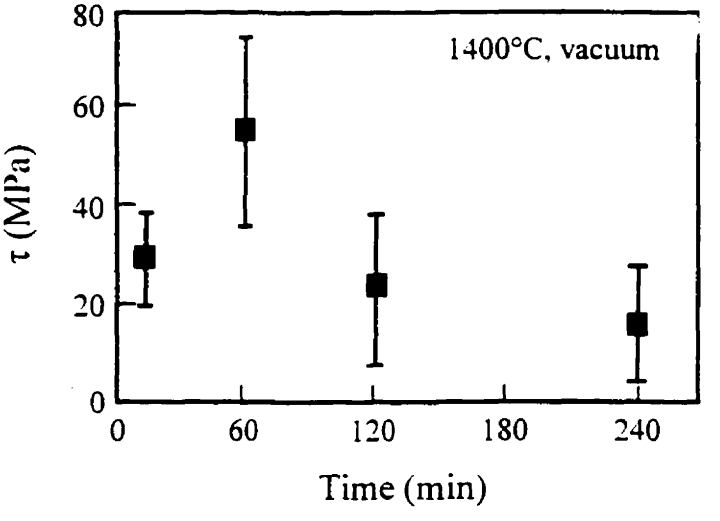

Figure 2.14. Plot of shear strength as a function of time for SiC/Mo samples hot-pressed at 1400°C. Error bars obtained from 4 to 6 samples per point[59].

*d) **Surface Roughness.*** Surface preparation before bonding is usually necessary for joint components and inserts. There are three main objectives: the first is the production of surfaces that are free of mobile contaminants such as oil films and surface layers of fragile or thick corrosion products, and any other protective layer that might inhibit bonding. Having produced clean surfaces, it is then necessary to ensure that there is macroscopic conformity between the mating surfaces of the components to be bonded. Without this, a

lack of surface conformity of components to be diffusion bonded may limit good intimate contact when joining either directly or via thin interlayers. Finally, it is important to create microscopic topographic features on each material surface in order to encourage bonding.

The presence of asperities on the bonding surfaces prevents large-scale plastic deformation at the surface because the metal is affixed between the asperities and limits the total area of contact between the metal and oxide-free ceramic, and, in addition, large voids are rarely closed [60, 61]. Therefore, it is necessary to polish the bonding surfaces prior to joining, improving the initial area of contact between the metal and ceramic and prevent the formation of large voids. The removal of rust and other thick corrosion products and the creation of desired macroscopic and microscopic topographies can often be achieved by mechanical treatment of the surfaces. Grinding can be used to prepare both metal and ceramic surfaces. In practice it can be useful also to avoid producing very smooth surface finishes because microscopic asperities can assist the disruption of surface oxides.

Particular attention should be paid to the uniformity of appearance of the treated surfaces since patches of incorrectly prepared surfaces can result in unbonded areas being present within the joint. Figure 2.15 shows cross-sections through a very simple rough surface in which the vertical scale is grossly exaggerated compared with the horizontal one. The dashed horizontal lines on the sections show the locations of the nominal surface such that the cross-sectional areas of the true surface peaks above, and of the valleys below, are exactly balanced.

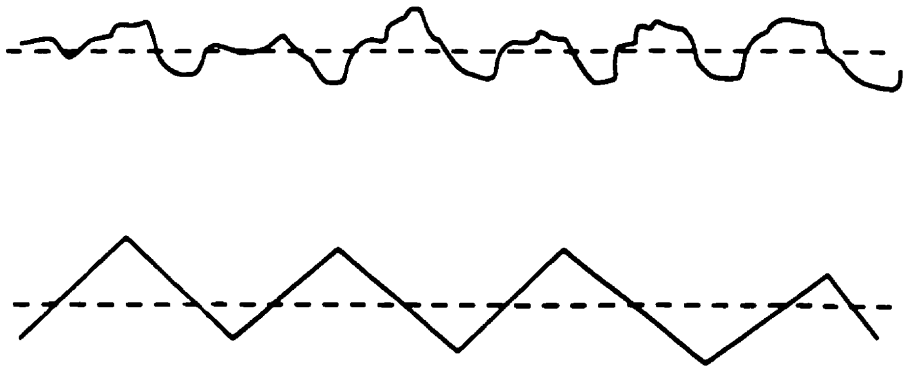

Figure 2.15. Cross-sections through roughened surfaces [61].

*e) **Bonding Environment.*** The selection and control of the gaseous environment is a crucial aspect for successful and reproducible brazing and diffusion bonding. The environment affects the surface chemistry of both the components to be joined and the joining materials themselves and hence exerts a fundamental influence on the process since joining is the conversion of surfaces to interfaces. The gaseous environment used to effect joining is seldom air because it generally causes the formation of oxide films that act as barriers to the direct contact between the component materials that is needed to create an interface. Diffusion bonding is usually carried out in vacuum or in the presence of a gas with low oxygen activity, e.g. argon or nitrogen. If one of the reaction products is a gas, such as nitrogen in Si_3N_4-metal systems, the environment affects the thermodynamics of the system and the kinetics of the reactions. For example, increasing the partial pressure of nitrogen in the environment may promote the formation of metal-nitrides in a situation not observed when joining is carried out under vacuum [62].

The three main types of gaseous environment used during diffusion bonding are vacuum, inert gases or gas mixtures such as Ar or He. Perhaps the biggest single barrier to the successful achievement of diffusion bonded joints is the presence of oxide films on the surfaces of diffusion bonding interlayers and metal components. These oxides form initially by reacting with the O_2 present in air, but they can thicken substantially when heated if O_2 is available. Relatively low O_2 arrival and oxide reformed rates also assist the removal of oxide films by other processes, such as chemical interaction with their substrates. Thus the most significant fact about the use of an evacuated furnace chamber is that it has a low partial pressure of oxygen. Non-reactive environments can be produced also by using inert gases such as Ar or N_2 at a pressure of generally about *100 kPa (≅ 1 atm)*. The prime attraction of these gases to user is of course their virtually complete chemical inertness, but there are physical differences between the gases that could affect their efficiency as joining environments. There are, however, drawbacks to use of inert gas environments. Thus they are of little effectiveness in removing oxide barriers already on the surfaces of metal components or joining materials and hence it is crucially important to use thorough oxide removal processes before loading the components into the bonding equipment. Similarly, it has been commented already that using gaseous environments can be a cause of problems when diffusion bonding involves gas entrapment at the joint interfaces. The presence of such gas pockets will prevent direct contact between the surfaces to be bonded and the application of a bonding pressure (typically 1 to 100 MPa) will compress the trapped gas and hence increase the partial pressure and chemical activity of trace constituents such as H_2O, O_2 and N_2.

2.2.2. Interfaces Between Metals and Ceramics

Metal/ceramic interfaces are involved in a great number of technologies, where specific electrical, optical, magnetic or mechanical properties are required. These properties often depend on the characteristic of the interfaces, such as their atomic structure and composition, as well as the nature of the interfacial bonds. In general, when ceramics and metal are joined, interfacial morphologies are classified into three groups mainly, as illustrated in Figure 2.16 [63]. ***i) Interfaces with Non-Reaction and Non-Diffusion Layer:*** the interfaces are microscopically planar and coherent (epitaxial) or incoherent growth, as in the case of alumina-niobium and alumina-platinum [34]. For non-reactive systems the physical approach of adhesion shows that three types of forces can appear during contact between two materials [61] namely, long range forces related to polarization mechanisms (dielectric materials), medium range forces (some nm) corresponding to van der Waals interactions and short range forces (0.1-0.2 nm) involving strong inter-molecular chemical bonds. No new phases grow at the interface. ***ii) Interfaces with Diffusion Layer:*** the interfaces are originated from interdiffusion between the metal and ceramic, as in the case of Si_3N_4-stainless steel [64]. ***iii) Interfaces with a Reaction Layer:*** the majority of metal-ceramic joints reacts chemically at the interface. In some couples many kinds of compounds are formed at the interface result from a chemical reaction between a ceramic and metal, as in the SiC-Mo system [65].

For reactive systems, when the reaction occurs at the interface, the strength of the bond is more complex to analyze and depends on adhesion properties of the new phases.

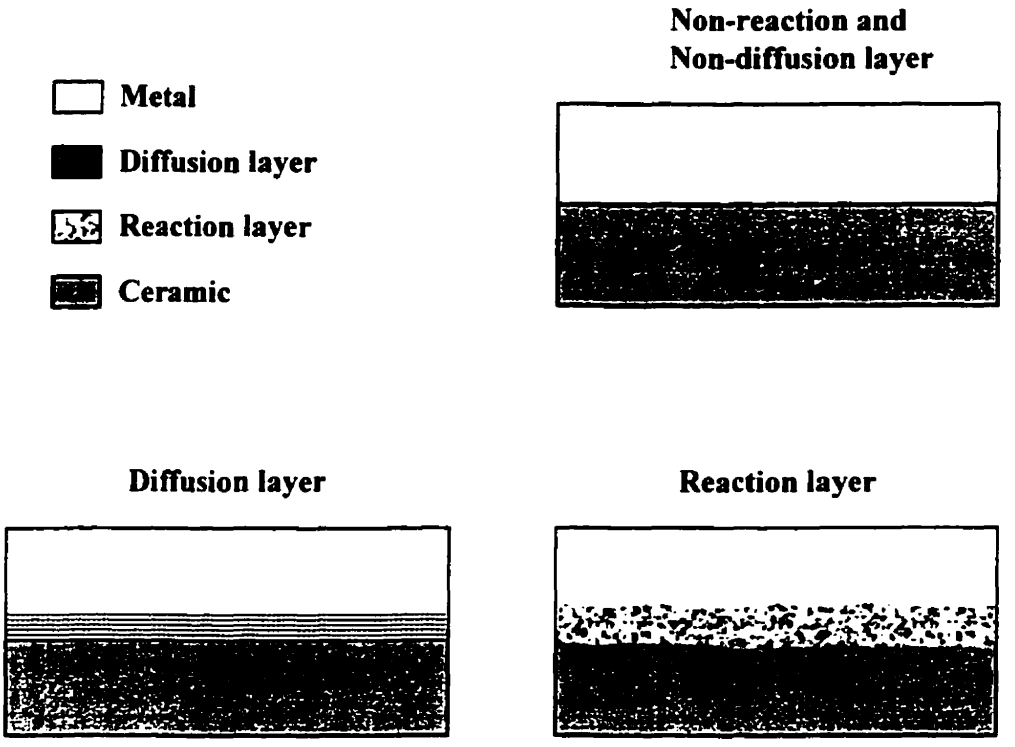

Figure 2.16. Common classes of metal/ceramic interfaces [63].

Chemical reaction during solid-state bonding occurs when there is mass transfer across the interface, resulting in the formation of interfacial reaction layer with properties that differ from those of either the metal or ceramic components. Such reaction products can have a drastic effect on the interface properties. Whether or not new phases form depends on the thermodynamic properties of the metal/ceramic system and on the experimental condition. Chemical reactions take place when the formation of a reaction product reduces the total Gibbs free energy of the system. Because interfacial reactions are an irreversible process, chemical reaction at metal/ceramic interfaces is usually considered

from the viewpoint of equilibrium thermodynamics, where the possible reaction products and conditions are determined from equilibrium thermodynamic data available for various systems as a function of time, temperature and pressure [66].

Diffusion and reaction layers primarily grow into metals but only slightly into ceramics because atomic diffusion is far easier in metals than in ceramics [67]. There are two significant factors governing the characteristics of interfacial bonding: *chemical bonding, and lattice matching.* Ceramic/metal interfaces have structural discontinuity especially in electronic state. Ceramics have covalent or ionic bonding but not metallic bonding involving free electrons. This difference in chemistry sometimes prevents formation of strong bonds at the interface.

2.2.3. Establishment of Metal-Ceramic Interface

The key step in the formation of a ceramic/metal interface is to achieve adequate contact between the two materials at the interface. A solid/solid interface in which at least one of the surfaces is a metal can be formed by pressure, especially at an elevated temperature, resulting in displacement of impurities and adjustment of irregularities due to localised deformation. A solid/liquid interface can be formed if the liquid wets or spreads thereby penetrating between irregularities at the solid surface. It has been widely considered that wetting is an essential prerequisite for the creation of a good bond. It is understood, however, that wetting alone is not sufficient to guarantee good adhesion since

wetting can occur with either van der Waals or stronger 'chemical' bonding across the interface.

The surface of any phase has an associated free energy. That energy, γ (J/m^2), is always positive, and it is equivalent to the energy required to create a unit area of new surface in the material. The driving force for the formation of a ceramic/metal interface in solid-state bonding is the reduction in the surface energy that occurs when intimate contact is established between the metal and the ceramic surfaces. This energy change per unit area (ΔG) is expressed by the Young-Dupré equation: [68, 69]

$$\Delta G = \gamma_m + \gamma_c - \gamma_{cm} \qquad (2.2)$$

Where: γ_m and γ_c are the surface energies of the metal and the ceramic respectively, and

γ_{cm} is the ceramic/metal interfacial energy.

If physical bonding occurs, i.e., no chemical reaction takes place at the ceramic/metal interface, and there is negligible energy dissipation during interfacial failure, then the energy (ΔG) is identical to the work of adhesion W_{ad}, which corresponds to the energy necessary to separate a unit area of interface into the two original surfaces.

Substituting W_{ad} for ΔG in equation *(2.2)*

$$W_{ad} = \gamma_m + \gamma_c - \gamma_{cm} \qquad (2.3)$$

This shows that two materials form a stable bond when the work of adhesion is negative; e.g., creating the metal-ceramic interface gives a net decrease in the free energy of the system by eliminating the high positive free energy of the interface.

Rearranging the terms in equation *(2.3)*

$$\gamma_{cm} = \gamma_m + \gamma_c - W_{ad} \qquad (2.4)$$

Which shows that the ceramic/metal interfacial energy, γ_{cm}, decreases as W_{ad} increases, which facilitates bonding. Therefore, in systems with high W_{ad} and low interfacial energy, strong interfaces are formed between the metal and ceramic.

Since direct measurements are not possible, owing to dissipation during fracture, W_{ad} must be indirectly obtained. There are two ways to calculate W_{ad} depending on the ceramic/metal system. If there is melting at the ceramic-metal interface, for example, molten glass on a metal or a braze alloy on a ceramic, W_{ad} is calculated by

$$W_{ad} = \gamma_m (1 + \cos\theta) \qquad (2.5)$$

where θ is the metal contact angle between the metal and the ceramic, which can be measured using the sessile-drop technique, and knowledge of the surface energy of the metal in equilibrium with its vapor. At equilibrium in the absence of chemical reaction, a metal droplet will assume a characteristic contact angle, θ, on a ceramic substrate that is determined by a balance of forces between the metal surface tension γ_m, the ceramic surface energy γ_c, and the ceramic/liquid metal interfacial energy, γ_{cm}. The contact angle decreases as γ_c exceeds γ_{cm}. Subsequently γ_m can be determined from the profile of the metal droplet. Values of γ_m can be found in the literature for just a few solid-solid systems, most of them involving Al_2O_3. From Table 2.2 it can be seen that, in general, γ_{cm} for

Al_2O_3-metal systems tends to increase with the cohesive energy of the metal, which is directly related to its melting temperature [70]. On the other hand, if the ceramic-metal is a solid-solid system, W_{ad} can be estimated by measuring the dihedral angle, ϕ, associated with residual voids on diffusion-bonded interfaces [71].

Table 2.2. Interfacial energies of solid-solid Al_2O_3-metal systems [70].

System	γ_{sm} (J/m^2)	T_m of Metal (°C)
Al_2O_3-Ag	1.57 at 700°C	960
Al_2O_3-Au	1.80 at 1000°C	1063
Al_2O_3-Cu	2.21 at 900°C	1083
Al_2O_3-Ni	2.20 at 1000°C	1453
Al_2O_3-Fe	2.73 at 1000°C	1536

If the interface ruptures in a brittle fashion, ϕ can be measured using an atomic force microscope and W_{ad} is then obtained by

$$W_{ad} = \gamma_m (1 - \cos\phi) \qquad (2.6)$$

For a given ceramic, one predicts that metals with high surface energies that form low energy ceramic/metal interfaces would form the stronger bonds. Higher melting point metals tend to have higher surface energies and thus, might be expected to form stronger bonds. Another important consequence of equation *(2.2)* is that a stable interface requires a

positive ΔG *(or* W_{ad}*)*. For a number of ceramic-metal systems, W_{ad} varies with the temperature, which provides an explanation for the minimum temperature requirements to achieve bonding. Chemical reactions, when present, further lower the free energy of the system, improving bonding. Although adhesion is difficult to model theoretically, recently first principles calculations [70] have provided W_{ad} values for some metals on oxides, which are similar to experimentally, measured values based on Equation *2.5*.

2.2.4. The Formation of Metal-Ceramic Interfaces

The driving force for the formation of an interface between materials is the energy decrease of the system resulting from its establishment. The interfacial energy should reach the lowest achievable value as the bond is formed, otherwise further changes that could degrade the stability of the bond may occur under operating conditions. Interaction between the ceramic and the metal requires the surfaces to be in direct intimate contact, and hence the surfaces must be free of contaminants. Thus the atmosphere is important in achieving the maximum energy decrease. In practice, formation processes are usually carried out at elevated temperatures so that the rates of interaction are rapid. Solid state bonding involves heating the system under an applied mechanical load to establish contact between the materials. In this process the formation of a continuous interface is mainly determined by the surface quality of the ceramic. Surface irregularities introduced by machining or due to grain boundaries hamper the formation of a continuous interface.

Increasing the load will increase the contact area, however, the plastically flowing metal cannot fill sharp grooves completely because of opposing metal surface energy effects. Even if the plastic deformation is extremely large, pores will be left at the interface. As long as the diffusion coefficient of the ceramic is much lower than that of the metal, the ceramic does not make a significant contribution to the process. Interface pores can only be eliminated by transport of matter.

Solid-state bonding can produce a stable interfacial structure at high temperature. A high pressure and temperature are necessary, however, for a good contact between the surfaces of metal and ceramic. Under this condition the metal deforms first to make the contact between both surfaces complete. Next, the metal at the interface recrystallizes to produce a coherent interface (epitaxial interface) or a chemical reaction occurs between the metal and the ceramic. In the latter case, the species of the metal and the ceramic diffuse into the other side or produce new compounds at the interface. As a result, the interface forms into a laminated structure and new interfaces are created. In addition, diffusion removes voids at the interface, simultaneously nucleating voids at the inner region of the metal by the Kirkendall effect [72]. If gas evolution takes place at the interface as the result of a reaction, the gas may be left as voids or pores at and near the interface. It may be removed by diffusion along the interface or through the metal. When compounds are formed as the result of the chemical reaction at the metal-ceramic interface, the coherency of the interfaces between the compound and metal and between the compound and ceramic has been investigated only for few conditions. This was from the viewpoint of interfacial energy or crystallography, which is indirectly related to the bond strength of the joint.

The main process parameters in diffusion bonding are temperature, time and pressure. Temperature is, however, the most important one due to the fact that: *(i)* in thermally activated processes, a small change in temperature will result in the greatest change in process kinetics (diffusion, creep) compared with other parameters; and *(ii)* virtually all mechanisms in diffusion bonding are sensitive to temperature (plastic deformation, diffusion, creep). On joining of metals to silicon nitride (Si_3N_4), an additional difficulty is introduced by the presence of nitrogen gas at the interface. Nitrogen gas is formed upon the dissociation of Si_3N_4, and it may or may not diffuse into the metal, depending on its solubility at the bonding temperature. The nitrogen solubilities of nickel (Ni), molybdenum (Mo), cobalt (Co) and tungsten (W) are too small to occlude the nitrogen gas. As a result, voids are observed as defects in the vicinity of the interface. In order to prevent this, it is desirable for the metals to be strong nitride forming elements such as zirconium (Zr), titanium (Ti), niobium (Nb) and vanadium (V), which serve to scavenge nitrogen [73].

Many ceramic/metal combinations are classified as reactive systems. Reaction products are generally brittle. As the layer of these products become thicker, the bond strength, at first, increases and reaches its maximum at a specific thickness, and then decreases. Therefore, the reaction products are to be controlled in thickness to enhance bond strength. In diffusion bonding, sufficient strength is provided by elemental interdiffusion resulting in chemical reactions. Hence, the formation of a reaction zone will take place. The thickness of an interfacial reaction zone, as a function of temperature, T, and time, t, can be expressed by [74]:

$$x = K_p \cdot t^n \qquad (2.7)$$

where: x is the thickness of the reaction layer,

K_p is the coefficient of penetration,

t is the bonding time.

The temperature term is implicit in the coefficient of penetration, which follows an Arrhenius-type relationship:

$$K_p = K_0 \exp(-Q / R T) \qquad (2.8)$$

where: K_0, is the pre-exponential factor,

Q is the activation energy for growth of the interface,

R is the gas constant,

T is the absolute temperature.

The rate constant, K_0, in equation *(2.8)* contains the frequency factor of atomic migration at the interface.

Reaction products of the reactive ceramic/metal combinations grow parabolically with time, following Fick's law with n equal to *0.5* in equation *(2.7)*. However, occasionally it has been reported that the parabolic law is not followed. For example, Figure 2.17 shows that the growth rate of reaction layers in Fe-SiC couples becomes extremely large at high temperatures [75]. This has been attributed to the large solubilities of carbon and silicon in iron.

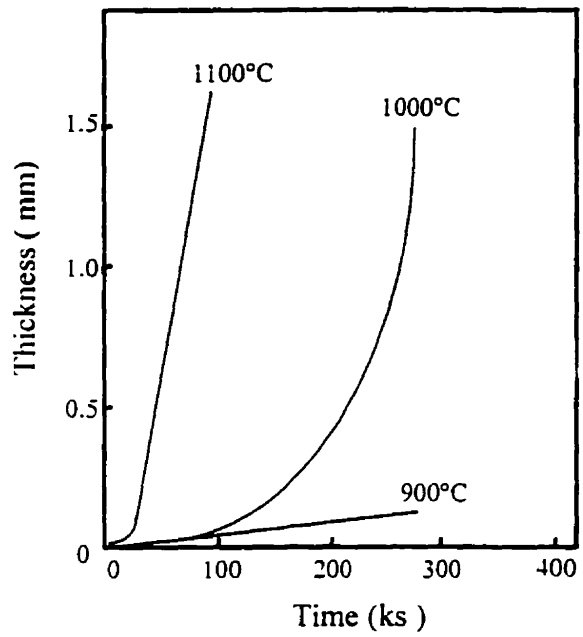

Figure 2.17. Changes in thickness of reaction layers in Fe-SiC couples as a function of time, for different temperatures [75].

2.2.5. The Si_3N_4 - Ti System

Chemical reactions at the metal/ceramic interface are the key factor in adherence since they decrease further the energy of the ceramic/metal system once intimate contact is established and physical interaction has occurred. Chemical descriptions of bonding processes should be in terms of irreversible thermodynamics, but the requirement of data makes this approach impractical. The kinetics of the reaction has to be determined experimentally, but guidance as to the nature of the reactions can be derived from equilibrium thermodynamic data. The driving force for the reaction is the chemical potential of the species involved, which

causes charge transport across the interface. Usually, but not always, mass transport also occurs, which can lead to the formation of interfacial layers.

When metals and ceramics are in contact with each other at high temperature, chemical reactions will often take place, leading to new phases. Sometimes only solid solutions will develop by diffusion of constituents from the ceramic in the metal. Often the isothermal cross-section through the phase diagram allows us to predict what actually will happen in such a system if thermodynamic equilibrium at the interfaces is assumed; however the relative mobilities may also be of importance. Heat of formation, ΔH_f, or free energy of formation, ΔG_f, data has commonly been used to predict the behavior of the compounds when various solids and gases are present. Using Ellingham diagrams, a first indication can be obtained as to whether a metal in contact with a ceramic will react with its non-metallic component. It also follows the relative positions of the lines in the diagram it is possible determine if an oxide for example, can be reduced by a metal, or which of the compounds is the most thermodynamically stable.

This analysis and the ability of metals to dissolve the metallic and non-metallic components of a ceramic form the basis of metal/ceramic joining by chemical reactions. Thus the study of phase diagrams of metal/ceramic systems is essential to understanding joining processes. The use of equilibrium thermodynamic data in a ceramic/metal reaction can be illustrated by reference to the Si_3N_4-Ti system in a low-pressure environment. The Ellingham diagram for some nitrides is shown in Figure 2.18 [76].

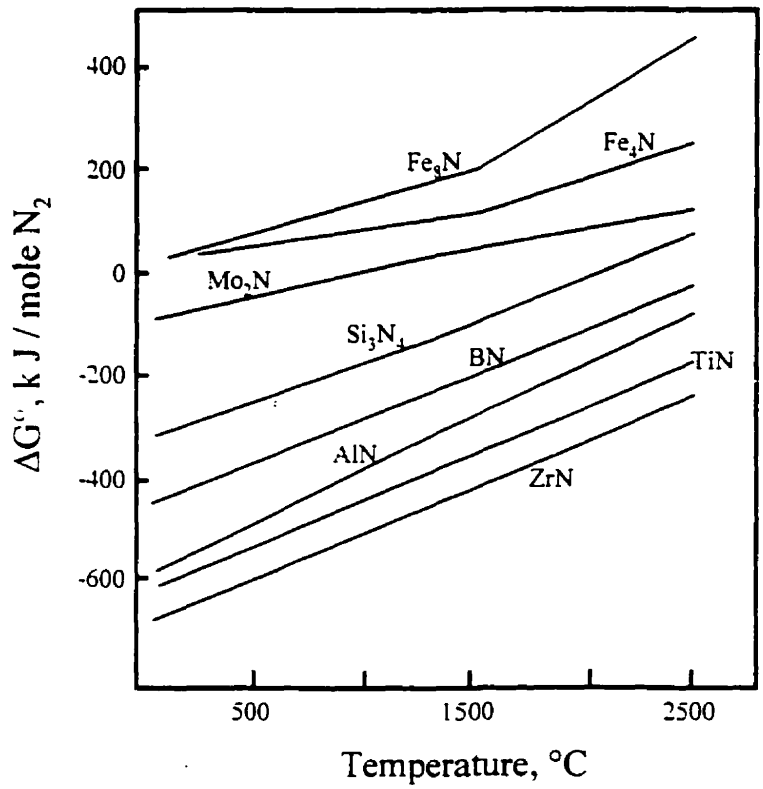

Figure 2.18. The standard free energy of formation of nitrides per g-mole nitrogen, gas [76].

The free energy of formation of Si_3N_4 and of TiN per mole N_2 can be represented by the equations:

$$\Delta G°_F(Si_3N_4) = -396480 + 206.64\,T \qquad (2.9)$$

$$\Delta G°_F(TiN) = -679140 + 191.52\,T \qquad (2.10)$$

Comparison with the free energy of oxide formation for silicon and titanium represented by the equations:

$$\Delta G°_F(SiO_2) = -873600 + 178.08\,T \qquad (2.11)$$

$$\Delta G°_F(TiO_2) = -911400 + 176.82\,T \qquad (2.12)$$

show that the nitrides are less stable. This implies that the oxygen partial pressure in the reaction environment should be extremely low to prevent the Si_3N_4 and titanium from oxidizing. Equations *(2.9)* and *(2.10)* show that Si_3N_4 is less stable than TiN, and so TiN will form when titanium is in contact with Si_3N_4 and the silicon liberated will react to form titanium silicides.

2.2.6. Titanium Silicides

The equilibrium solid phases of the Ti-Si system are shown in the phase diagram illustrated in Figure 2.19 [77]. The transformation of the initial *α-Ti* to *β-Ti* occurs approximately at 865°C. The melting point of pure titanium is established as 1670°C. The solubility of silicon in titanium increases as the temperature increases, until it reaches approximately 0.5 at. % in α-Ti and 3.5 at. % in β-Ti at 1330°C. Two eutectic points have been observed in the Ti-Si system at 1330°C corresponding to 13.5 at. % Si, and another corresponding to 83.8 at. % Si. A third eutectic point has been observed, at 1480°C corresponding to 64.2 at. % Si. Some properties of the three titanium silicides and titanium nitride are shown in Table 2.3 [78].

Similarly a section through the ternary phase diagram calculated for the Ti-Si-N system at temperatures between 700°C to 1000°C and illustrated in the Figure 2.20 shows that Si_3N_4 is only stable in the presence of TiN [79]. Free Si, according to the ternary phase diagram, is a thermodynamically stable decomposition product of the Ti/Si_3N_4 reaction.

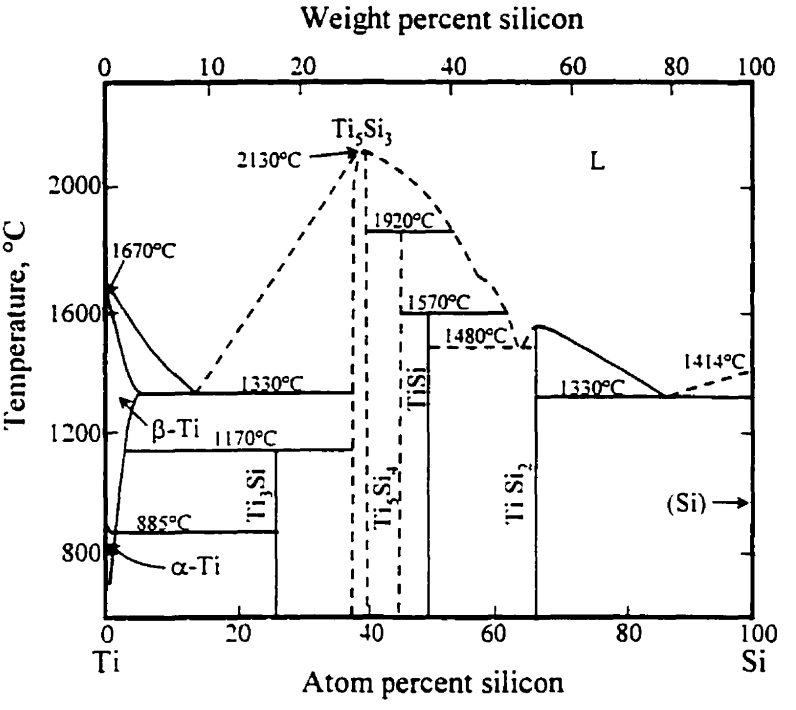

Figure 2.19. Ti-Si phase diagram [77].

Table 2.3. Properties of titanium silicides and nitride [78].

	Ti_5Si_3	TiSi	$TiSi_2$	TiN
Structure	Hexagonal	Orthorhombic	Orthorhombic	Cubic
CTE ($°C^{-1}$. 10^{-6})	11 (170-1070°C)	8.8 (170 - 370°C) 10.4 (370-1070°C)	8.9 (200-1200°C)	9.35 (25-1100°C)
Density (x-ray)	4.36 g/cm^3	4.24 g/cm^3	3.85 g/cm^3	5.44 g/cm^3
Melting Point	2130°C	1570°C	1480°C	2950°C

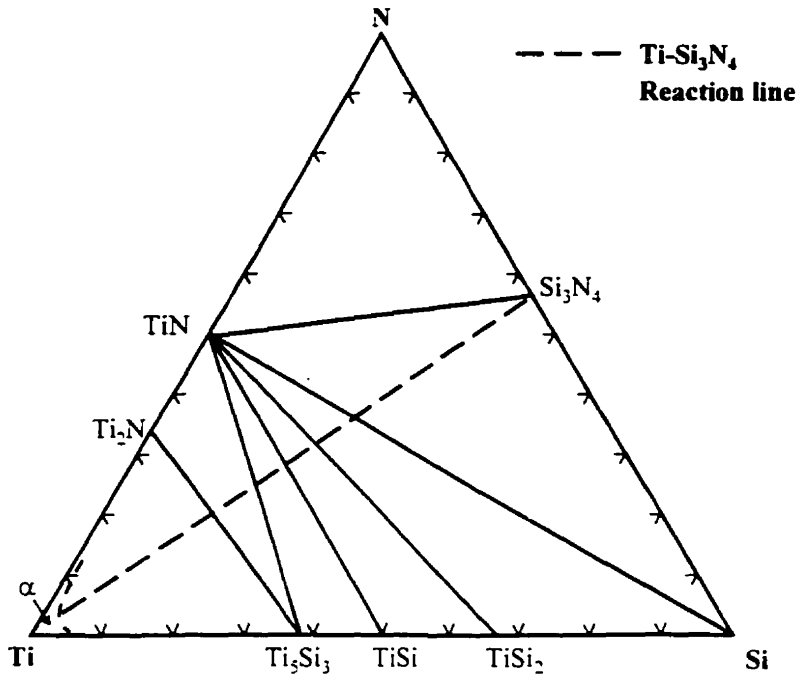

Figure 2.20. Section through the ternary Ti-Si-N phase diagram at temperatures between 700°C to 1000°C [79].

The tie lines remain the same in the temperature range of 700-1000°C. On joining of Ti-Si_3N_4 system, an additional difficulty is introduced by the presence of nitrogen gas at the interface. Nitrogen gas is formed upon the dissociation of Si_3N_4, and it may diffuse into the metal, depending on its solubility at the bonding temperature. This means that the behavior of the system has to be considered for non-standard conditions.

As already mentioned, equilibrium thermodynamics are only useful for determining the conditions in which a ceramic/metal system can react, but they do not say anything about the reaction kinetics. These have to be determined experimentally by using available

data on the diffusion of the ceramic species into the metal. The formation of non-metallic or intermetallic compounds should be prevented as far as possible because these compounds almost always have a detrimental effect on the mechanical properties of the ceramic/metal joint.

2.3. Metal/Ceramic Joint Evaluation

It is important to distinguish between joints made between *similar* materials, whether they be metals, ceramics, composites, and joints which involve interfaces between *dissimilar* materials, e.g. metal bonded to ceramic, glass or ceramic bonded to glass. In the case of *dissimilar* materials, the engineering compatibility of the two components must be considered. Mismatch of the elastic modulus is a common form of mechanical incompatibility, which leads to stress concentrations and stress discontinuities at the bonded interface between the two materials. Figure 2.21 shows an example in which, a normal load is transferred across the interface between two materials with different elastic modulus [80, 81]. The stiffer, higher modulus, component restricts the lateral contraction of the more compliant, lower modulus, component, and generating shear stresses at the interface that may lead to debonding.

Thermal expansion mismatch represents a lack of physical compatibility and is a common problem in metal/ceramic joints. Thermal expansion mismatch leads to the development of thermal stresses which, tend to be localized in the joint and reduce its load-

carrying capacity, ultimately leading to failure of the component. Poor chemical compatibility is commonly associated with undesirable chemical reaction in the region of the joint. Chemical reactivity between the components may lead to undesirable interface reactions and the products of these reactions are often brittle. Reactions accompanied by a volume change generate local stresses and the mechanical integrity of the joint will be threatened. Thermal expansion mismatch has a great influence not only on the absolute value of strength but also on the reliability of joints.

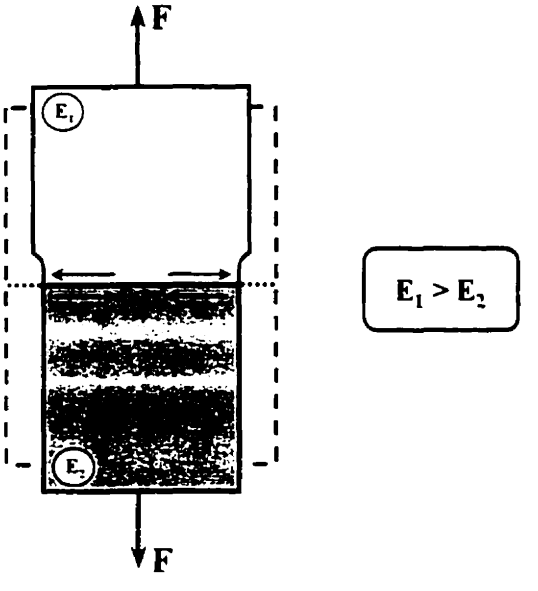

Figure 2.21. Mismatch in the elastic modulus of bonded components results in elastic constraint, which generates shear stresses parallel to the interface under normal loading conditions [80].

A large thermal stress increases the scatter of joint strength because of the presence of defects induced during the joining process. One should insert an appropriate interlayer

to relax the stress between a ceramic and a metal. Surface roughness also has some influence on the reliability, a roughly ground bond surface leads to scatter in strength and scratches must be removed before joining. The reliability of a ceramic/metal joint structure has not been surveyed consistently yet, because most ceramic/metal joints fracture in a quite brittle manner.

2.3.1. Problems of Joining Ceramics to Metals

Factors influencing the reliability of a joint can be classified into several categories. Figure 2.22 shows the schematic illustration of several important defect categories, which may cause scatter in strength directly [82]. From the microscopic view, the reaction structure caused by wetting or by chemical and physical bond-ability between two faces may be of concern.

These factors will reflect the distribution of unjoined or weakly bonded island-like defects on interfaces resulting in substantial reduction in joint strength. Unjoined areas reduce joint strength especially in solid-state joining. From the more macroscopic view, when a reaction layer grows thick, cracking in the layer frequently influences joint strength to a great extent. Thermal or residual stress in a joint becomes another important factor. The final goal for joining research will be in establishing a technique producing a tightly bound interface by eliminating these defects and by accommodating thermal stress. The development of residual stresses at the interface when the material is cooled down from the

bonding temperature to room temperature is one of the major problems in ceramic/metal joining. These residual stresses reduce the strength of the bonded material, and in some cases lead to joint failure during or after the joining process.

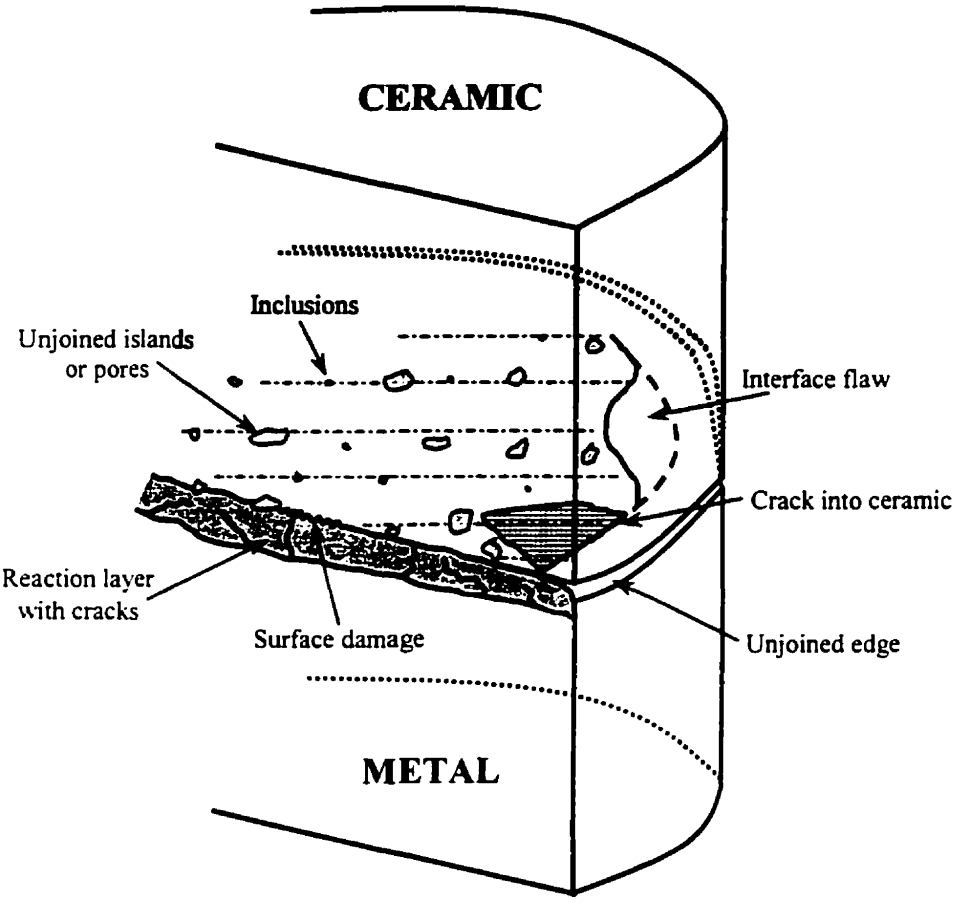

Figure 2.22. Schematic illustration of various defect structures in ceramic/metal joint [82].

The thermal stress may be relieved by two different methods. One method inserts a metal with approximately the same thermal expansion coefficient as that of the ceramic to decrease the magnitude of thermal stress generated, while the other method involves thermal stress relief by using a ductile metal that easily develops plastic deformation under thermal stress [83, 84]. These two methods may also be employed in combination. Figure 2.23 shows a schematic illustration of thermal stress at a joint interface and the mode of cracking due to difference of thermal expansion coefficient [85, 86]. When the thermal expansion coefficient, α_C, of the ceramic is smaller than that of the metal, α_M; the ceramic is subjected to tension stress and cracks at the edges, as schematically illustrated in Figure 2.23a: on the other hand, when the thermal expansion coefficient, α_M, of the metal is smaller than that of the ceramic, α_C; tensile stress acts on the core of the ceramic and cracks the ceramic, not at the edges, but transversely at the core, as shown in Figure 2.23b.

The amount and distribution of residual stresses in a ceramic/metal joint depends on parameters such as the coefficient of thermal expansion *(CTE)* and elastic modulus of the metal and ceramic. Geometry of the joint, bonding temperature, and thickness of reaction layers also have an important influence [87, 88].

High concentrations of residual stresses are generally found close to the interface and to the free surface. In cylindrical samples, the amplitude of stresses increases with the diameter of the joint. For rectangular samples, the corners of the joint faces act as point of high stress concentration. Careful design along with proper selection of joining materials for intended applications can alleviate the residual stresses developed during joining.

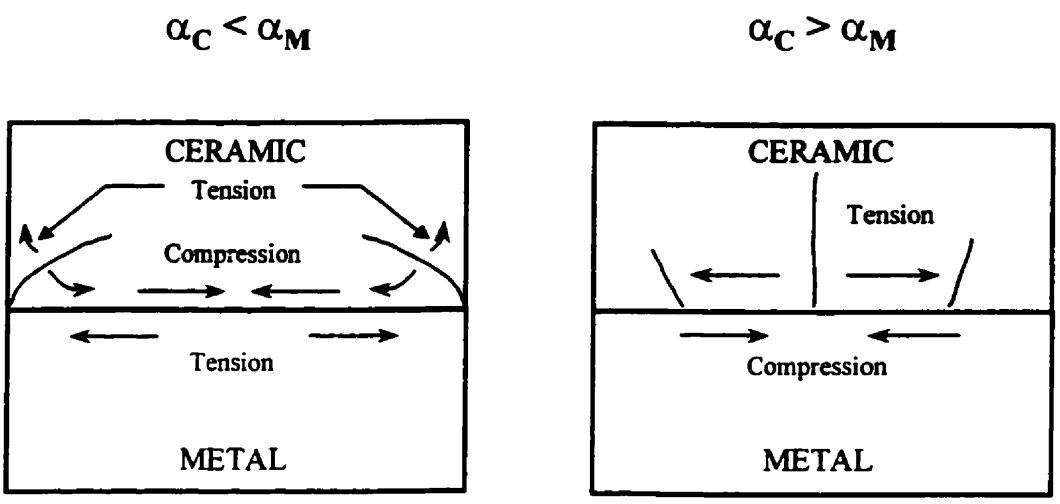

a) Edge cracks in ceramic **b) Core cracks in ceramic**

Figure 2.23. Schematic illustration of thermal stress in joint interface and mode of cracking due to difference of thermal expansion coefficient [85, 86].

2.3.2. Mechanical Evaluation of the Joint

As the use of advanced ceramic materials for critical structural components increases, reliability in ceramic/metal joints becomes a critical issue. Ensuring reliable performance in a ceramic/metal joint means being able to predict with a high degree of certainty whether a component will fail under typical operating conditions. This requires an accurate description of the stresses likely to be encountered in service, as well as knowledge of the mechanical properties of the joint. There are a variety of different properties to be considered in the ceramic/metal joints, e.g. mechanical, electrical, thermal properties, etc. Depending on the application of the joint, some properties are more

important than others. However, the mechanical properties are some of the most important properties for any joint. Joints without any mechanical strength can be regarded as unsuccessful joints. A description of the mechanical behavior of ceramic-metal joints requires the determination of their strength along with the distribution of residual thermal stresses. For the evaluation of the joint properties, it is essential to establish proper testing methods so that effects of the processing can be detected accurately and consistently [89, 90].

In the production of metal/ceramic joints, the required strength of the joints is an important criterion in the selection of an appropriate joining technique. In contrast to homogeneous materials, such as steels or other metals, the strength of the joint is not a material-specific parameter, which can be found in reference books, but is influenced considerably by the following factors [91, 92]:

- *The selection and mechanical properties of the individual joint partner materials.*
- *Differences in the thermal expansion coefficients of the partner materials.*
- *Selection of the joining technique.*
- *Interface reactions between the joining partners.*
- *The design of the joining geometry.*

By the selection of the materials to be joined, the material specific constants like Young's modulus and thermal expansion coefficient are determined. The resulting strength of the joint depends to a large extent on the preparation of the materials and the joining technique. Diffusion processes between solid materials can also affect bonding of materials. With this technique the polished surfaces of the material partners are brought into contact under the application of pressure, they are then heated to a high temperature just below the lowest melting point of the two material partners. The materials are kept at

this temperature for a specific time and then cooled very slowly. In order to determine the success of the respective joining technique and the joining parameters used, and the reproducibility of the joining technique, the strength of the joint must be tested [93]. Strength is one of the critical properties for structural applications. Although there is an *ASTM* standard (tensile test), for the metal/metal joints, most of researchers have used their own method for the evaluation of the ceramic/metal joint strength. Because the normal *ASTM* method requires complex shape tensile specimen, an alternative test method needed to be established. The mechanical characterization of a metal/ceramic joint is a complex problem. Even if there are no residual stresses from the bonding process, the difference in elastic properties on each side of a metal/ceramic joint will lead to interfacial stress concentrations in the absence of a defect. Once a crack is initiated and failure commences the different strain energy release rates in the metal and ceramic components can lead to deflections of the crack away from the interface. Therefore it may be necessary to adopt a component-based approach to bond strength analysis where many factors of design, and not just the mechanical properties of the bond, are considered. Several methods have been used to measure joint strength. At present, the most common methods include tensile, bending or flexural and shear tests, where the stress to fracture the bonded surfaces is used to characterize the joint strength [94, 95]. The schematics of various tests methods of joint strength are shown in Figure 2.24. Tensile tests are generally performed in double joint specimens, ceramic/metal/ceramic, whereas three-point and four-point bending can be performed in both single and double joints. Shear tests can only be performed on single joints as a consequence of their intrinsic geometry.

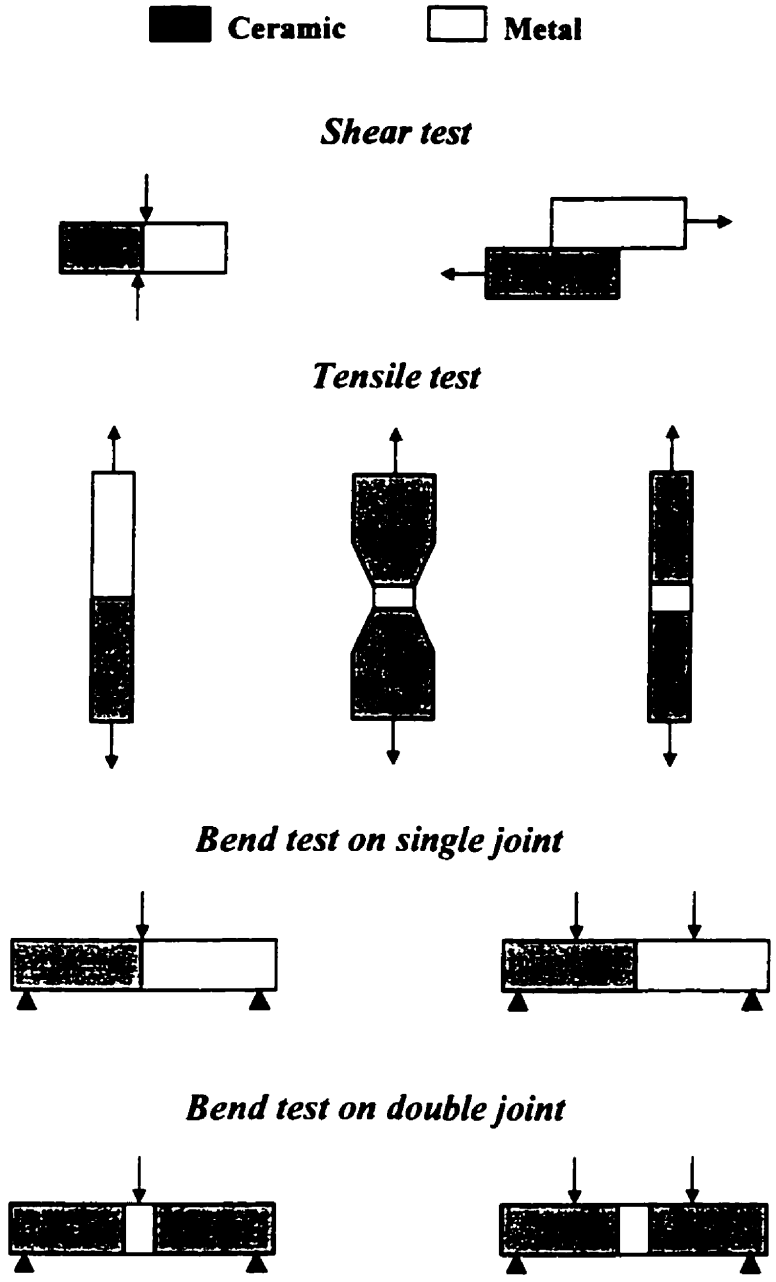

Figure 2.24. Schematics of various mechanical tests methods performed on ceramic/metal joints [94, 95].

The characterization of the interfacial strength by pull-off or shear-off tests has several limitations. The first one is related to the variety of techniques used by different research groups, making it difficult to establish a mutual comparison of results. The shear test provides an alternative way to assess the mechanical strength of interfaces. Samples are easily produced, but the results are generally lower than those obtained for bend and tensile tests. The selection of an appropriate method for measuring the bond strength is dictated by the purpose of testing, but the bonding process and parameters affecting the mechanical quality of the bond can be monitored by both fracture mechanics and conventional testing methods. The bond strength values obtained also depend on the testing technique chosen. Bend test values are generally higher than tensile test values for joints and for brittle ceramic materials. The shear test is one of the simplest methods. However, the shear stress at the interface is not simple shear and it always contains a component of tensile stress that originates from a bending moment, which cannot be neglected. The influence of a slight change of the push position and the fixing condition on the stress distribution is very important. Therefore, the shear test is not recommended for the common evaluation method. Bending and tensile test have almost the same stress distributions as those derived from analytical equations. However, the elastic constant mismatch between ceramics and metal induces inhomogeneity in stress distribution [96].

The tensile test requires a careful preparation of test specimen and a strict alignment of the load train. These difficulties in testing will influence the reproducibility of the strength measurements. On the contrary, bending tests have greater flexibility compared to the tensile test. However, in the case where plastic deformation occurs in the

metal the analytical equation for bending stress becomes complicated. Figure 2.25 shows a schematic comparison of the tensile stress distribution for three-point, four-point and uniaxial tensile test specimens [97].

In the case of three-point bending the peak stress occurs only along a single line on the surface of the test bar opposite the point of loading. The tensile stress decreases linearly along the length of the bar into the thickness of the bar, reaching zero at each bottom support and at the neutral axis, respectively. The probability of the largest flaw in the specimen being at the surface along the line of peak tensile stress is very low. Therefore, the specimen will fracture at either a flaw smaller than the largest flaw or a region of lower stress. Four-point bend testing results in lower strength values for a given ceramic material than does three-point bending. The peak for the stress distribution in a four-point bend specimen is present over the area of the tensile face between the load points. The tensile stress decreases linearly from the surface to zero at the neutral axis and from the load point to zero at the bottom supports. The area and volume under peak tensile stress or near peak tensile stress is much greater for four-point bending than for three-point bending, and thus the probability of a larger flaw being exposed to high stress is increased. As a result, the modulus of rupture or bend strength measured in four-point is lower than that measured in three-point. Uniaxial tensile strength results in lower strength values for a given ceramic than does bend testing. Figure 2.25 illustrates that in the case of uniaxial tension the complete volume of the gauge section of a tensile test specimen is exposed to the peak tensile stress. Therefore, the largest flaw in this volume will be the critical flaw and will result in fracture.

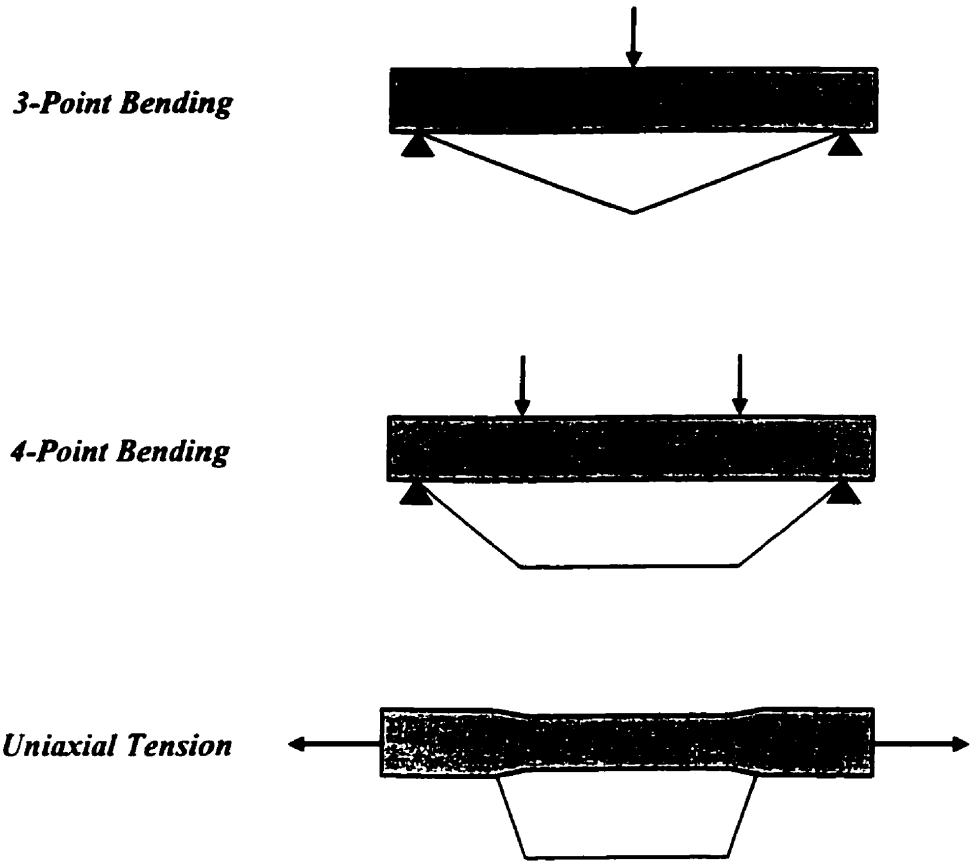

Figure 2.25. Comparison of the tensile stress distributions for three-point, four-point, and uniaxial tensile test specimens. Shaded area represents the tensile stress, ranging from zero at each support of the bend specimens to maximum at midspan, and being uniformly maximum along the whole gauge length of the tensile specimen [97].

The strength of metal/ceramic joints materials is generally characterized by bend testing, also referred to as flexure testing. The test specimen can have a circular, square, or rectangular cross section and is uniform along the complete length. As shown in Figure 2.24, the test specimen is supported near the ends and the load is applied either at the center, for three-point loading, or at two positions for four-point loading.

Three-point bending

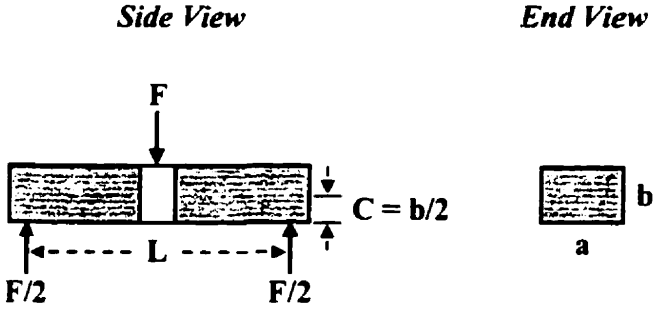

Four-point bending

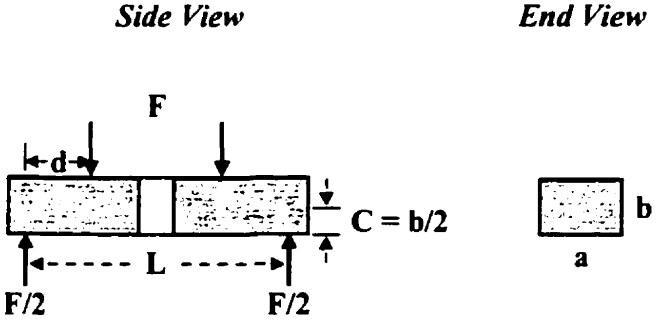

Figure 2.26. Derivation of the modulus of rupture equation for three-point and four-point bending.

The bend strength is defined as the maximum tensile stress at failure and is often referred to as the *modulus of rupture (MOR)*. The bend strength for a rectangular test specimen can be calculated using the general flexure stress formula:

$$S = M.C / I \qquad (2.13)$$

where M is the moment, C the distance from the neutral axis to the tensile surface, and I the moment of inertia.

For a rectangular test specimen:

$$I = a.b^3 / 12 \qquad (2.13)$$

and

$$C = b / 2 \qquad (2.14)$$

where b is the thickness and a is the width of the specimen [97, 98].

From Figure 2.26, it is possible to illustrate the derivation of the three-point and four-point flexure formulas for rectangular bars. We can observe that; $M = (L / 2).(F / 2)$ in the case of three-point and $M = (F / 2).d$ for four-point test. Therefore, for three-point bending:

$$S = \sigma_{3\text{-}pt} = 3.F.L / 2.a.b^2 \qquad (2.15)$$

and for four-point bending test:

$$S = \sigma_{4\text{-}pt} = 3.F.d / a.b^2 \qquad (2.16)$$

For most ceramic materials, the apparent strength will decrease when going from three-point to four-point to tensile testing and as specimen size increases.

Chapter 3:

Objectives

In order to assess the potential and functionality of a given specific ceramic/metal combination for structural applications, the physical and mechanical properties of the joining materials are an important aspect. However, it is also important to understand the mechanisms of interface formation between the metal and ceramic. In particular, the Si_3N_4/Ti is a reactive system, and the presence of an interface reaction layer may affect the final properties of the joint.

Some investigations have studied the interaction of Ti powder and joining of Ti-alloys with Si_3N_4, however no work has addressed the use of commercially pure Ti for joining of Si_3N_4. From the above, this research is focused on the study of some of the aspects of joining Si_3N_4 to Ti by diffusion bonding at high temperature, using the hot-uniaxial pressing technique.

In summary, the main objective of this study is the fabrication, characterization, and evaluation of hot-pressed Si_3N_4/Ti diffusion joints.

Other objectives of this work are focused on the study of the interfacial reaction of the ceramic/metal interface and to compare the results with thermodynamic analysis carried out for the Si_3N_4/Ti system. As well as:

i) Study the possible use of a Ti interlayer during hot-pressing of Si_3N_4/Si_3N_4 joints through diffusion bonding.

ii) Evaluate the effect of the surfaces roughness and sample preparation on joining as well as characterization of the resulting interfacial reaction.

iii) Optimize the process parameters in terms of time, temperature, and pressure in order to obtain a desirable joint.

iv) Assess the mechanical properties of the joints and correlate the results with the interface microstructure.

Chapter 4:

Experimental Methodology

This chapter presents the characterization of the starting materials used in this work, as well as the description and operation of the equipments used in the preparation of the diffusion samples. A short description of the elements of the F*A*C*T* program used in the thermodynamic analysis is presented, as well as the various techniques employed in the characterization and evaluation of the bonded materials.

4.1. Starting Materials

The starting materials used in the preparation of the diffusion samples in this work were Si_3N_4 Ceralloy 147-31N *(Ceradyne Inc, Costa Mesa, CA, USA)* and commercially pure Ti-rod and Ti-foil, 99.7%, *(AESAR Division Johnson & Matthey, Toronto, Canada)*. The original rods were cut into small blocks of cylindrical geometry with thickness of 3 mm and diameter of the supplied rods *(12.7 mm for Ti and 14.2 mm for Si_3N_4)*, the

thickness of the foil was of 0.89 mm. The Si_3N_4 used in this work was hot-pressed β-Si_3N_4 *(HPSN)* using Al_2O_3 and Y_2O_3 as additives. The material had been produced by hot pressing the Si_3N_4 powder plus additives in a graphite die at temperatures between 1700 and 1800°C, using a boron nitride *(BN)* powder protection. The final product is a high strength material, which achieved a density >99.5% of the theoretical density. Table 4.1 contains some physical and mechanical properties of this material [99].

A sample of Ceralloy 147-31N Si_3N_4 was fractured and cleaned with isopropanol in an ultrasonic bath for 5 minutes and etched using hydrofluoric acid *(HF)* for 25 minutes. Figure 4.1 shows a fracture surface of a dense Ceralloy Si_3N_4 sample and illustrates the typical fibrous nature of the microstructure. The elongated grain structure of the β-Si_3N_4 phase can be observed, which has a strong influence on the mechanical properties of the material.

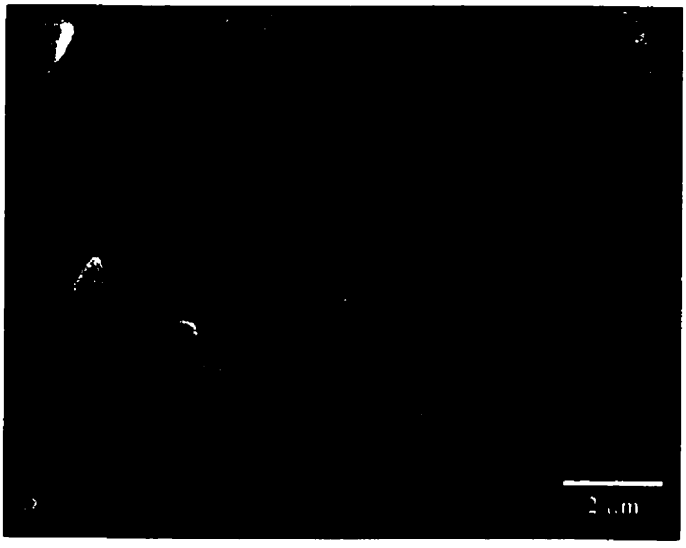

Figure 4.1. Typical microstructure of Ceralloy 147-31N Si_3N_4.

Table 4.1. Physical and mechanical properties of Ceralloy 147-31N Si_3N_4.

PROPERTY	SILICON NITRIDE (Si_3N_4)
Decomposition temperature under 1 atm N_2	1900 °C
Density	3.21 g / cm ^{3} (99.5% of theoretical density)
Coefficient of Thermal Expansion, CTE,	3.1 X 10 $^{-6}$ °C $^{-1}$ (25°C – 1000°C)
Thermal Conductivity	26 W / m . K
Flexural Strength	800 MPa at 25°C 545 MPa at 1200°C 365 MPa at 1400°C
Young' Modulus	310 GPa
Poisson's Ratio	0.27
Vickers Microhardness	18 GPa
Fracture Toughness	5.8 – 6.0 MPa $m^{1/2}$

A sample of Si_3N_4 was also analyzed by X-ray diffraction *(XRD)* and the resulting spectrum is shown in Figure 4.2. The diffraction pattern indicated the presence of β-Si_3N_4, and an additional crystalline phase identified as N-melilite, an intergranular phase often found in Si_3N_4 when Y_2O_3 is used as sintering additive, and having composition $Y_2O_3.Si_3N_4$. Although alumina was also used as a sintering additive, no peaks corresponding to any other compound were found, indicating the possible presence of an amorphous intergranular phase containing both Al_2O_3 and SiO_2.

A collection of properties for the Ti-rod supplied by Johnson & Matthey is shown in Table 4.2 [100]. A sample of Ti was also ground and polished using alumina suspension *(0.05 μm)*, and finished with colloidal silica *(0.06 μm)*.

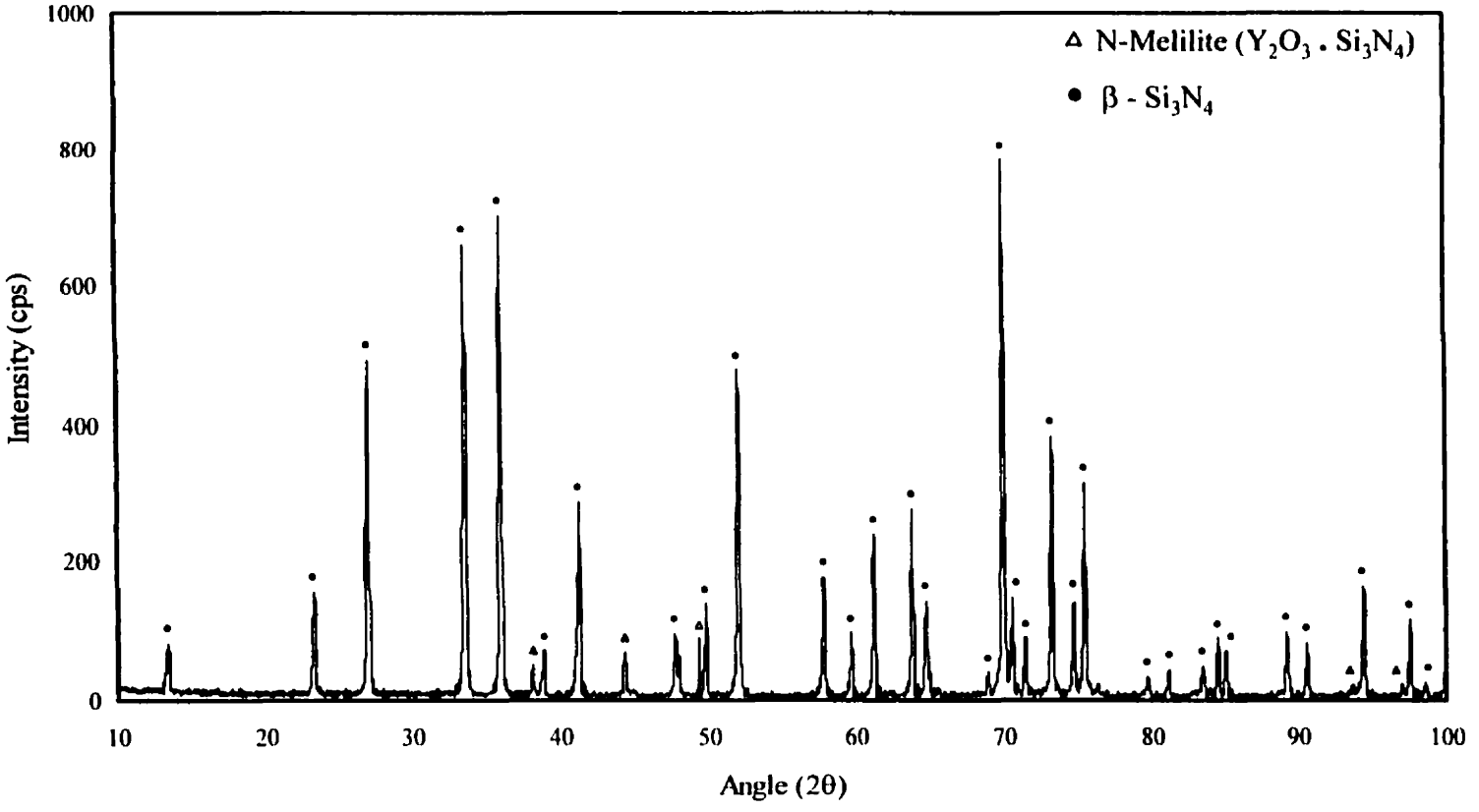

Figure 4.2. XRD pattern of a Ceralloy 147-31N Si_3N_4 sample.

Figure 4.3 shows an optical photograph of a titanium sample etched with Kroll's reagent [101], *(3 ml HF, 6 ml HNO_3, H_2O to 100 ml)*, for 50 seconds. A typical equiaxed titanium microstructure can be observed.

Table 4.2. Physical and mechanical properties of Ti-rod.

PROPERTY	TITANIUM
Melting Point	1668 ± 10 °C
Density	4.51 g / cm ^{3}
Coefficient of Thermal Expansion, CTE	8.64 X 10 $^{-6}$ °C $^{-1}$
Thermal Conductivity	22.4 W / mK at 25°C 20.7 W / mK at 1000°C
Tensile Strength	475 MPa at 25°C
Young' Modulus	102.7 GPa at 25°C
Poisson's Ratio	0.41
Vickers Microhardness	175 kg/mm^2

4.1.1. Sample Preparation

Diffusion bonding processes depend for their success on a combination of factors. One of the most important is the surface roughness of the materials because it controls the initial area of interaction between the diffusion couples.

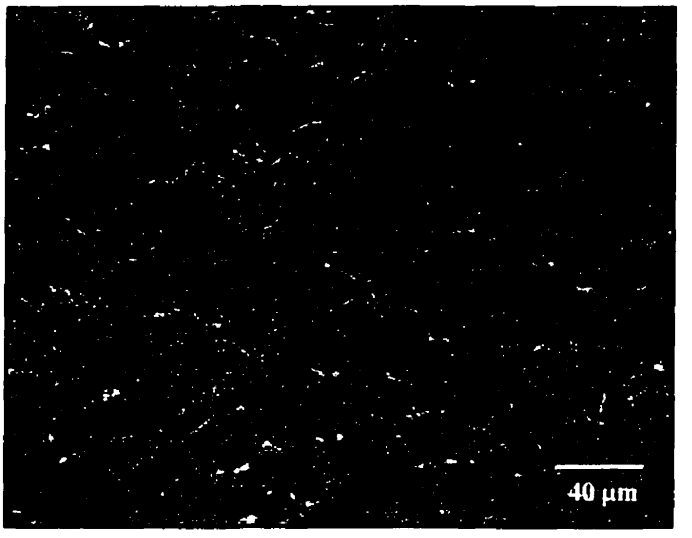

Figure 4.3. Typical microstructure of an etched Ti sample.

The hot-press diffusion bonding experiments started with the preparation of the materials to be joined. Si_3N_4 and Ti were supplied as rods of 14.2 cm and 12.7 cm in diameter, respectively. The original rods were cut into small blocks of cylindrical shape having a thickness of 3 mm and the diameters of the supplied rods, using a diamond blade in a high-speed wafering saw. In order to assure reproducibility of the surface preparation of the samples, an automatic polishing procedure was followed. The surfaces of the samples to be joined were ground using a diamond-grinding disc, following by silicon carbide paper of 400 and 600 grit, under a load of 5 psi *(34.5 kPa)* using a rotation speed of 150 rpm. The polishing step was carried out using a load of 2 psi *(13.8 kPa)* initially with diamond paste and finished with alumina suspension *(0.05 μm)* in the case of Si_3N_4 samples. Colloidal silica *(0.06 μm)* was used in order to provide a final finish to the

titanium samples. In order to study the effect of the surface roughness of the materials to be joined, a series of unpolished samples was prepared. These samples were only ground and used without final polishing. The samples were cleaned with isopropanol in an ultrasonic bath for 5 minutes prior to bonding experiments.

4.2. Thermodynamic Evaluation

A thermodynamic analysis of the Si_3N_4-Ti system was carried out with the aid of a computer program named *F*A*C*T* (Facility for the Analysis of Chemical Thermodynamics). The results obtained from this database were used in conjunction with available literature information, and isothermal cross-sections of Ti-Si-N phase diagrams. *F*A*C*T* is a fully integrated thermochemical database program capable of performing thermodynamic calculations, as well as supplying data and properties of various stoichiometric compounds and binary solutions [102]. The analysis carried out in the present work is based on the routines *EQUILIBRIUM* and *REACTION* to predict the probable product and calculate the standard Gibbs free energy for the formation of Ti-Si-N compounds. The *EQUILIBRIUM* routine determines the chemical species when specified elements or compounds react or partially react to reach a state of chemical equilibrium. The *REACTION* routine calculates changes in extensive thermochemical functions such as enthalpy *(H)*, entropy *(S)*, internal energy *(U)*, and Gibbs free energy *(G)* for a species, a group of species, or for a chemical reaction for a specified change in the state of a system.

The temperature, hydrostatic pressure, phase and activity of each species may also be specified. The determination of most stable phase is based on the one with the lowest Gibbs energy. The standard Gibbs free energy *($\Delta G°$)* for the formation of Si_3N_4 was obtained and plotted along with $\Delta G°$ for the formation of Ti-Si (Ti_5Si_3, TiSi, $TiSi_2$), and Ti-N (TiN) compounds for the Ti-Si-N system. Temperatures up to 1800°C were investigated and a hydrostatic pressure of *20 Pa (2 X 10^{-4} atm)* was used in order to simulate typical vacuum conditions. The values of ΔG were normalized for *1 mol* of Si_3N_4, *i.e.*, the formation of any reaction product corresponding to the decomposition of the same amount of Si_3N_4.

4.3. Joining Experiments

Joining experiments started with the preparation of the diffusion couples as described in 4.1.1. The diffusion samples consisted of a block of Si_3N_4 mounted axially with a block of Ti, in the case of single samples. Sandwich samples consisted of two blocks of Si_3N_4 samples mounted axially with Ti-foil between.

The hot-press used to join the diffusion couples consisted of a hydraulic press combined with a graphite resistance furnace as depicted in Figure 4.4. The pressure applied to the sample during the hot-pressing was monitored by a load cell placed underneath the furnace (Figure 4.4). The load cell generates an output voltage signal that is sent to an *OMEGA DP-80* digital display. Calibration of the load cell is necessary periodically against the *ENERPAC* gauge and maintains a precision of 5 % of the nominal applied load.

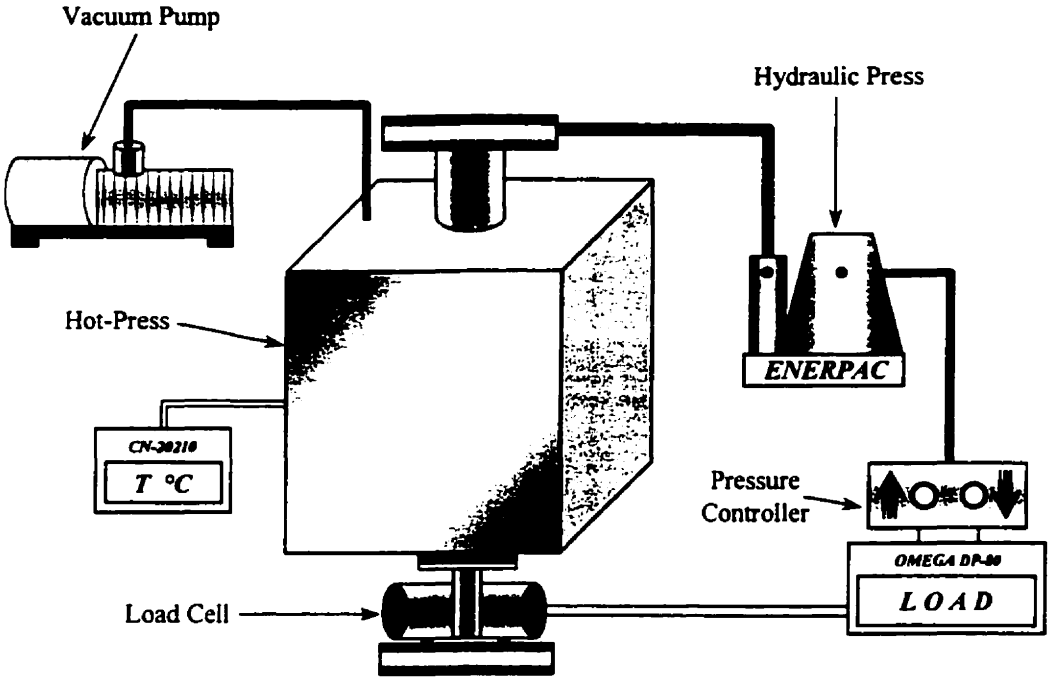

Figure 4.4. Experimental apparatus used during the Si_3N_4/Ti joining experiments.

Figure 4.5 shows a schematic representation of the sample assembly and a front view of the hot-press chamber. Individual samples were inserted in a graphite die and embedded in 99.5% pure *BN* (boron nitride) powder *(Johnson & Matthey, Toronto, Canada)*. The purpose of the powder-bed was to avoid contact between the sample and the internal walls of the graphite die, and to aid in the distribution of the hydraulic pressure applied to the sample. The graphite die containing the sample was then placed in-line with the remaining graphite punches.

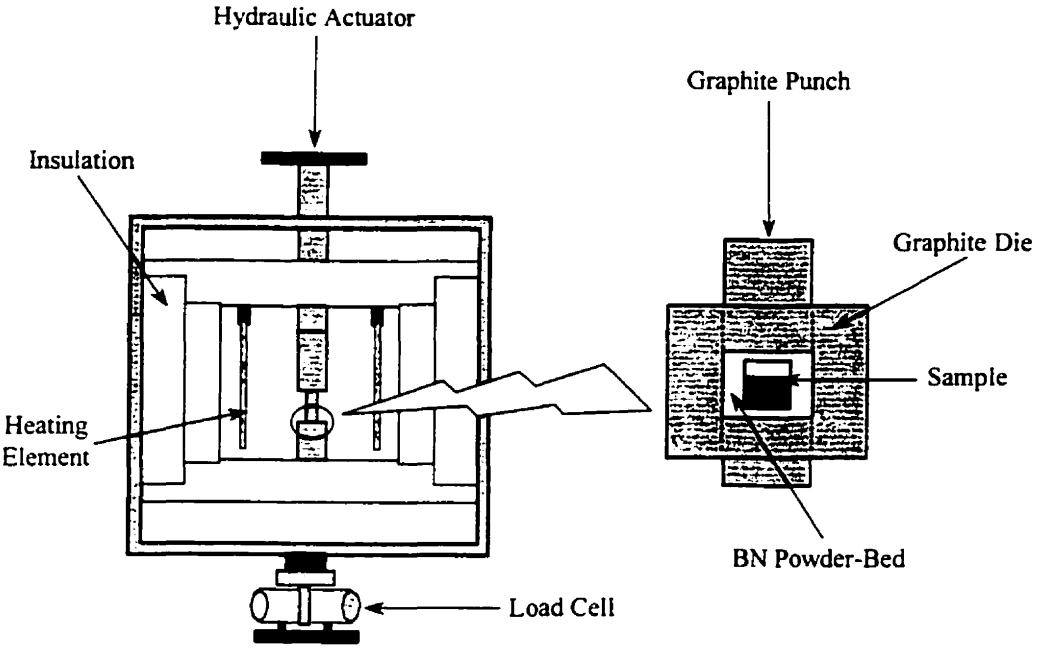

Figure 4.5. Schematic representation of the front view of the hot-press chamber.

The sample holder and punches used to apply the uniaxial load to the sample during the experiments were manufactured from high strength graphite grade *AQ-30 (Speer Canada)* used especially for hot-pressing applications. Some of the properties of this material are [103]: compressive strength of *98.5 MPa*, thermal conductivity of *105 W/m.K*, coefficient of thermal expansion of 3.5×10^{-6} $°C^{-1}$, and density 1.75 g/cm^3.

The joining temperature was measured using a two colors infrared pyrometer *MIKRON M-600*, which eliminates immiscibility problems, inserted at the back of the furnace and is shown in Figure 4.6. The target tube consists of a glassy graphite cylinder

connected to a fiber-optic lens assembly. When the temperature increases the target tube glows, and the fiber-optic send an infrared signal to a control box, where an output voltage signal is generated, simulating a type-C thermocouple, which is sent to a programmable temperature controller *OMEGA CN2021* as shown Figure 4.4. The pyrometer was periodically calibrated against a type-C thermocouple *(Tungsten-5% Rhenium / Tungsten-26 % Rhenium)*, placed in contact with the sample. The testing temperature was within a range of 6°C of the nominal value. Two graphite elements were used for heating, and graphite fiber insulators surrounded the hot zone.

Once the sample was assembled in the graphite die, it was positioned in the furnace and it was closed and evacuated to a pressure of 2×10^{-4} atm (20 Pa), at room temperature. After the joining environment was established, the furnace was heated up to the preset joining temperature at a rate of 15°C/min. When the temperature in the furnace was 10°C lower than the set point, the load was carefully applied and monitored by the load cell positioned at the bottom of the furnace. The temperature and pressure profiles followed during the joining experiments are shown in Figure 4.7.

Joining experiments were carried out for temperatures ranging from 1200°C to 1500°C for holding times varying from 30 minutes to 3 hours. After the holding time elapsed, the sample was cooled at a rate of 5 °C/min until 900°C, i.e. below the phase transformation temperature of the titanium, followed by furnace cooling for the remainder of the cycle. The applied load was carefully removed during the initial stages of cooling.

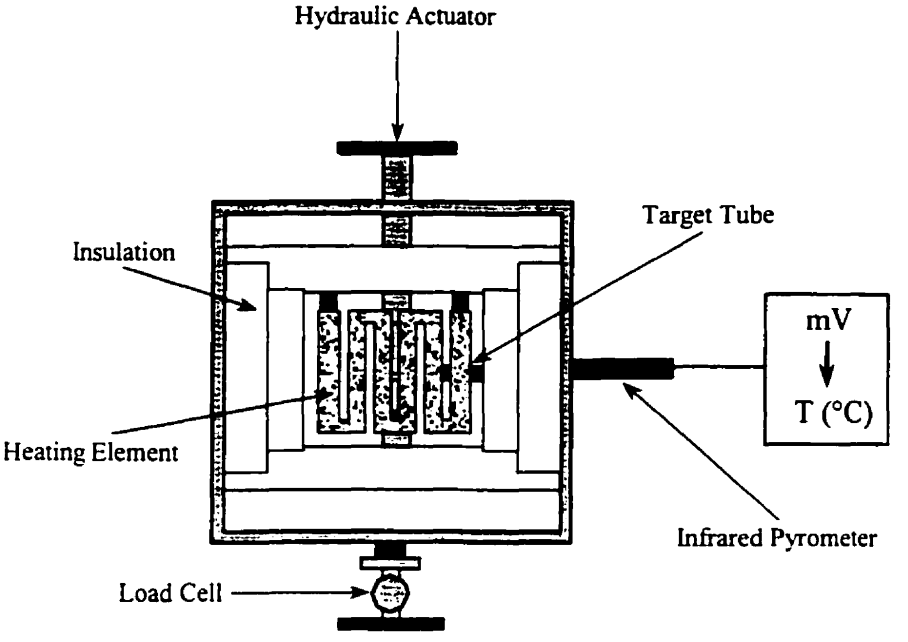

Figure 4.6. Schematic representation of the side view of hot-press chamber.

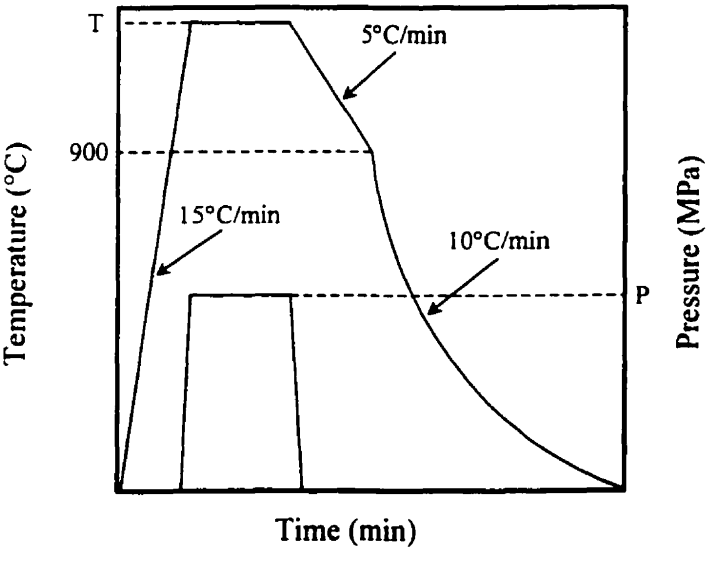

Figure 4.7. Typical heating and pressure profiles follows during the joining-press experiments.

4.4. Sample Examination

In order to investigate the composition and morphology of the Si_3N_4/Ti interfaces, transverse sections of each joint were cut using a low-speed diamond cut-off wheel operated with an oil coolant to protect the specimens from over-heating. The specimens were mounted in a cold-setting epoxy resin and an automatic polishing procedure was followed, in order to assure reproducibility of the preparation of the samples.

The samples were ground using a 45 μm diamond-grinding disc, following by SiC paper of 400 and 600 grit, under a load of 5 psi *(34.5 kPa)* using a rotation speed of 120 rpm. The polishing was carried out using diamond paste *(6 and 1 μm)* under a load of 2 psi *(13.8 kPa)* finished with colloidal silica *(0.06 μm)* to provide a final finish. The samples were then cleaned with isopropanol in an ultrasonic bath for 5 minutes.

4.4.1. Microstructural Characterization

The microstructural examination was performed on the polished joints and fracture surfaces of samples. The thickness of the resulting interfaces was measured directly from the micrographs obtained using both the secondary electron image (SEI) and back-scattered electron image mode (BEI) in a *JEOL JSM-840A* scanning electron microscope, equipped with an energy dispersive spectroscopy unit. In order to prevent a negative charge build up on the specimen surfaces, all the SEM samples were Au-Pd coated prior to examination. Further

compositional analysis was performed using electron probe microanalysis *(EPMA)* of interfacial phases in a *CAMEBEX* electron microprobe with wavelength dispersive system *(WDS)* using an accelerating voltage of 10 kV and a beam current of 0.7 nA. The standards consisted of SiO_2 for Si, Al_2O_3 for Al and O, TiN for N and Ti, and $Y_3Fe_5O_{12}$ for Y. Carbon-coated using an *EDWARDS E306A* coating system when EPMA analysis was required.

4.4.2. Atomic Force Microscope Analysis

In order to characterize the surfaces roughness of the materials, an analysis of the surfaces was carried out using Atomic Force Microscopy *(AFM)* with a DI 3100 Scanning Probe Microscope. *AFM* is a relatively new tool for examination at the atomic levels of sensitivity. This method has attracted considerable interest because it enables real-space examination of atomic level details on surfaces [104]. AFM provides true atomic resolution on surfaces, enabling visualization of the finest details and the images represent do not a synthesis of information derived over a large region, but rather reflect the real defect and imperfections that exist on any surfaces. AFM can be operated in a variety of environments and it can be used to investigate both insulating and conducting materials [105].

AFM works by sensing the force applied between a tip and a sample surface maintained in close proximity to each other. The tip of a flexible force-sensing cantilever stylus is raster scanned over the surface of the sample. The force acting between the cantilever and the sample surface causes minute deflection of the cantilever. The deflection

is detected and utilized as the feed back signal. By keeping the force small and constant, a topographic image at *constant force* that follows the surface contours is obtained. A schematic diagram of an AFM is shown in Figure 4.8. The sample is mounted on top of a tube scanner. The tip, mounted at the end of a flexible spring (cantilever), is brought into gentle contact with the sample surface. The cantilever provides a restoring force to counter that arising from the interaction between the sample and tip. By actuating the tube scanner, the tip is raster scans the sample surface.

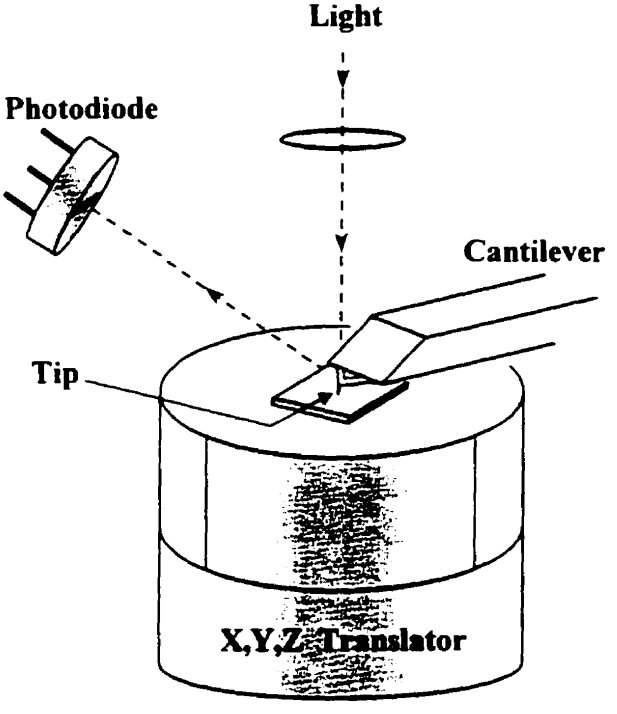

Figure 4.8. The atomic force microscope (AFM) [106]. Deflection of the tip is monitored by an "optical lever' formed by reflection of laser light off the tip on to a sectored photodiode.

The signal, after amplification, is compared with a reference value. The difference in signal is again amplified to drive a feedback circuit. A constant-force topographic image of the surface structure is obtained. The surface roughness term commonly used is: average roughness ***R***. For N measurements of height z and average height $\bar{z}$, the average roughness is the mean deviation of the height measurement as expressed by:

$$R = \frac{1}{N} \sum_{i=1}^{N} \left| z_i - \bar{z} \right| \qquad (4.1)$$

Several surface roughness measurement techniques are in common usage. The optimum method will depend upon the type and scale of roughness to be measured for a particular application.

4.4.3. X-Ray Diffractometry

In order to make a qualitative phase analysis, X-ray diffraction was carried out on fracture surfaces of the joint components, using CuKα radiation on a PHILIPS PW1710 X-Ray diffractometer. The angular range between 10 to 100 of 2θ was scanned with an angular velocity of 0.6°/min, using an accelerating voltage of 40 kV, and current of 20 mA. Similar conditions were used on samples of the starting materials. The phases present in the samples were identified by comparing the diffraction patterns obtained with the *XRD* reference patterns available on the PC-identification database of the computer derived from JCPDS index.

4.5. Mechanical Evaluation

The effect of the joining conditions on the room temperature mechanical properties can be investigated by increasing the specimen size so as to produce standard specimens. The interfacial strength of $Si_3N_4/Ti/Si_3N_4$ joints was determined by four-point bending test using an *INSTRON Dynamic Testing System TINIUS OLSEN H25K-5* with a maximum load cell of 25 kN, and a bending jig represented schematically in Figure 4.9.

4.5.1. Four-Point Bending Test

The specimens consisted of butt-joined ceramic/metal/ceramic diffusion samples. They were carefully placed in the bottom part of the jig, with the interface plane parallel to the plane of vertical displacement of the plunger. The load was applied at a vertical speed of 0.5 mm/min until the applied load resulted in fracture of the specimen. The load-displacement curves were obtained on a *x-y* chart recorder connected to the testing equipment.

The bend strength is defined as the maximum tensile stress at failure and is often referred to as the modulus of rupture *(MOR)*. The bend strength for a circular test specimen can be calculated using the general flexure stress formula described in equation:

$$S = M.C / I \qquad (4.2)$$

where: M is the moment,

C is the distance from the neutral axis to the tensile surface,

I is the moment of inertia.

For a circular test specimen:

$$I = \pi D^4 / 64 \qquad (4.3)$$

and

$$C = D / 2 \qquad (4.4)$$

where D is the diameter of the specimen.

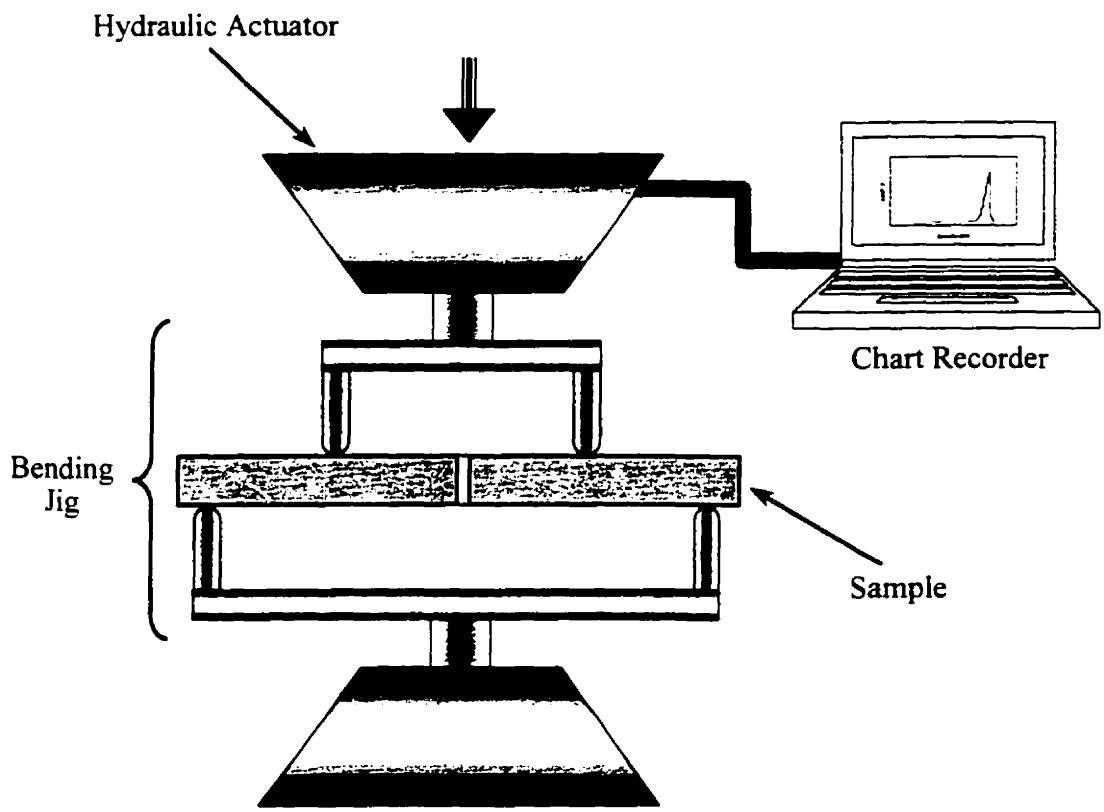

Figure 4.9. Assembly used in four-point bending tests.

For the four-point test:

$$M = (F / 2).d \qquad (4.5)$$

therefore:

$$S = \sigma_{4\text{-}pt} = 16.F.d / \pi D^3 \qquad (4.6)$$

where: F is the load at fracture,

d is the distance between the outer and inner span of the four-point bend jig

D is the diameter of the specimen.

The distance of the inner and outer span was of 20 mm and 40 mm, respectively. For each set of experimental conditions studied, temperature and time, an average of at least five samples of 50 mm in length and 7 mm in diameter, were used to determine the bending strength.

4.5.2. Microhardness Evaluation

Microhardness was measured in order to establish the differences in hardness between the materials and compounds forming at the interface. The microhardness was obtained using the Leco M-400-G2 microhardness tester. A load of 25 and 50 g was used. The resulting indentation was measured (width and length) and the calculated hardness value was recorded. At least twelve tests were carried out for each compound and on different samples to verify the accuracy. Similar conditions were used on samples of the starting materials.

Chapter 5:

Thermodynamic Predictions and Si_3N_4 - Ti Interaction Behaviour

The main objective of this chapter is to present the results obtained from hot-pressing of Si_3N_4/Ti diffusion couples. At the beginning of this chapter, a thermodynamic analysis of the Ti-Si-N system is presented. Emphasis will be made on the characterization of the resulting ceramic/metal interfaces produced upon the hot-pressing of single Si_3N_4/Ti samples.

5.1. Thermodynamic Analysis

A thermodynamic evaluation of the Si_3N_4-Ti system was carried out using F*A*C*T (Facility for the Analysis of Chemical Thermodynamics) program and its database. The analysis is based on the stability of Ti-Si-N compounds that result from the interaction of Si_3N_4 to Ti under a vacuum of 2×10^{-4} atm. (20 Pa), which was the experimental joining

environment. In general the chemical reaction occurring between silicon nitride (Si_3N_4) and metal (Me) follows one of the following three routes:

$$Me + Si_3N_4 = Me\ silicide + Me\ nitride \quad (5.1)$$

$$Me + Si_3N_4 = Me\ silicide + N_{2(g)} \quad (5.2)$$

$$Me + Si_3N_4 = Si + Me\ nitride \quad (5.3)$$

Comparing the thermodynamic stability of Si_3N_4 with those of metal silicides and nitrides it is possible to predict the probable products. When the bonding temperature is above the minimum temperature as is required for reaction *(5.2)*, it proceeds and forms an intermetallic compound at the interface. The free N produced by this reaction diffuses into the metal when the metal has a high solubility for N. It can then escape from the joint or remains as gas voids at, or near, the interface. If reaction *(5.2)* occurs, the silicide grows and prevents direct contact between the metal and ceramic. This decreases the amount of the metal supplied to the ceramic side and results in the formation of another silicide with higher Si content. On the other hand, the change in the free energy for reaction *(5.3)* can be calculated from the changes of the standard free energy for the formation of nitrides. Zr, Ti, Nb and V promote reaction *(5.1)* above the minimum temperature of reaction *(5.2)* and below the minimum temperature in the case of reaction *(5.3)*.

A plot of the Gibbs free energy of formation (ΔG) of Ti-Si-N compounds as a function of temperature, for 2×10^{-4} atm., is shown in Figure 5.1. When Si_3N_4 is in contact with Ti, it decomposes into Si and $N_{2(g)}$ and a reaction is predicted to occur. According to Figure 5.1, the reaction should follow route *(5.2)*, initially forming Ti_5Si_3 and $N_{2(g)}$ gas. For

temperatures higher than 1000°C, route *(5.1)* is more favorable, because TiN is more stable than Si_3N_4. The silicide present could be TiSi or $TiSi_2$, formed from the diffusion of Si into Ti_5Si_3. In Figure 5.1, it can be seen that Si_3N_4 is more stable than any other Ti-Si-N compound from room temperature to approximately 100°C. Hence, no reaction is expected to take place in that temperature range. Above 100°C, Ti_5Si_3 becomes more stable than Si_3N_4, and is predicted to form.

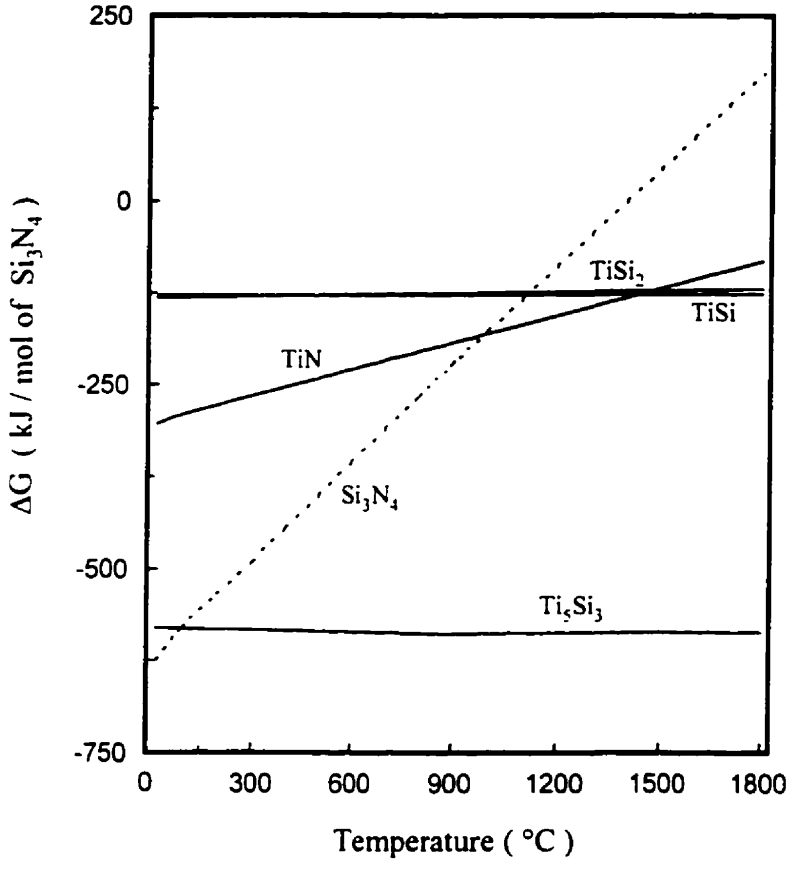

Figure 5.1. Free energy of formation of Ti-Si-N compounds as a function of temperature, data obtained from F*A*C*T.

The process starts with the decomposition of Si_3N_4 into silicon (Si) and nitrogen (N) according to,

$$Si_3N_4 = 3\,Si + 2\,N_{2(g)} \qquad (5.4)$$
$$\Delta G^\circ_1 = 744.753 - 0.468 * T \quad (kJ/mol\ K)$$

where $\Delta G^\circ_1 > 0$, since the formation of Si_3N_4 has associated with it a $\Delta G^\circ < 0$. In the next step, Si diffuses into Ti and reacts forming a silicide as follows,

$$5\,Ti + 3\,Si = Ti_5Si_3 \qquad (5.5)$$
$$\Delta G^\circ_2 = -579.057 - 7.731 * T \quad (kJ/mol\ K)$$

Combining *(5.4)* and *(5.5)*, and selecting 1200°C as the joining temperature result in,

$$Si_3N_4 + 5\,Ti = Ti_5Si_3 + 2\,N_{2(g)} \qquad (5.6)$$
$$\Delta G^\circ_3 = -498.88\ kJ/mol$$

According to reaction *(5.6)*, $N_{2(g)}$ is formed along with Ti_5Si_3. If $N_{2(g)}$ diffuses into Ti and forms TiN, the reaction at 1200°C is expressed by,

$$Ti + \tfrac{1}{2}\,N_{2(g)} = TiN \qquad (5.7)$$
$$\Delta G^\circ_4 = -156.27\ kJ/mol$$

combining *(5.4)*, *(5.5)* and *(5.7)* result in,

$$Si_3N_4 + 9\,Ti = Ti_5Si_3 + 4\,TiN \qquad (5.8)$$
$$\Delta G^\circ_5 = -1123.95\ kJ/mol$$

comparing *(5.6)* and *(5.8)*, it can be seen that $\Delta G^\circ_5 < \Delta G^\circ_3$, indicating that the reaction expressed by *(5.8)* is thermodynamically more favorable than *(5.6)*. Therefore, the formation

of TiN and Ti_5Si_3 at the Si_3N_4/Ti interface is expected to occur during joining experiments at 1200°C in vacuum. Infact, Figure 5.1 shows that, in a vacuum of 2 x 10^{-4} atm., TiN is unlikely to form in the temperature range from 0 to 1000°C because its free energy is higher than the free energy of formation of Si_3N_4. Depending on the concentration of Si within the interface, Ti_5Si_3 can be converted to TiSi. At 1200°C, this reaction is expressed by:

$$Ti_5Si_3 + 2\,Si = 5\,TiSi \qquad (5.9)$$
$$\Delta G^\circ_6 = -54.858\ kJ/mol$$

combining *(5.4)*, *(5.6)* and *(5.9)*, gives,

$$Si_3N_4 + 3\,Ti = 3\,TiSi + 2\,N_{2(g)} \qquad (5.10)$$
$$\Delta G^\circ_7 = -296.731\ kJ/mol$$

If $N_{2(g)}$ diffuses into Ti to form TiN, the reaction at 1200°C is expressed by,

$$Ti + Si = TiSi \qquad (5.11)$$
$$\Delta G^\circ_8 = -128.503\ kJ/mol$$

which gives,

$$Si_3N_4 + 7\,Ti = 3\,TiSi + 4\,TiN \qquad (5.12)$$
$$\Delta G^\circ_9 = -921.799\ kJ/mol$$

comparing *(5.10)* and *(5.12)*, it can be seen that the reaction expressed by *(5.10)* is thermodynamically less favorable that the one expressed by *(5.12)*.

Similarly, Ti_5Si_3 can be converted to $TiSi_2$. At 1200°C, this reaction is expressed by:

$$Ti_5Si_3 + 7\,Si = 5\,TiSi_2 \qquad (5.13)$$
$$\Delta G^\circ_{10} = -33.306\ kJ/mol$$

combining *(5.4)*, *(5.6)* and *(5.13)*, which gives,

$$Si_3N_4 + (3/2)\ Ti = (3/2)\ TiSi_2 + 2\ N_{2(g)} \qquad (5.14)$$
$$\Delta G^\circ_{11} = -97.511\ kJ/mol$$

If $N_{2(g)}$ diffuses into Ti to form TiN, the reaction at 1200°C is expressed by:

$$Ti + 2\ Si = TiSi_2 \qquad (5.15)$$
$$\Delta G^\circ_{12} = -124.193\ kJ/mol$$

resulting in,

$$Si_3N_4 + 11/2\ Ti = 3/2\ TiSi_2 + 4\ TiN \qquad (5.16)$$
$$\Delta G^\circ_{13} = -722.579\ kJ/mol$$

comparing the reactions expressed by *(5.8)*, *(5.12)* and *(5.16)*, it can be seen that because $\Delta G^\circ_5 < \Delta G^\circ_9 < \Delta G^\circ_{13}$, the sequence of reactions $Ti_5Si_3 \rightarrow TiSi \rightarrow TiSi_2$, is thermodynamically favorable. Figure 5.2 represent the relations between the standard Gibbs free energy (ΔG°) per mol of Ti of reactions *(5.8)*, *(5.12)* and *(5.16)* as a function of temperature. Thermodynamic analysis reveals that when temperature is lower than 1100°C, reaction *(5.16)*, that represents the formation of TiN and $TiSi_2$, is more favorable than others. However, it can be observed that when temperature is higher than 1100°C, the formation of TiN and Ti_5Si_3, reaction *(5.8)*, is thermodynamically more favorable than the others. Therefore, these phases, Ti_5Si_3 and TiN, are expected to form during joining experiments in the range of 1200°C to 1500°C in vacuum. Diffusion is the dominating reaction mechanism in diffusion joining, consequently silicide transformations may or may not be observed depending on the joining parameters, such as bonding temperature and time,

because these parameters affect the concentration of diffusing silicon at the interface, and therefore, the nature of the resulting silicide.

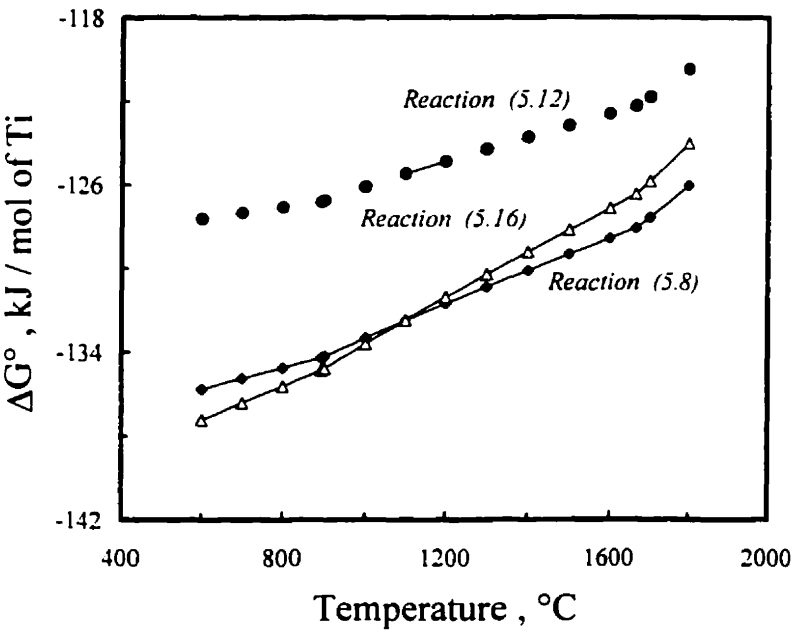

Figure 5.2. Relation between standard Gibbs free energy as a function of temperature.

According to the Ti-Si phase diagram, Figure 2.19, liquid formation can occur when the samples are hot-pressed at temperature >1330°C, until the amount of Si is sufficient to stabilize the solid Ti_5Si_3 phase. As result, the interface growth rate could be affected during the initial stages of the interface formation due to the formation of a liquid.

5.2. Si_3N_4/Ti Joining Experiments

Diffusion couples of silicon nitride, Si_3N_4, and titanium, Ti, were hot-pressed in vacuum at temperatures varying from 1200°C to 1500°C and for times from 15 minutes to three hours. A schematic representation of the hot-pressed samples is shown in Figure 5.3. In order to select the applied pressure for the sample, a preliminary study was carried out hot-pressing Si_3N_4/Ti diffusion couples using loads in the range of five to 50 MPa.

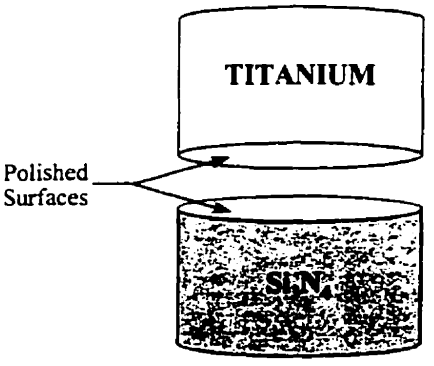

Figure 5.3. Schematic representation of the hot-pressed samples.

It could be observed that pressures in excess of 30 MPa resulted in substantial deformation of the Ti and even in some cases the metal was squeezed out of the Si_3N_4 sample, especially at high joining temperatures. Therefore, the pressure was limited to values between five and 20 MPa.

Joining temperature and time were the main parameters studied. Table 5.1 summarizes the results obtained for joining conditions used to hot-press Si_3N_4/Ti samples. Ti could not be bonded to Si_3N_4 for samples hot-pressed lower than 1400°C. For the different variables studied, even for holding times of the order of three hours, the samples always peeled apart at the interface during cooling.

Successful joining was achieved at 1400°C and 1500°C. However, for Si_3N_4/Ti samples hot-pressed at 1400°C at holding times of 120 to 180 minutes the joint strength was insufficient and the sample debonded during sample preparation for SEM. Nevertheless, joining of Si_3N_4/Ti samples hot-pressed at 1500°C occurred for all the conditions studied.

Table 5.1. Experimental results of hot-press Si_3N_4/Ti samples.

Temperature (°C)	Joining Time (minutes)	Bonded (✓) Not bonded (×)
1500	15 to 180	✓
1400	30 to 90	×
	120 to 180	✓
1300	30 to 180	×
1200		

In order to determine the interfacial interaction during the hot-pressing, X-ray diffraction analysis was carried out on the fractured Si_3N_4 and Ti surfaces. The diffraction spectra obtained revealed the presence of Ti_5Si_3 and a trace of TiN on the metal surface of samples hot-pressed at 1200°C and 1300°C. Figure 5.4 shows the diffraction patterns

obtained on both (a) Si_3N_4 and (b) Ti fracture surfaces for a sample hot-pressed at 1400°C for 30 minutes under a load of 5 MPa. It could be observed that most of the interface remained attached to the metal.

Comparing the pattern obtained on the Si_3N_4 surface (Figure 5.4a), with that observed on the original Si_3N_4 material (Figure 4.2), it can be observed that the main peaks from the fracture surface corresponded to the original Si_3N_4 Ceralloy 147-31N, i.e. hexagonal β-Si_3N_4. No peaks could be attributed to any Ti-nitride phase, confirming that most of the interface remained attached to the metal Ti. In the case of the X-ray diffraction pattern corresponding to the Ti fracture surface, Figure 5.4b, some peaks corresponding to the metal could be observed mainly at values of 2θ of 36.24°, 39.44°, 62.32°, and 86.96°. The main peaks observed in the spectrum of the Ti fracture surface correspond to hexagonal Ti_5Si_3. The presence of cubic TiN phase is clearly observed in the peaks corresponding to 2θ of 36.58°, 61.72°, 74.02°, 77.08°, and 93.32°. Some low intensity peaks corresponding to the TiSi phase were also observed mainly at high angles, 2θ of 83.6°, 84.88°, and 88.24°.

5.3. Interface Behavior of Si_3N_4/ Ti Joints

Successful joining was achieved for samples hot-pressed at 1500°C and for times ranging from 15 minutes to three hours. Joining occurred by the formation of a reactive interface on the Ti side of the sample by diffusion of N and Si.

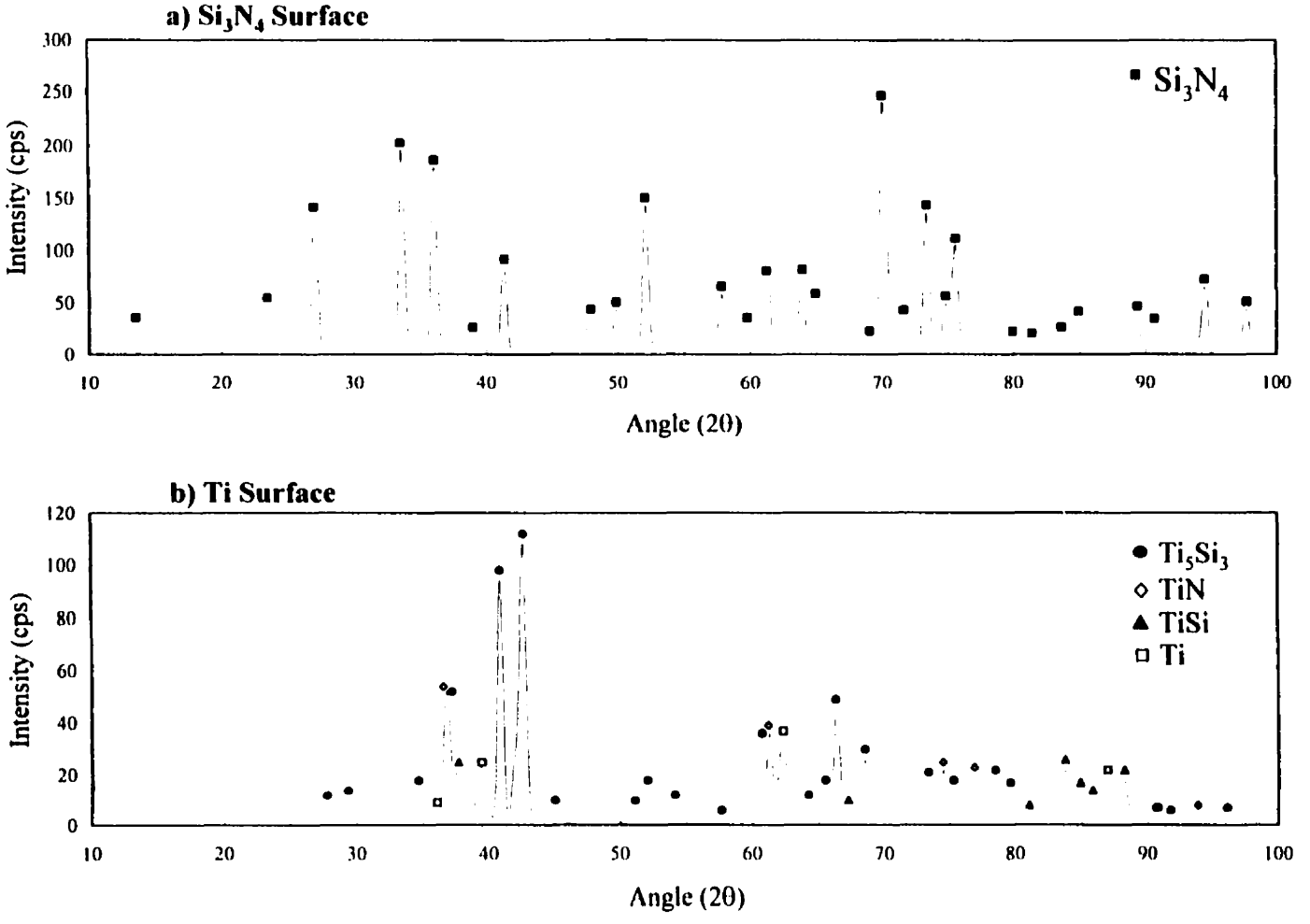

Figure 5.4. X-ray diffraction of (a) Si_3N_4 and (b) Ti fracture surfaces of the sample hot-pressed at 1400°C for 30 minutes using a load of 5 MPa.

The reaction started with the decomposition of Si_3N_4 into Si and $N_{2(gas)}$ and diffusion of these species into the Ti. Because diffusion is a thermally activated process, reaction became significant for this high joining temperature. For the range of bonding times investigated in samples hot-pressed at 1500°C, the formation of Ti-silicide and Ti-nitride occurred even for a time of 15 minutes, however the sample debonded during cooling and effective joining started to take place after about 30 minutes. The interface consisted initially of one reaction layer containing two intermixed phases, and can be observed in the SEM photograph of this sample shown in Figure 5.5. The formation of liquid produced by the interaction between Ti and Si and the high affinity of Ti for Si resulted in the rapid formation of silicides, initially Ti_5Si_3, preventing extensive diffusion of Si into the Ti. The diffusion of N into Ti resulted in zone (B) formation.

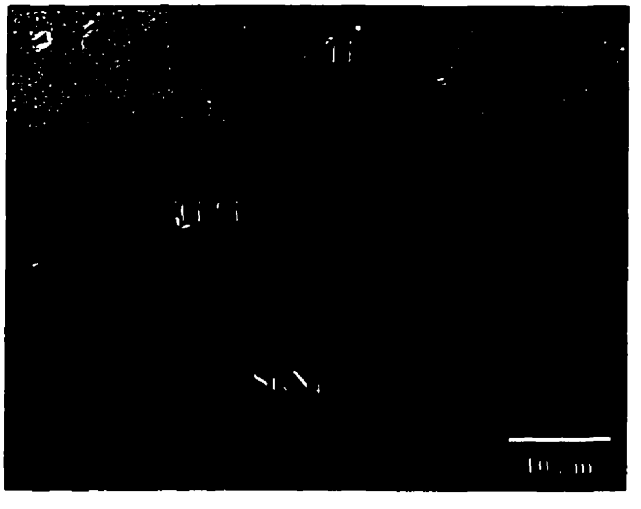

Figure 5.5. Secondary electron image (SEM) of Si_3N_4/Ti interface for a sample hot-pressed at 1500°C for 30 minutes and 20 MPa.

Figure 5.6 shows the interface of a sample hot-pressed at 1500°C for 45 minutes. The interface consisted once more of Ti_5Si_3 and zone (B) in separate interfacial layers. The average thickness of this interface was 12.23 μm. It can be observed that increasing the holding time from 30 to 45 minutes did not significantly increase the interface thickness. Some thermal cracking can be observed within the interface, mainly in the Ti_5Si_3 region. EPMA showed a composition of the zone (B), which, corresponded to TiN but containing Al, Y, O, and a trace amount of Si. Liquid formation plays an important role in the joining process, because it increases the rate of the interface formation, improving the contact area between the bonding materials, and consequently the interaction is higher, promoting rapid diffusion of the materials, since liquid diffusion is much faster than the diffusion in the solid-state.

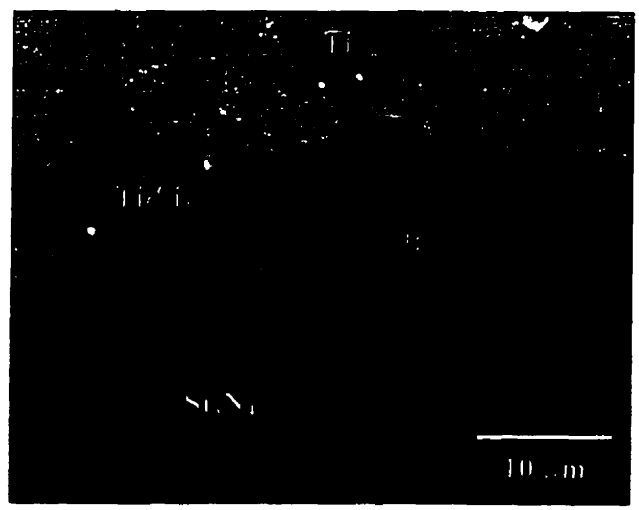

Figure 5.6. Secondary electron image (SEM) of Si_3N_4/Ti interface for a sample hot-pressed at 1500°C for 45 minutes and 20 MPa.

The interface of samples hot-pressed at 1500°C for 60 minutes and 120 minutes are shown in Figure 5.7 and 5.8 respectively. It can be observed in the interface shown in Figure 5.8 that a TiSi phase is produced by the transformation of the Ti_5Si_3, by reaction with Si produced by the decomposition of Si_3N_4.

In the case of the interface shown in Figure 5.8, the final thickness of this interface is 26 μm. Figure 5.8 also illustrates a more defined interface between Si_3N_4 and Ti, which is composed of three reaction zones: i) zone (B) in contact with Si_3N_4; ii) an intermediate reaction layer corresponding to Ti_5Si_3, and iii) a reaction zone containing both Ti_5Si_3 and TiSi, produced by an excess amount of Si at the interface resulting in the transformation of Ti_5Si_3 into TiSi.

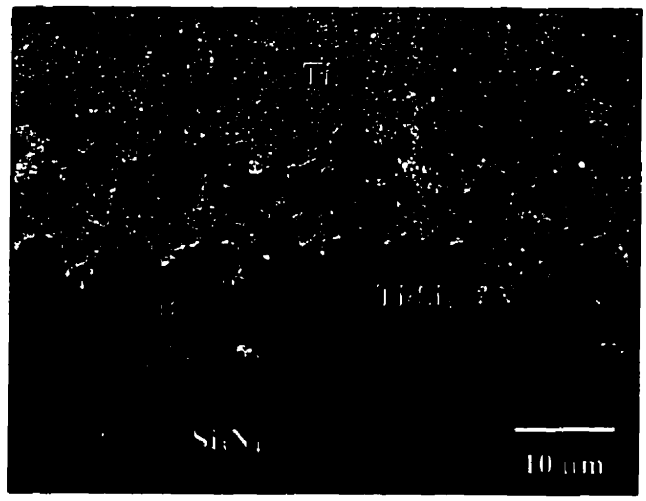

Figure 5.7. Secondary electron image (SEM) of Si_3N_4/Ti interface for a sample hot-pressed at 1500°C for 60 minutes and 20 MPa.

Figure 5.8. Secondary electron image (SEM) of Si_3N_4/Ti interface for a sample hot-pressed at 1500°C for 120 minutes and 20 MPa.

Therefore, the sequence of reaction within a Si_3N_4/Ti interface can be summarized as follows: when Ti came in contact with nitrogen, it reacts to produce TiN which precipitates at the interface adjacent to Si_3N_4, the final average thickness of this phase was of 1 µm. However the interaction of Ti with Si forms a eutectic when the sample is hot-pressed at temperature higher than 1330°C and promotes the formation of a liquid. As the liquid saturates with Si, Ti_5Si_3 precipitates quickly and grows inside the Ti.

The formation of TiSi occurred as a consequence of further diffusion of Si, as predicted by the thermodynamic analysis of the Si_3N_4/Ti system and can be observed in the Ti-Si phase diagram shown in Figure 5.9. It can be observed from Figure 5.9 that Ti_5Si_3 transforms to different Ti-silicides (Ti_5Si_4, TiSi, or/and $TiSi_2$) when the Si amount increases.

The final product depends on the amount of Si in the interface, an ample study carried out to investigate the Ti-silicides phases within the interface is presented in chapter 6.

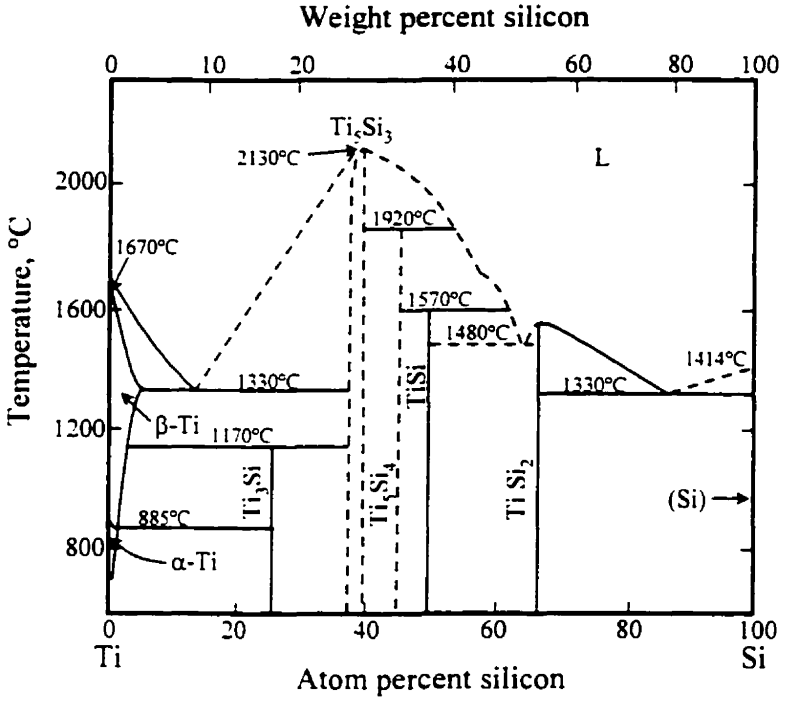

Figure 5.9. Ti-Si phase diagram [77].

5.4. Interface Characterization

Electron-probe microanalysis was performed on the different phases observed at the interface of the hot-pressed samples in order to further characterize the reaction layer of the joined samples. EPMA performed on Si_3N_4/Ti samples produced at 1500°C, is shown in

Figure 5.5 to Figure 5.8 and indicates that the phases present are Ti_5Si_3, TiSi, and also a zone (B) containing Ti, N, Y, Al, O, and traces of Si at the Si_3N_4 interface. A complete characterization of the reaction layer observed at the Si_3N_4/Ti interface and in particular of the zone (B) was made with X-ray diffraction, X-ray mapping and quantitative WDS-line scanning and the results are presented in the following sections.

5.4.1. X-Ray Diffractometry

In order to obtain a good overview of the different components in the interface, a sample joined at 1500°C for 45 minutes was fractured at the interface and the two fracture surfaces were examined. X-ray diffraction analysis was performed on these two surfaces and the corresponding spectra from (a) Si_3N_4 and (b) Ti surfaces are shown in Figure 5.10. The main peaks from the fracture surface of Si_3N_4 spectrum (Figure 5.10a), corresponded to the original silicon nitride Ceralloy 147-31N, hexagonal β-Si_3N_4. Low intensity peaks attributed to TiN were observed at 2θ of 36.58° and 61.72°. It can be observed that most of the interface remained attached to the metal Ti.

The presence of predominantly Ti_5Si_3 and TiN are clearly evident on the X-ray spectrum corresponding to the Ti surface (Figure 5.10b). Low intensity peaks corresponding to TiSi phase were also observed, mainly at high angles. These results support the thermodynamic predictions performed on the Si-N-Ti system.

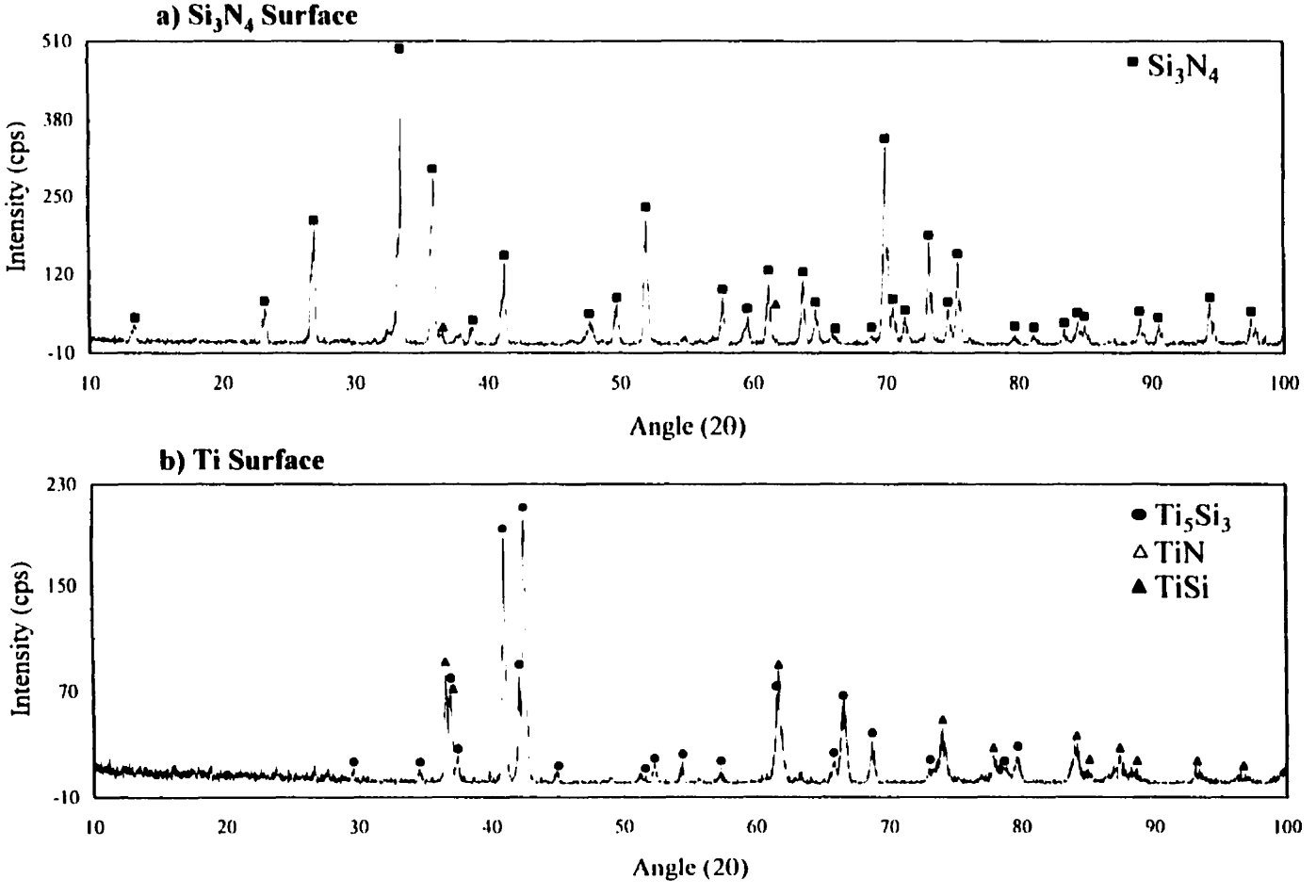

Figure 5.10. X-ray diffraction of (a) Si_3N_4 and (b) Ti fracture surfaces of the sample hot-pressed at 1500°C for 45 minutes.

The lattice parameters of the different phases observed at the interface of the samples were calculated and are shown in Table 5.2. Comparing the values of the lattice parameters obtained for β-Si_3N_4, (a = 7.6783 Å, c = 2.8809 Å, c/a = 0.375) after hot-pressing with the corresponding values before pressing (a = 7.609 Å, c = 3.172 Å, c/a = 0.417), it can be observed that the unit cell of the β-Si_3N_4 phase had expanded in the ***a*** direction, but contracted along the ***c*** axes. In the case of the Ti, comparing the values of the lattice parameters before pressing (a = 2.9608 Å, c = 4.6698 Å, c/a = 1.577), with the corresponding values after pressing (a = 2.5979 Å, c = 4.9698 Å, c/a = 1.913), it can be a contraction of the Ti unit cell in the ***a*** direction, and an expansion in the ***c*** direction, due to the alloying (N_2 or O_2 dissolution) of the metal. On the other hand, the values of the lattice parameters obtained in the case of the TiSi, Ti_5Si_3, and TiN phases are in good agreement with those reported in the standard JCPDS tables.

5.4.2. Electron Probe Micro-Analysis

The atomic distribution of elements across the Si_3N_4/Ti interface was studied using EPMA-EDS by X-ray mapping across the interface of the joint, hot-pressed at 1500°C for 45 minutes. The main elements analyzed were titanium (Ti) and silicon (Si). However, since Y_2O_3 and Al_2O_3 were the additives used during the sintering process of the Si_3N_4 Ceralloy 147-31N, then yttrium (Y) and aluminum (Al) were also analyzed. The corresponding maps

are shown in Figure 5.11, where the interface is aligned in the vertical direction with the Ti sample on the left side and the Si_3N_4 on the right. The different contrast from dark to white corresponds to the increase in the concentration of the specific element.

Table 5.2. Lattice parameter of the different phases found in the interface of Si_3N_4/Ti hot-pressed samples.

Phase	Structure	Lattice Parameters (Å)
β-Si_3N_4	Hexagonal	A = b = 7.6783, c = 2.8809, c/a = 0.375
TiN	Cubic	A = b = c = 4.2473
Ti_5Si_3	Hexagonal	A = b = 7.4368, c = 5.1412, c/a = 0.691
TiSi	Orthorhombic	A = 6.4047, b = 3.6296, c = 5.0398
Ti	Hexagonal	A = b = 2.5979, c = 4.9698, c/a = 1.913

In the Ti-map, the different contrast from left to right corresponds to the decrease in concentration of Ti from pure Ti to pure Si_3N_4, passing through the interface composed of Ti_5Si_3 and zone (B). No diffusion of Ti into the ceramic can be observed, resulting in the dark region corresponding to Si_3N_4. For the Si-map, a decrease in the intensity corresponding to a

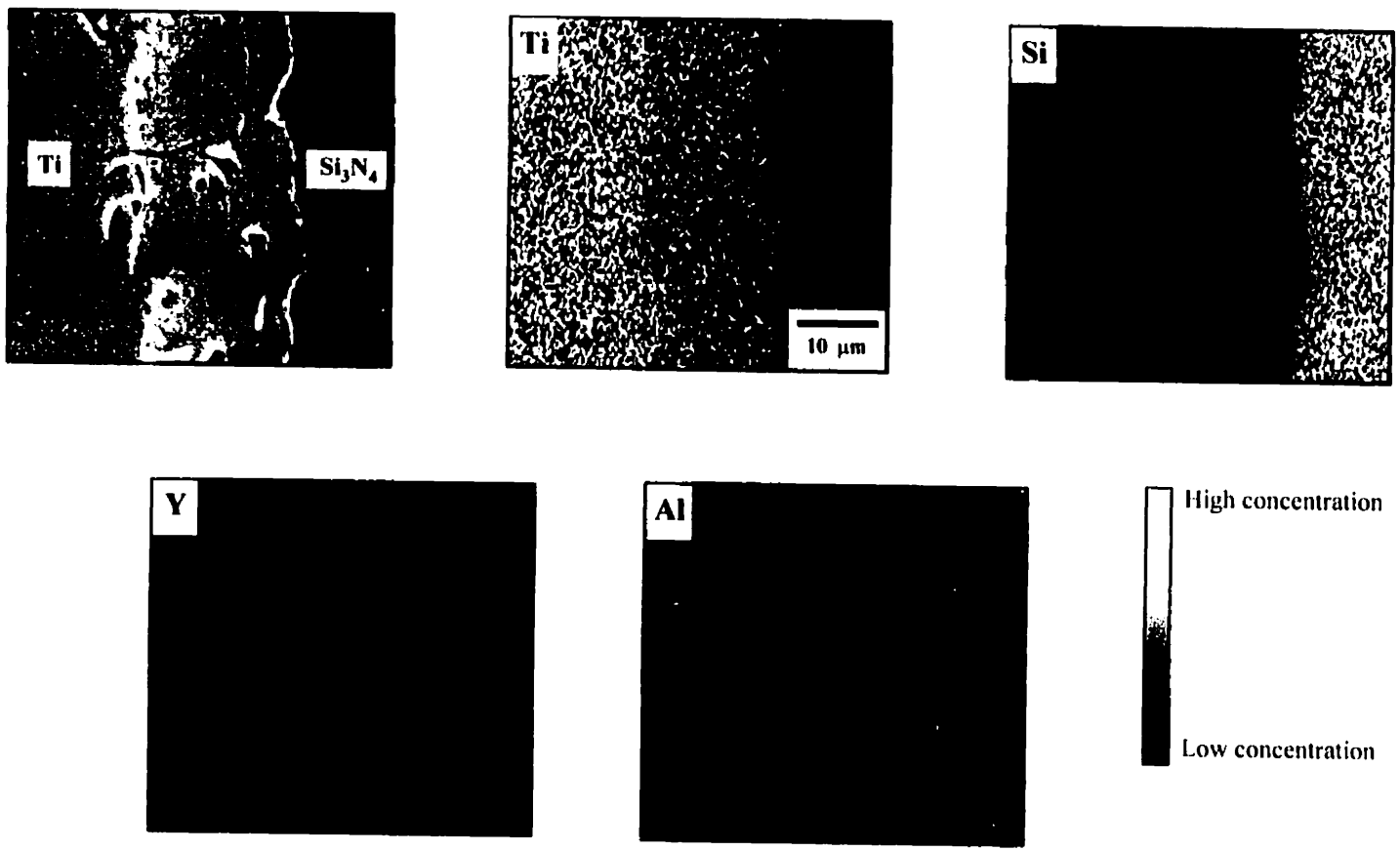

Figure 5.11. Atomic distribution across the interface of a sample hot-pressed at 1500°C for 45 minutes and 20 MPa using EPMA.

decrease in the concentration of Si is observed in the direction of Ti, passing through the zone (B) and Ti_5Si_3 layers. A decrease of Si can be observed in the interface delineating clearly the region corresponding to zone (B). The concentration of Y and Al increased close to the ceramic interface, clearly delineating the zone (B). However, some traces of Al diffusion into zone (B) can be observed. A slight increase of Al can be observed in the region when the Si content has decreased. Unfortunately, the N peak at 379 eV and the Ti peak at 387 eV overlap and therefore the peak height in this energy range is given by a superposition of the Ti and N peaks, making it difficult to obtain a N map.

In order to obtain a quantitative overview of the different components in the interface, diffusion profiles were obtained in a Si_3N_4/Ti sample hot-pressed at 1500°C for 60 minutes and a load of 20 MPa, (Figure 5.7.), by WDS line analysis. This method also resulted in an acceptable profile for oxygen, and consequently, it was possible to establish the presence of oxide phases. Again, unfortunately a profile for N was not obtained because of overlapping of the N and Ti peaks. The results are illustrated in Figure 5.12 where the Ti and Si_3N_4 are on the left and right, respectively. The scan line was chosen to start on the Ti side of the sample through the interface, Ti_5Si_3 and zone (B), finishing on the Si_3N_4 side.

The amount of Ti detected in the Si_3N_4 was less than 0.15 wt%, i.e. within the detection limits of the EPMA, thus confirming that no Ti diffused into the Si_3N_4. The main element present was Si with maximum concentration of 54.8 wt%, which is in good agreement with the nominal concentration of this element in Si_3N_4: 60 wt% for Si and 40 wt% for N.

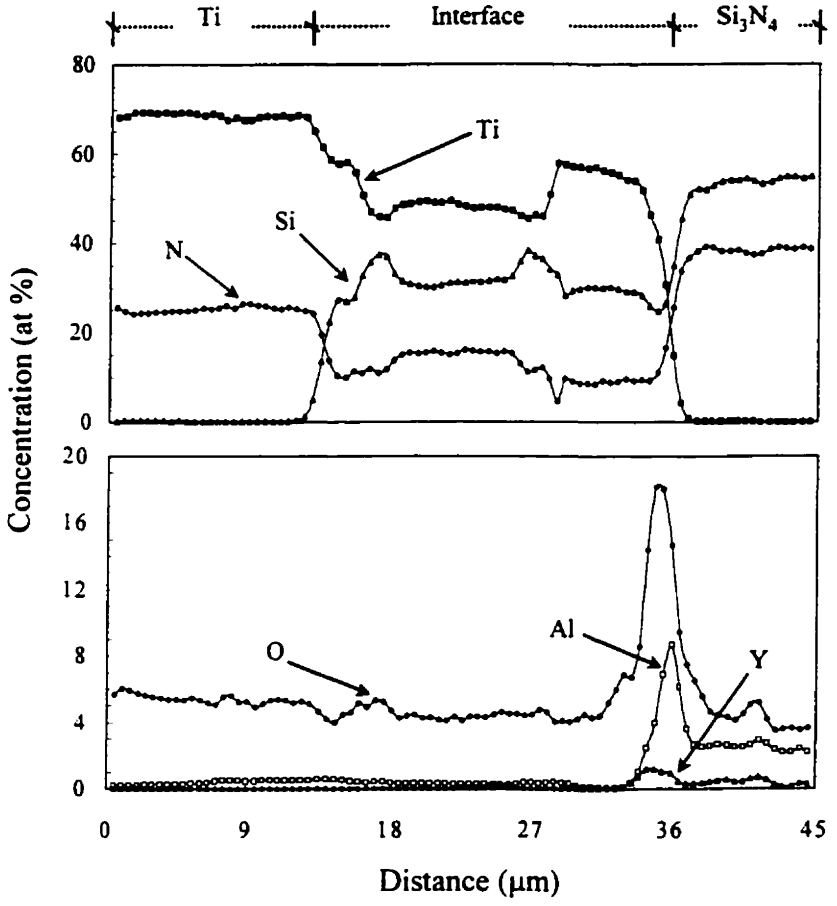

Figure 5.12. Quantitative EPMA line analysis across the interface obtained in a sample hot-pressed at 1500°C for 60 minutes shown in Figure 5.7.

The Ti and Si profiles showed good agreement with the data obtained from X-ray mapping. The different interfacial phases, Ti_5Si_3 and TiSi, could be observed through the variation of the intensities of the WDS signal for these two elements. It can be seen that an increase of the Ti intensity is matched by a decrease in the Si signal indicating the transition from one Ti-silicide to another. The Si signal reached its maximum at the Ti_5Si_3-zone (B)

boundary where the Ti signal reached its minimum. In the region corresponding to zone (B) high levels of Al, Y, and O were obtained, as well a trace of Si. The increase in the Y and O signals would suggest that this was segregation of the sintering additive (Al_2O_3 and Y_2O_3), into the interface. The Al profile indicated the presence of a residual and well distributed concentration of Al, of 2 wt%, across the Si_3N_4 area. The maximum concentration of Y and Al were 3.2 wt% and 8.1 wt%, respectively. In the O profile a maximum concentration of 8.12 wt% is observed in the same fraction as the maximum Al peak. A residual intensity of about 2.3 wt% was observed along the entire profile, and is probably related to the presence of a surface oxide. Therefore, the presence of O in the silicide layers and in Ti metal is not clear. Y and Al were not observed outside the zone (B) in the direction of Ti, confirming the results observed in the corresponding X-ray mapping, and indicating that these elements did not diffuse into the metal, but, remained trapped along the region corresponding to zone (B). In the N profile, a high concentration of N (8.4 wt%) can be observed in the Ti and within the interface (2.94 wt%). This could be caused by overlapping of the Ti and N peaks or dissolution of N in Ti. Thus, the presence of N at the interface and in Ti metal is not clear.

These results indicated that, upon decomposition of Si_3N_4, silicon was the main diffusing element into the metal. Therefore, in accordance with the thermodynamic analysis, EPMA, and X-ray diffraction results, zone (B) is TiN combined with the sintering aids, Y_2O_3 and Al_2O_3, which segregated to the interface during the decomposition of the ceramic. The latter is most likely to be an amorphous alumino-silicate, since no additional phases were detected at the interface by the X-ray diffraction analysis.

Chapter 6:

Characterization of Si_3N_4/ Ti / Si_3N_4 Joints

The main objective of this chapter is to present the results obtained during hot-pressing of Si_3N_4/Ti/Si_3N_4 joints. Emphasis will be made on the characterization of the resulting ceramic/metal interfaces formed during the hot pressing of the samples. The effect of the surfaces roughness and sample preparation on joining and the resulting interfacial reaction kinetics was studied. Finally, the mechanical properties of the joints are presented and correlated to the interface microstructure.

6.1. Si_3N_4/Ti/Si_3N_4 Joining Experiments

Sandwich-like ceramic/metal samples of silicon nitride (Si_3N_4) and titanium (Ti) were hot-pressed in vacuum at temperatures varying from 1200°C to 1500°C using different

holding times. The pressure applied to the samples was limited to 20 MPa, and was selected based on the results described in chapter 5.

A schematic representation of the hot-pressed samples is shown in Figure 6.1. Table 6.1 shows a matrix of the results obtained for different joining conditions. It can be seen from Table 6.1 that Ti could not be bonded to Si_3N_4 for samples hot-pressed at temperatures lower than 1400°C, where no liquid formation occurs to promote bonding. Even for holding times of the order of nine hours, the samples always peeled apart at the interface during cooling.

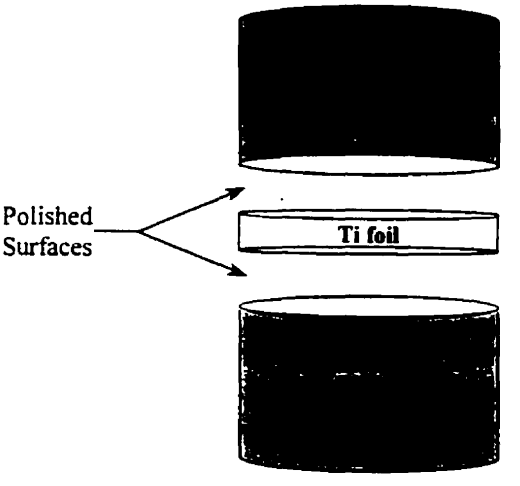

Figure 6.1. Schematic representation of the hot-pressed samples.

However, successful joining was obtained at temperatures higher than 1400°C. Results obtained for samples hot-pressed at 1400°C showed that they debonded for holding times of less than 120 minutes, joining of Si_3N_4 to Ti occurred but these samples debonded during sample preparation for SEM. However, successful joining was achieved in the case of two hours and longer. On the other hand, joining of samples hot-pressed at 1500°C was obtained for all the joining conditions studied.

The joining process starts with the decomposition of Si_3N_4 into Si and N gas and subsequent reaction with the Ti metal. Liquid formation can occur at the beginning of the

process, by the interaction of the decomposed Si with Ti, on the surface of the metal when the samples are hot-pressed at temperatures higher than 1330°C, according to the Ti-Si phase diagram, until the amount of Si is enough to precipitate solid Ti_5Si_3 phase. As result, the interface growth rate would be initially fast and would decrease as the amount of liquid decreases. On the other hand, liquid would not be formed in samples hot-pressed at 1200°C and 1300°C, and as a consequence longer times would be necessary to form an interface.

Table 6.1. Experimental results of hot-press Si_3N_4/Ti/Si_3N_4 samples.

Temperature (°C)	Joining Time (minutes)	Bonded (✓) Not bonded (×)
1500	30 to 180	✓
1400	30 to 90	×
	120 to 180	✓
1300, 1200	180 to 540	×

In order to determine the interface interaction during the hot-pressing experiments, X-ray diffraction analysis was performed on the Si_3N_4 and Ti fracture surfaces. The diffraction spectra obtained from Si_3N_4 and Ti fracture surfaces of samples hot-pressed at 1200°C and

1300°C (debonding occurred during cooling), revealed the presence of Ti_5Si_3 as the main phase and traces of TiN phase at the interface. It could also be observed that most of the interface remained attached to the metal, since the spectrum corresponding to the Si_3N_4 fracture surfaces showed peaks corresponding to the starting Si_3N_4 material only, and not to the interface.

6.2. Interfacial Characterization

6.2.1. Microstructural Evolution

Joints produced at 1400°C and 1500°C of Si_3N_4 to Ti occurred through the formation of a reactive interface on the metal side of the sample as a result of diffusion of N and Si. Because diffusion is a thermally activated process, the reaction rate became significant at high joining temperatures, as a consequence of liquid formation. The reaction started with the decomposition of Si_3N_4 into Si and N gas and interaction and diffusion of these species into Ti. The first step in the bonding sequence occurs with the interaction of Ti with Si to form a eutectic liquid (>1330°C). This liquid is formed instantaneously and is followed by a period of rapid dissolution of Si, in which the liquid tends to attain a constant composition, and precipitate Ti-silicides. In the first few minutes, the initial liquid formation, dissolution and precipitation occur extremely rapidly, with reaction products forming immediately. Figure 6.2 shows an interface obtained for a sample hot-pressed at 1400°C for 120 minutes. The interface consists of one layer with three intermixed phases.

Figure 6.2. Cross-section of the Si_3N_4/Ti/Si_3N_4 interface for a sample hot-pressed at 1400°C for 120 minutes in vacuum.

EPMA performed on this sample indicated that these phases were Ti_5Si_3, TiSi and the zone (B), which is a mixture of TiN containing Y, Al, O and Si. This is associated with segregation of the sintering aids, Y_2O_3 and Al_2O_3, during the decomposition of the ceramic to form an amorphous alumino-silicate. Several cracks can be observed in the reaction layer, mainly in the Ti_5Si_3 phase. The high affinity of Ti for N and Si resulted in immediate formation of TiN and a silicide, initially Ti_5Si_3. The TiSi phase was the result of the rapid transformation of Ti_5Si_3, which indicates considerable decomposition of Si_3N_4, and a large supply of Si. Although the reaction layer initially present is a mixture of Ti_5Si_3 with TiN, only Ti_5Si_3 phase extended inside the Ti. Some transformation of Ti_5Si_3 occurs forming an intermixed layer of Ti_5Si_3 with TiSi and extends from the Ti_5Si_3 inside the metal. This effect can be observed in a cross-section of the interface between Si_3N_4 and Ti obtained in a sample

hot-pressed at 1400°C for 180 minutes and illustrated in Figure 6.3. The average thickness of this interface was 27.3 μm and consisted once more of TiN and Ti-silicides. It could be observed that the TiSi phase did not extend into the Ti but formed an intermediate reaction zone mixed with Ti_5Si_3.

In order to investigate the different phases formed at the interface in a more clear manner. X-ray diffraction was performed after gradually removing interfacial material (layer by layer) from the Ti-fracture surface of a sample hot-pressed at 1400°C for 90 minutes. This sample debonded during cooling from the joining temperature. It can be seen that most of the interface remained attached to the Ti. The corresponding patterns, starting with (a) the original interface through (c) the final grinding and removal of interfacial material, are shows in Figure 6.4.

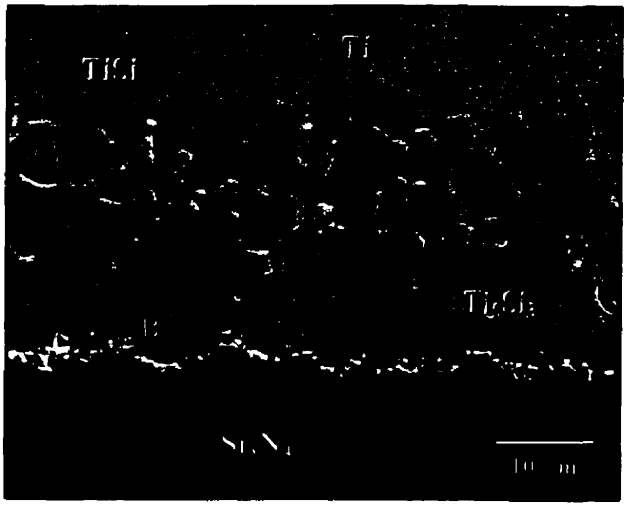

Figure 6.3. Cross-section of the Si_3N_4/Ti/Si_3N_4 interface for a sample hot-pressed at 1400°C for 180 minutes in vacuum.

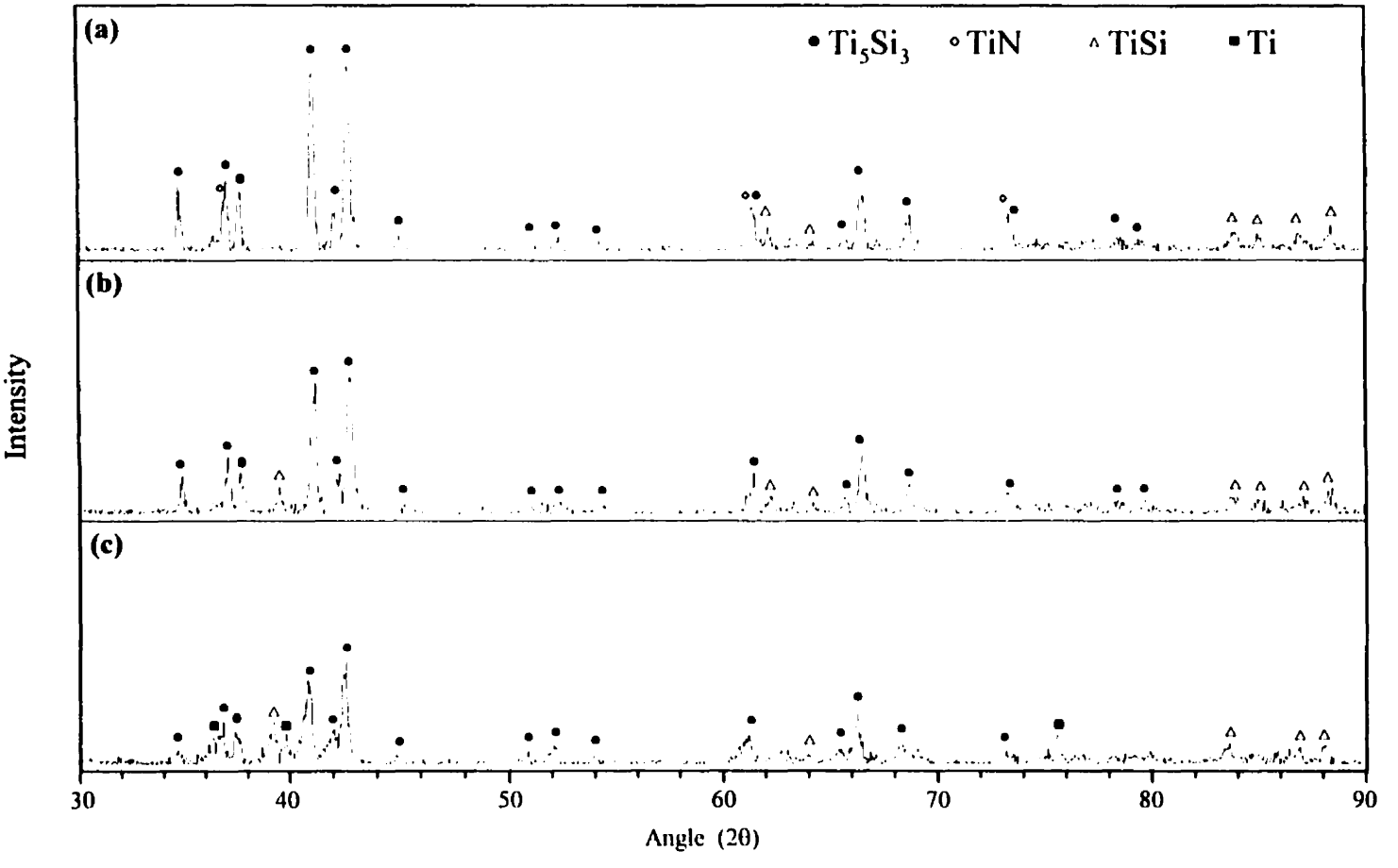

Figure 6.4. X-Ray diffraction for a Ti fracture surface of a sample hot-pressed at 1400°C for 90 minutes. (a) Original interface through (c) last grinding step of material.

First, the original interface was studied and the corresponding X-ray spectra, Figure 6.4a, confirmed the presence of cubic TiN and hexagonal Ti_5Si_3 as the main phases that form the reaction layer. Low intensity peaks corresponding to TiSi were identified at high diffraction angles. In the next step, the sample was ground to eliminate the TiN phase, and the X-ray diffraction was performed on the resulting surface producing the spectrum shown in Figure 6.4b. In general a reduction can be observed in the values of the intensity of the peaks compared with the spectrum in Figure 6.4a. However Ti_5Si_3 still was identified as the main phase. The spectrum is characterized by the appearance of a peak at 2θ of 39.56° and corresponds to TiSi, confirming the transformation of the Ti_5Si_3 to TiSi, and the presence of the intermixed reaction zone formed from these two phases. In the final grinding step, the sample was ground again and the X-ray pattern of the resulting surface is shown in Figure 6.4c. At this point approximately 18 μm has been removed. Some peaks corresponding to the metal could be observed. However, the main peaks observed in the spectrum correspond to either hexagonal Ti_5Si_3 and TiSi phase.

In the case of Si_3N_4/Ti/Si_3N_4 samples hot-pressed at 1500°C successful joints were obtained for all the conditions studied. Ti_5Si_3, TiSi and TiN in the zone (B) could be observed at the interface forming an intermixed layer. Figure 6.5 shows the interface obtained from samples hot-pressed at 1500°C for (a) 30 and (b) 60 minutes. The total thickness of the reaction zone for these samples was of about 13.6 μm and 20.5 μm, respectively. Figure 6.5a also illustrates a more defined interface between Si_3N_4 and Ti, which is composed of a layer of TiN in contact with Si_3N_4 and an intermixed reaction zone containing both Ti_5Si_3 and TiSi in contact with Ti.

(a)

(b)

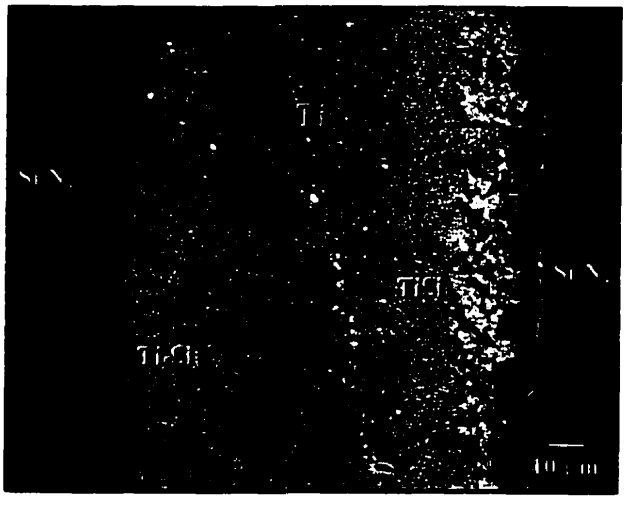

Figure 6.5. Cross-section of the interface for a Si_3N_4/Ti/Si_3N_4 sample hot-pressed at 1500°C for (a) 30 minutes and (b) 60 minutes.

6.2.2. Interface Growth Behavior

The activation energy and growth behavior of Si_3N_4/Ti/Si_3N_4 interfaces were studied. The thickness of the reaction zones was measured from SEM micrographs of the interfaces. The main process parameters in diffusion bonding are temperature and time. Temperature is, however, the most important one due to the fact that in thermally activated processes, a small change in temperature will result in a significant change in process kinetics compared with other parameters, and virtually all mechanisms including plastic deformation and diffusion are sensitive to temperature.

Figure 6.6 shows a plot of the thickness of the interfaces as a function of the square root of holding time for the samples hot-pressed at joining temperatures varying from 1200°C to 1500°C. The error bars are one standard deviation for the average thickness of at least twenty measurements for each sample. Figure 6.6 shows an excellent parabolic fit of the growth of the reaction zone resulting in a correlation coefficient greater than 0.96 for each line, and a time exponent of 0.5 in equation:

$$x = K_p \cdot t^{n} \qquad (6.1)$$

where: x is the thickness of the reaction layer,

K_p is the coefficient of penetration,

t is the bonding time.

The results are separated into two parts: (a) results obtained at temperatures where a eutectic liquid formation occurs, Figure 6.6a. These results suggest than diffusion of Si

into Ti was immediately followed by a liquid formation and fast precipitation of Ti silicide, which contributed to the rapid growth of the interfaces. On the other hand, in samples hot-pressed at temperature where solid-state reaction takes place, Figure 6.6b, the growth of the interface was slow and longer times were required. It can be observed that the rate of interfacial growth was higher when the temperature increased, which accounts for an increase in the value of K_p, coefficient of penetration in equation *(6.1)*, with increase in temperature.

In general, increasing the bonding temperature resulted in a faster growth of the reaction zones. In both cases, the interfaces grew in a parabolic fashion and, as a consequence, increasing the holding time from 30 minutes to three hours resulted in a significant increase in the interface thickness upon raising the temperature from 1400°C to 1500°C (Figure 6.6a) and is related to liquid phase formation. However, for temperatures in the range varying from 1200°C to 1300°C, longer times were necessary to increase the thickness of the interface, Figure 6.6b, and is associated with a solid-state reaction.

The activation energy, Q, for the formation of Si_3N_4/Ti/Si_3N_4 interfaces was calculated using equation *(6.1)* and equation *(6.2)*, which follows an Arrhenius-type relationship expressed by:

$$K_p = K_0 \exp(-Q / R T) \qquad (6.2)$$

where: K_0, is the pre-exponential factor,

Q is the activation energy for growth of the interface,

R is the gas constant,

T is the absolute temperature.

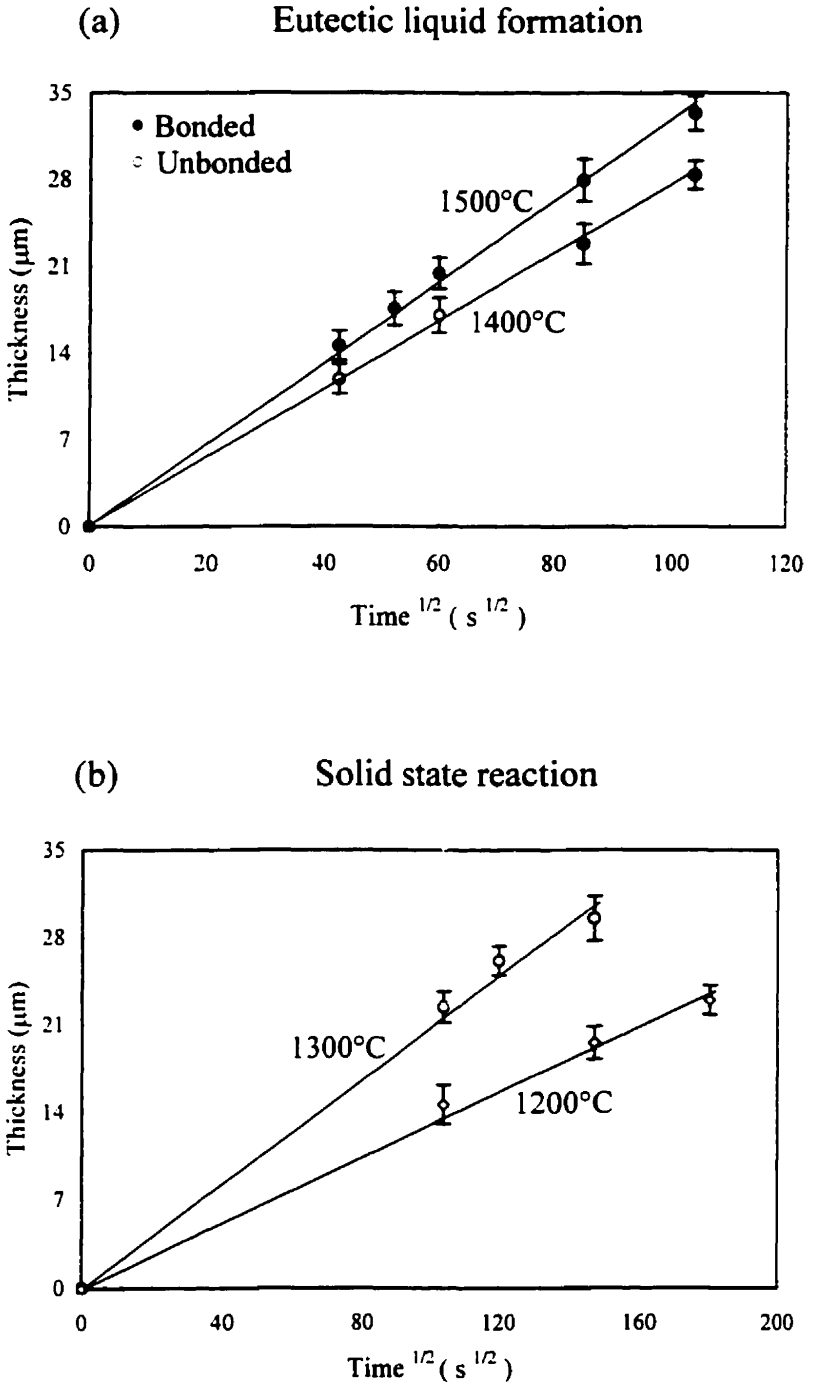

Figure 6.6. Thickness of the reaction zone as a function of joining time in Si_3N_4/Ti/Si_3N_4 samples hot-pressed at (a) 1400 and 1500°C and (b) 1200 and 1300°C.

The coefficient of penetration, K_p, is estimated from the thickness measurement of the corresponding interfaces and resulted in a plot of ln (K_p) as a function of the absolute temperature as shown in Figure 6.7. The activation energy for the formation of interfaces was calculated from the slope of the Arrhenius curve obtained for vacuum conditions. Two values have been calculated associated with the different mechanisms in the system, including eutectic liquid formation (Figure 6.7a) and solid-state reaction (Figure 6.7b). An activation energy of 72 ± 11 kJ/mol was obtained in the first case and a higher value, 123 ± 18 kJ/mol, more characteristic of a solid-state process.

6.3. Effect of Surface Roughness

Surface preparation of the materials during bonding is an important parameter because the presence of large asperities on the bonding surfaces prevents extensive plastic deformation on the surface due to poor contact between the asperities that limits the total area of contact between the metal and ceramic. In order to establish the effect of the surface roughness of the materials to be joined on the activation energy and interface growth, a series of unpolished Si_3N_4/Ti/Si_3N_4 samples were hot-pressed from 1200°C to 1550°C, for different times using 20 MPa pressure. These samples were as-ground, without final polishing. Figure 6.8 and 6.9 show typical surface roughness analyses obtained for polished and unpolished Si_3N_4 and Ti samples respectively, using the Atomic Force Microscopy (AFM).

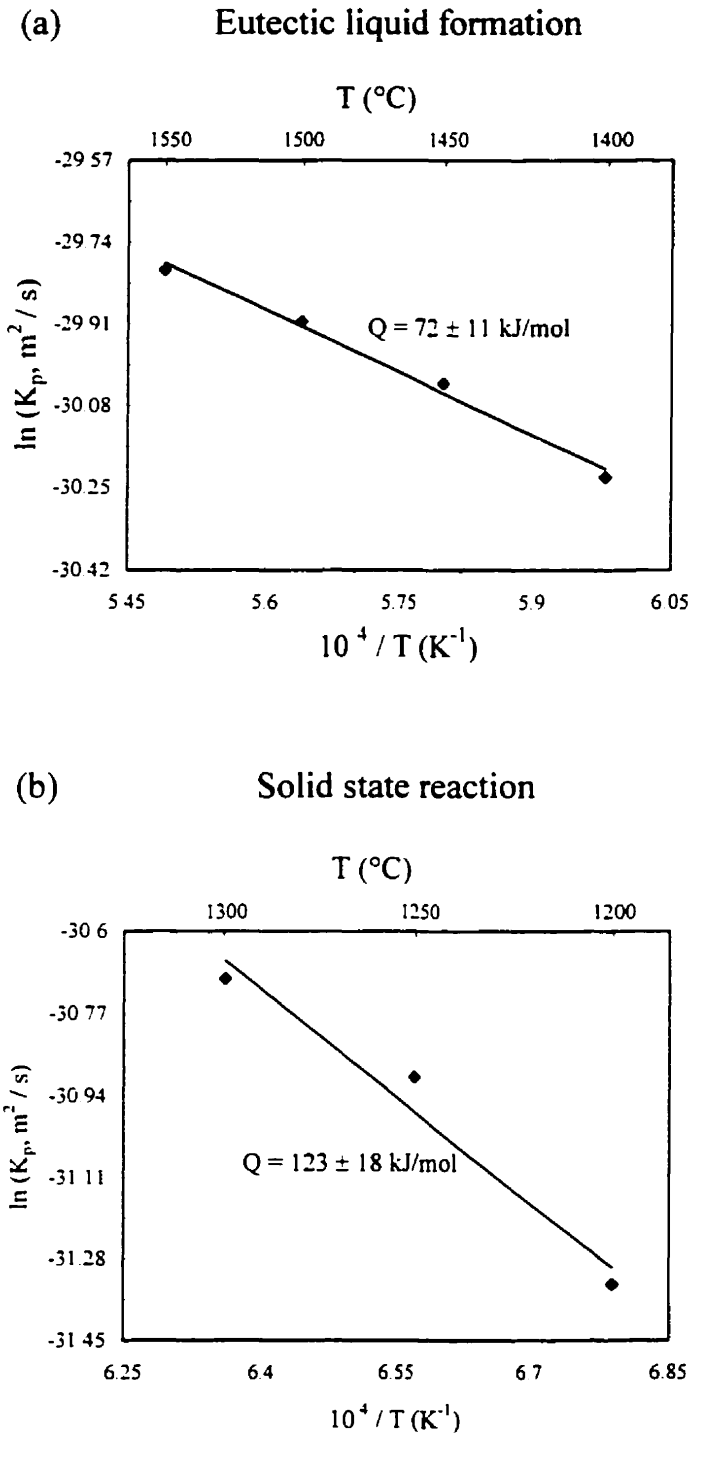

Figure 6.7. Arrhenius plots of the coefficient of penetration, K_p, as a function of temperature for polished samples.

Both polished and unpolished surfaces were examined over a *50 μm* by *50 μm* area for each analysis. Several areas at the center and edge of the sample were scanned by the AFM, and it was found that the surface roughness of the samples was quite homogeneous. The value of the surface roughness, *R*, represents the average difference between the maximum and minimum peaks obtained after sample scanning. The average surface roughness of polished Si_3N_4 and Ti surfaces (Figure 6.8) was *63.4 nm* and *53.4 nm*, respectively. By contrast the values for unpolished samples (Figure 6.9) were *584 nm* and *1140 nm* for Si_3N_4 and Ti, respectively.

In general, the bonding results for unpolished samples showed successful joining of Si_3N_4 to Ti when the samples were hot-pressed at a temperature of 1400°C and higher. However longer times were necessary compared with polished samples under the same conditions. Even when joining was unsuccessful, a reaction layer could be observed in the metal. For example, a cross section of the interface observed for unpolished samples hot-pressed at 1500°C for (a) 120 and (b) 180 minutes is shown in Figure 6.10.

An intermixed interface was formed and contained Ti_5Si_3 and TiN. However TiSi was not observed within the interface. The reaction layer thickness increased with time, but the morphology of the interface was quite wavy after joining, conforming to the original grinding grooves, which suggests that a eutectic liquid was present throughout the process.

(a) Si_3N_4 , R = 63.4 nm

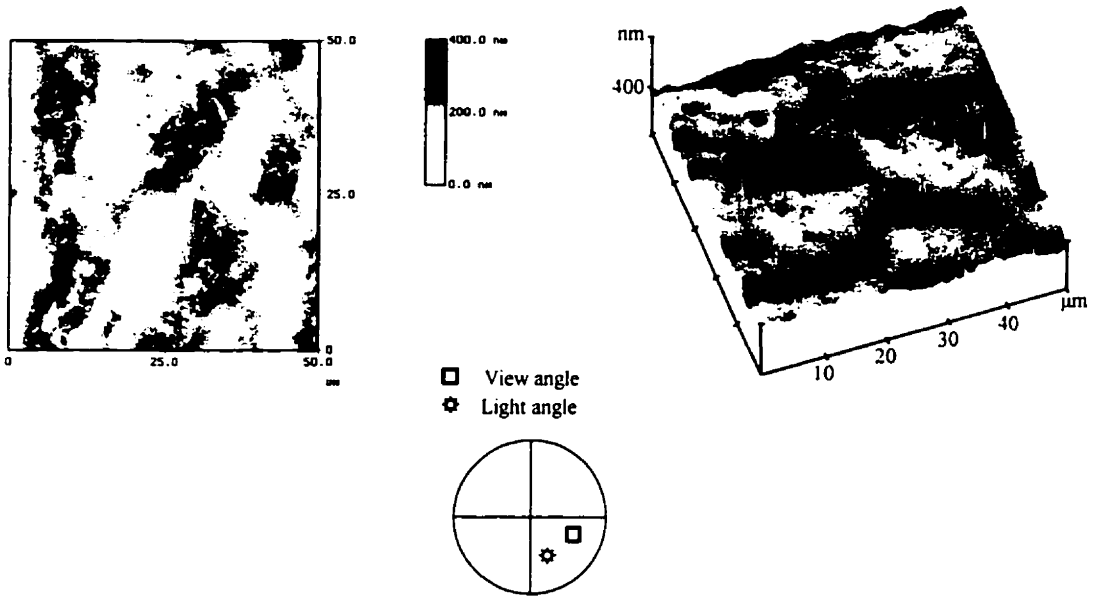

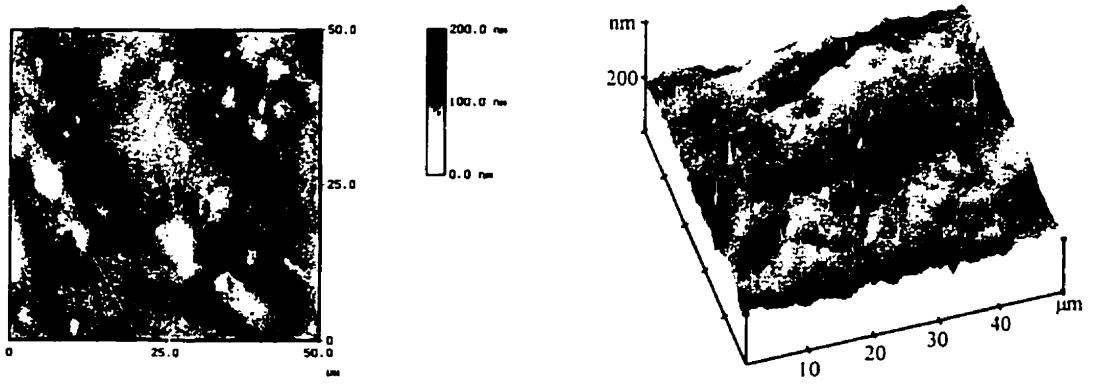

(b) Ti , R = 53.4 nm

Figure 6.8. Surface roughness analyses of polished a) Si_3N_4 and b) Ti samples.

(a) Si_3N_4 , R = 584 nm

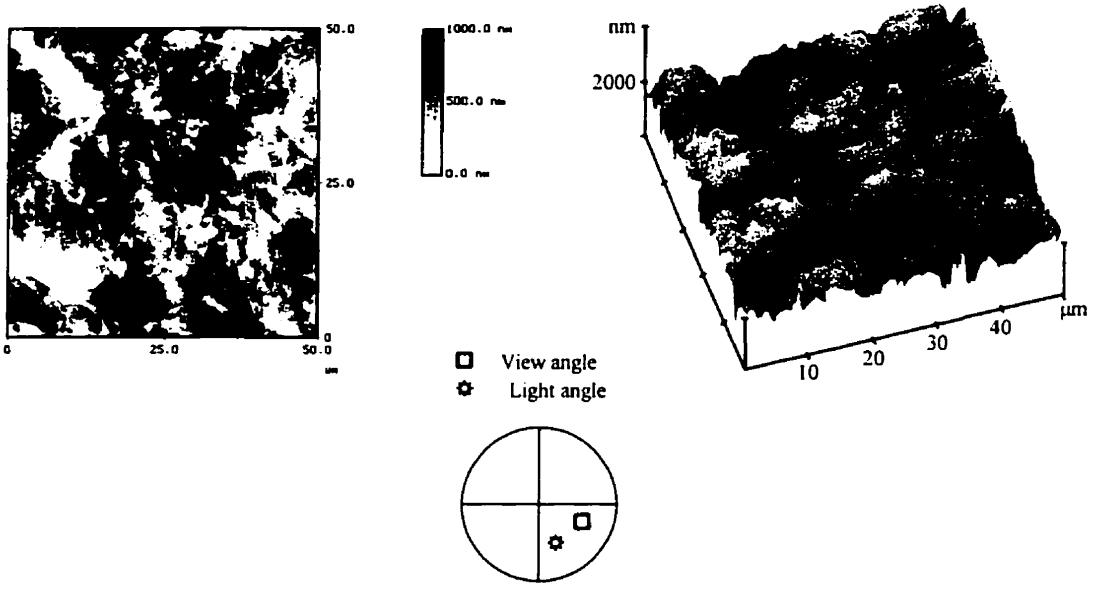

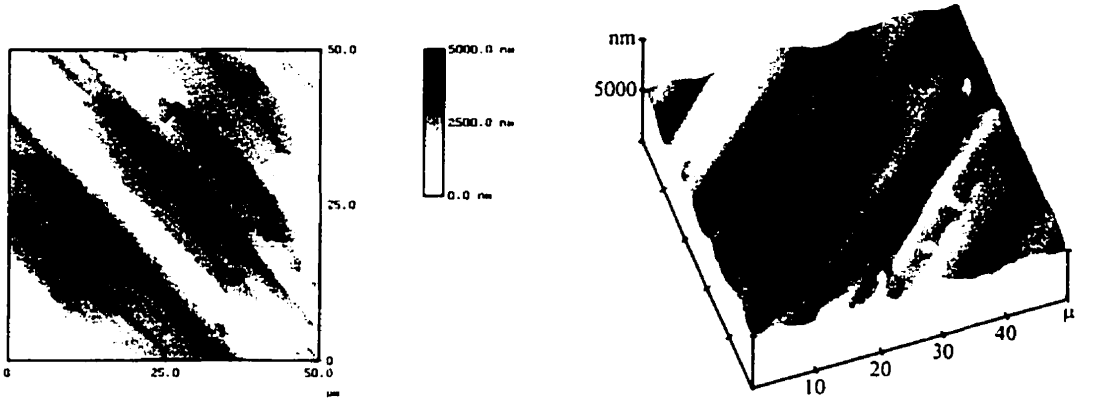

(b) Ti , R = 1140 nm

Figure 6.9. Surface roughness analyses of unpolished a) Si_3N_4 and b) Ti samples.

(a)

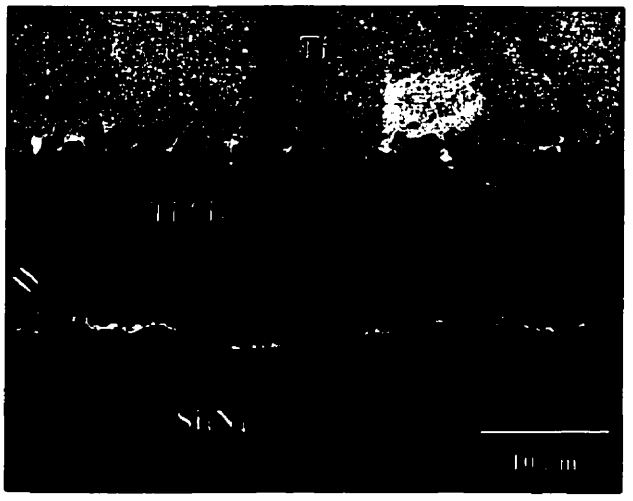

(b)

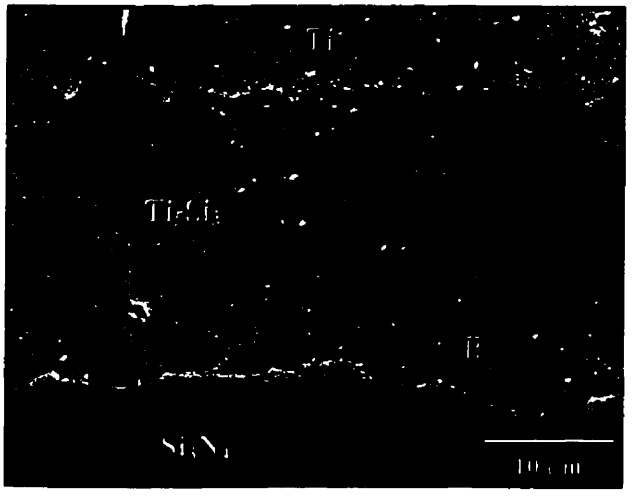

Figure 6.10. Cross-sections of the Si_3N_4/Ti/Si_3N_4 interface for unpolished samples hot-pressed at 1500°C for (a) 120 minutes and (b) 180 minutes.

A plot of the average thickness of the interface obtained for unpolished samples hot-pressed at 1500°C as a function of the square root holding time is shown in Figure 6.11. As with the polished samples the interface grew in a parabolic fashion, resulting in a time exponent of 0.5 in equation *(6.1)*. In consequence, it can be observed that the reaction zone resulted in a significant increase in the interface thickness with increasing holding time. An illustration of the thickness of the reaction zone as a function of temperature using both polished and unpolished materials for a time of two hours is shown in Figure 6.12. It can be observed that the interface obtained in samples hot-pressed with unpolished materials is significantly lower than that obtained with polished samples, however only a slight change is observed when the temperature is increased.

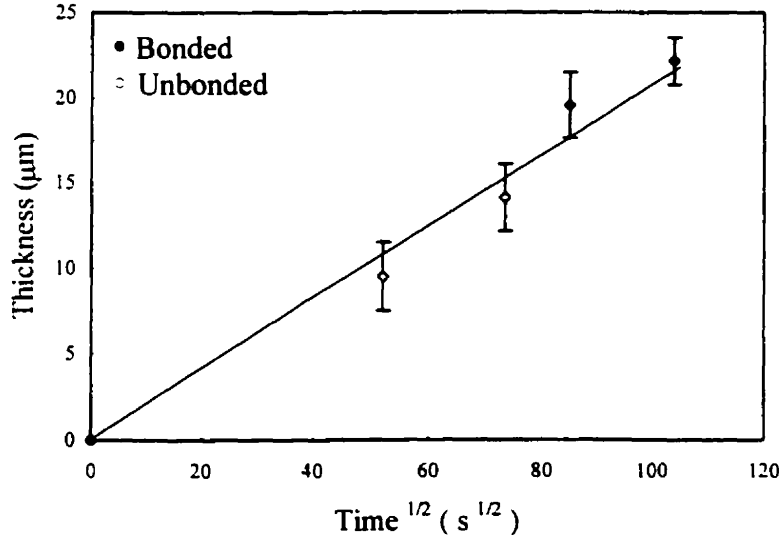

Figure 6.11. Thickness of the reaction zone as a function of time in unpolished Si_3N_4/Ti/Si_3N_4 samples hot-pressed at 1500°C.

Since bonding mainly occurs within the interface, the results show that surface roughness plays an important role in the diffusion bonding process especially at temperatures below 1330°C, where liquid formation does not occur. The activation energy for the formation of Si_3N_4/Ti/Si_3N_4 interfaces was calculated from the slope of the Arrhenius curve obtained for vacuum conditions using unpolished materials. The coefficient of penetration, K_p, is estimated from the thickness measured from the corresponding interfaces and resulted in a plot of the ln (K_p) as a function of the reciprocal of absolute temperature as shown in Figure 6.13. An activation energy of 90 ± 10 kJ/mol was obtained when a eutectic liquid forms (Figure 6.13a) and a value of 158 ± 22 kJ/mol was obtained in the case of a solid-state reaction joining (Figure 6.13b).

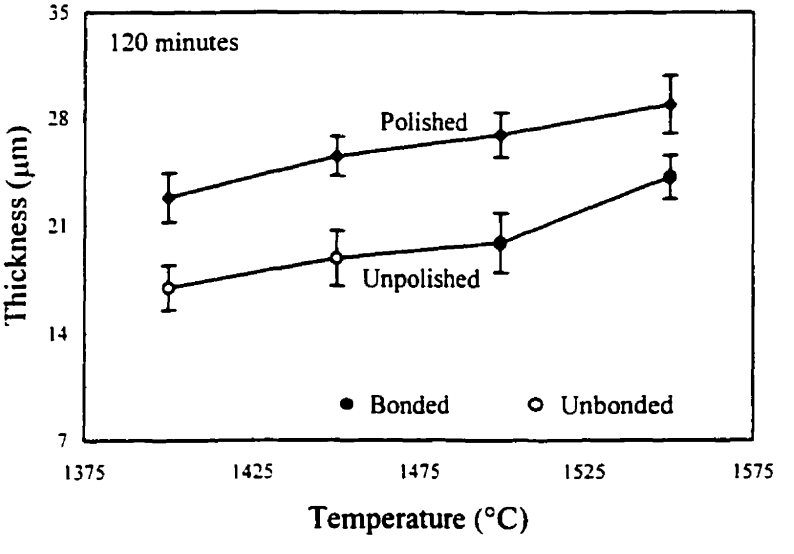

Figure 6.12. Thickness of the reaction zone as a function of temperature in polished and unpolished samples hot-pressed for 120 minutes.

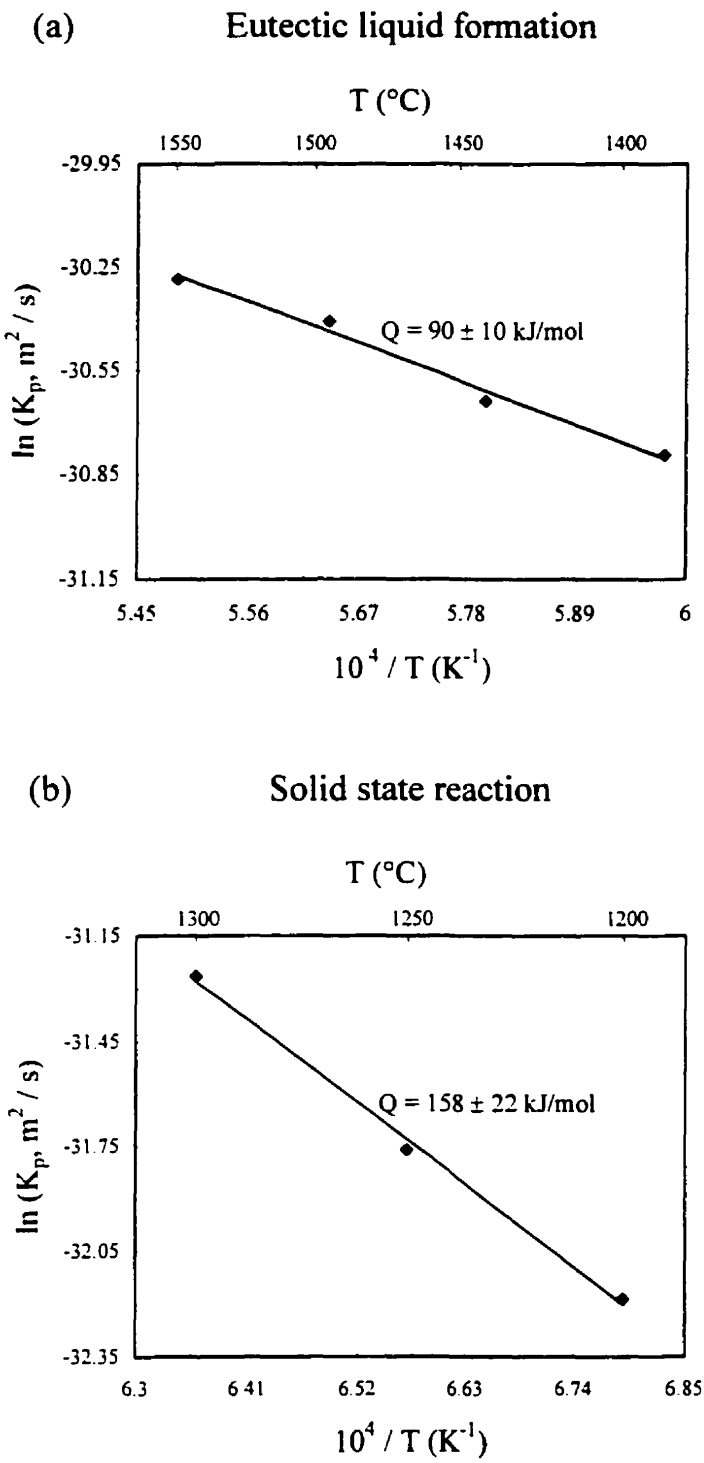

Figure 6.13. Arrhenius plot of the coefficient of penetration, K_p, as a function of temperature for unpolished samples.

Hot pressing using unpolished samples did not result in a significant change in the value of the activation energy. It can be observed from Table 6.2 that, within experimental error, these values for the activation energy are essentially the same. One difference between the curves for polished and unpolished samples was a shift of the frequency factor, K_0, to a lower value for the samples hot-pressed using unpolished samples, which accounts for the thinner interfaces compared to those produced with polished samples. This clearly indicates that diffusion bonding requires not only a surface free of contamination, but also a well polished and flat mating surface is very important to achieved rapid and effective bonding.

Table 6.2. Activation energy and rate constants for polished and unpolished samples.

	Temperature (°C)			
	< 1330		> 1330	
	K_0 (m^2/s)	Q (kJ/mol)	K_0 (m^2/s)	Q (kJ/mol)
Polished	2.714×10^{-11}	123 ± 18	8.051×10^{-10}	72 ± 11
Unpolished	1.408×10^{-11}	158 ± 22	5.983×10^{-10}	90 ± 10

6.4. Mechanical Strength

The strength of diffusion bonded ceramic/metal/ceramic joints depends on the nature and microstructure of the interface between the joining materials. The effect of the joining conditions on the room temperature mechanical properties can be investigated by increasing the specimen size so as to produce standard specimens. In order to establish a mechanical evaluation of joints in hot-pressed Si_3N_4/Ti/Si_3N_4 samples, a series of large samples were hot-pressed and the joint strength was measured using the four-point bending test method. The samples used for bending testing were of 50 mm in length and 7 mm in diameter, and were produced by diffusion bonding of two Si_3N_4 cylindrical samples of 25 mm each with a 0.89 mm Ti-foil sandwiched in between. An example of a test sample is shown in Figure 6.14.

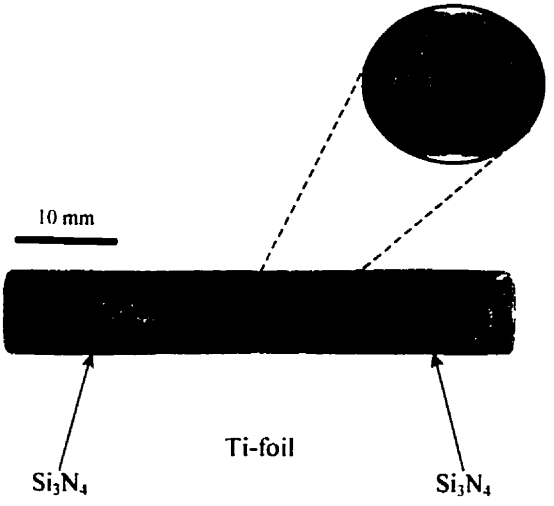

Figure 6.14. Example of a bend test sample hot-pressed at 1500°C and 90 minutes.

The maximum load at fracture was obtained from the load-displacements curves, an example is shown in Figure 6.15. The modulus of rupture (MOR) was calculated for Si_3N_4/Ti/Si_3N_4 samples hot-pressed at 1500°C and times varying from 30 to 180 minutes: the results obtained are shown in Figure 6.16. The error bar corresponds to plus or minus one standard deviation for the average joint strength of at least five samples for each set of experimental conditions.

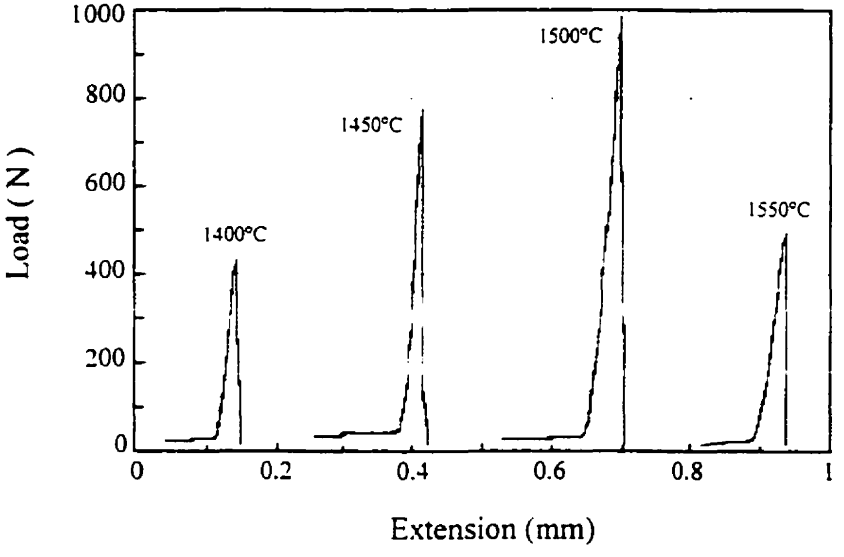

Figure 6.15. Typical load-displacements curves obtained in bending test for samples hot-pressed at various temperatures.

It can be observed that the strength of the joint increased from a value of 17.9 MPa and reached a maximum value of 147 MPa, when the time was increased from 30 to 120

minutes, respectively, and decreased beyond this time. The effect of the growth behavior of the reaction layer of the interface on the strength of the Si_3N_4/Ti/Si_3N_4 samples, can be observed when comparing the results of the interface thickness obtained for samples hot-pressed at 1500°C, Figure 6.6a. The detrimental effect of the thickness of the reaction layer can be observed in the case of samples hot-pressed for three hours, where the strength of the joint decreased compared with that obtained in the case of samples hot-pressed for two hours.

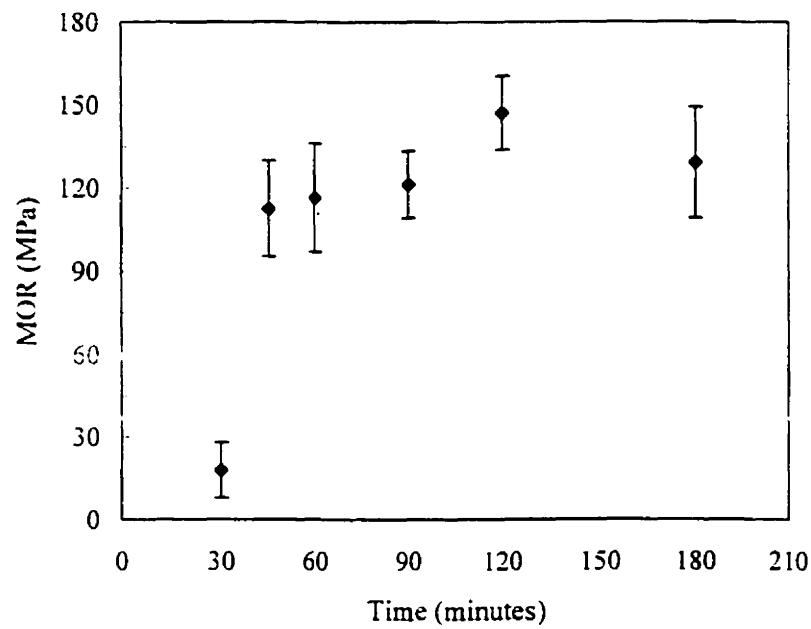

Figure 6.16. Modulus of rupture in function of time for Si_3N_4/Ti/Si_3N_4 samples hot-pressed at 1500°C in vacuum

The effect of the growth of the reaction layer on the modulus of rupture of the Si_3N_4/Ti/Si_3N_4 samples can be more clearly observed in Figure 6.17, which presents the

results of the bending strength as a function of temperature for Si_3N_4/Ti/Si_3N_4 samples hot-pressed under vacuum for a constant time of 120 minutes.

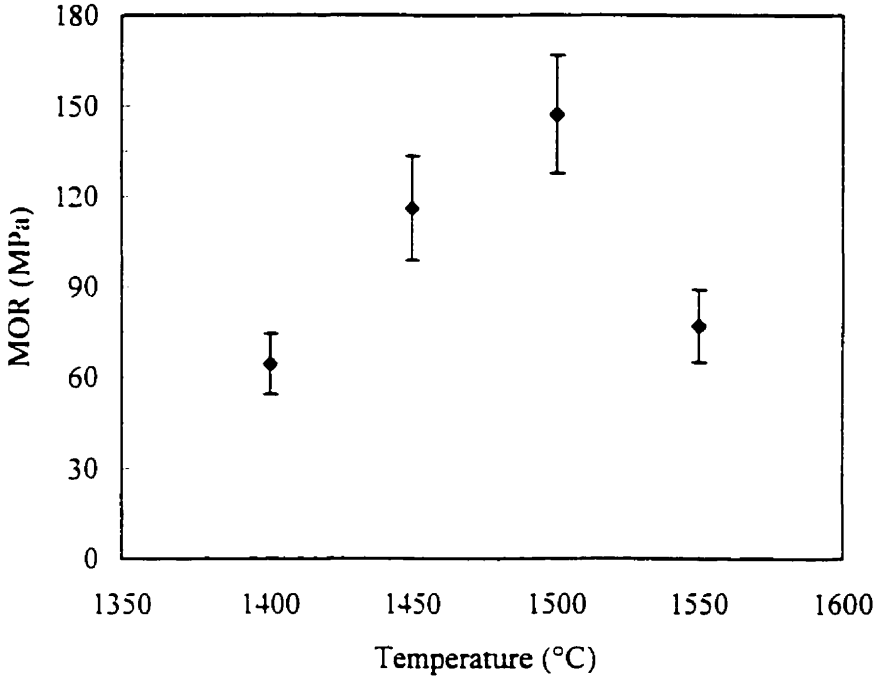

Figure 6.17. Modulus of rupture in function of temperature for Si_3N_4/Ti/Si_3N_4 samples hot-pressed in vacuum for 120 minutes.

The effect of the temperature was more pronounced than the effect of the time. It can be observed that the strength of the joint increased from 64 MPa to a value of 147 MPa when the temperature increased from 1400°C to 1500°C. However, the joint strength decreased, when the temperature was raised to 1550°C. In general, a schematic correlation between joint strength and interfacial microstructure for Si_3N_4/Ti/Si_3N_4 samples hot-pressed at 1500°C is shown in Figure 6.18. It can be observed that increasing the joining time to 120 minutes

increased the average joint strength up to 147 MPa. This improvement was attributed to the increase of interface reaction and formation of a chemical bridge between the two materials. The decrease of joint strength for times of three hours was attributed to the excessive thickness of the reaction layer. In summary, the choice of appropriate conditions to prepare ceramic/metal/ceramic joints requires a knowledge of the mechanism of reaction between the materials and the evolution of the interface. For the case of hot-pressed Si_3N_4/Ti/Si_3N_4 diffusion samples, the strongest joint was obtained for optimum joining conditions of 1500°C and 120 minutes, with a resulting average bending strength of 147 MPa, however excellent joint strengths were produced at 1500°C for times greater than 45 minutes.

All joints fracture samples showed the same type of fracture mode as shown in Figure 6.19. The fracture originated and mainly propagated along the Si_3N_4/reaction zone interface and passed through the Ti metal to the other side of reaction zone/Si_3N_4 interface. The main part of the fracture surface was on the Ti-silicide of the Si_3N_4/reaction zone interface. Ceramics are more brittle, stiffer, and have lower thermal expansion coefficients than metals, thus, the interface between the ceramic and the metal will be in a state of stress when cooled from the joining temperature. If the metal, Ti, undergoes plastic deformation during the cooling cycle, some of the interfacial stresses could be relieved, resulting in an increased joint strength. The amount of the plastic deformation depends on the yield strength of the metal. Generally the lower the yield strength, the more plastic deformation will occur and consequently this could lower the residual stresses. However the interface could have some defect or point of high stress concentration where fracture is initiated.

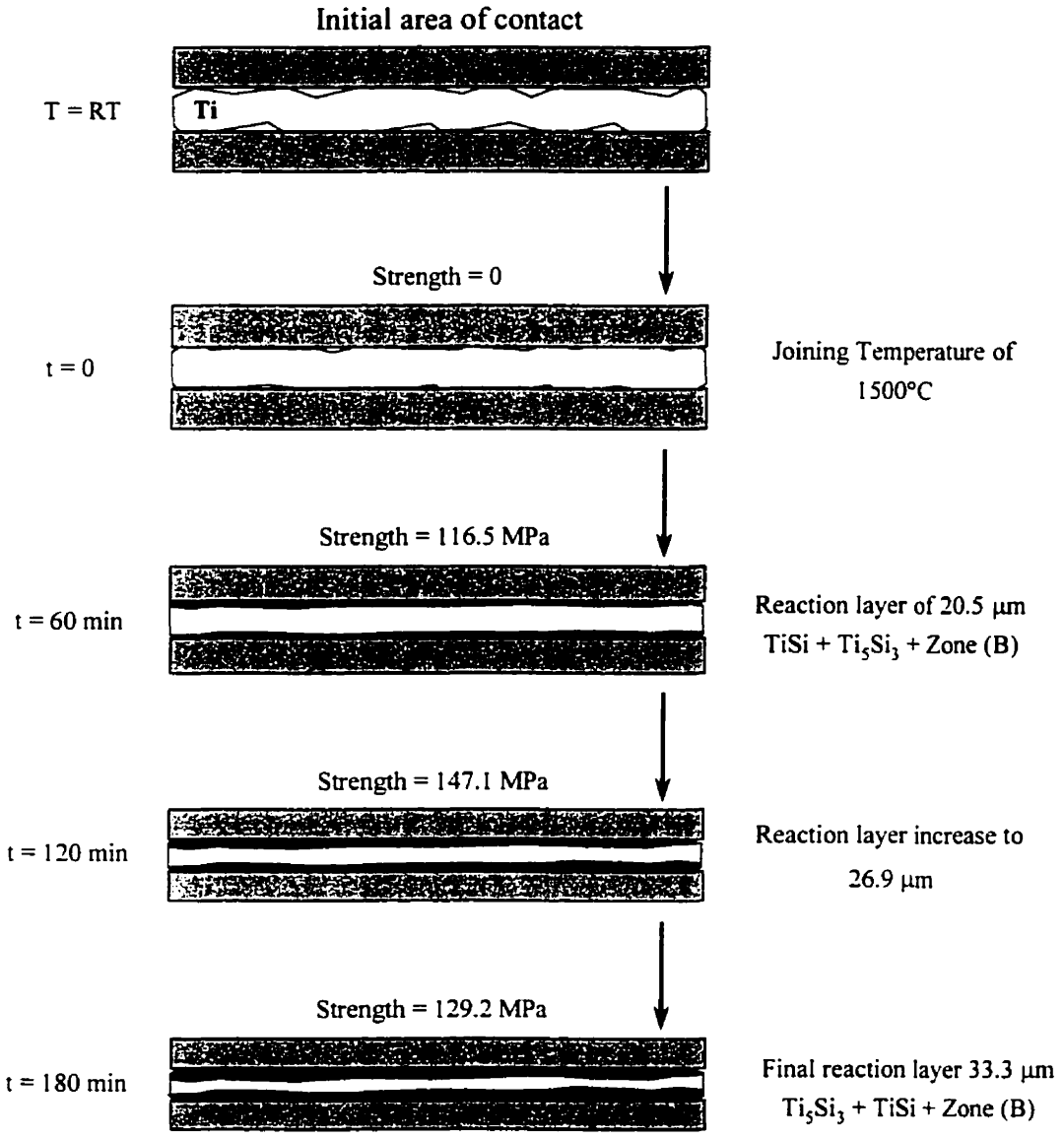

Figure 6.18. Correlation between joint strength and interfacial microstructure for Si_3N_4/Ti/Si_3N_4 samples hot-pressed at 1500°C.

(a) Hot-pressed at 1500°C for 120 minutes

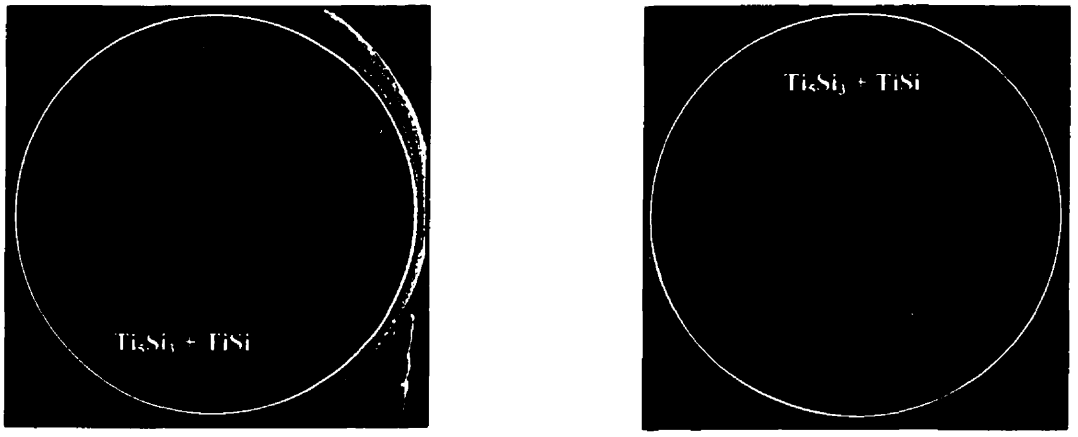

(b) Hot-pressed at 1500°C for 60 minutes

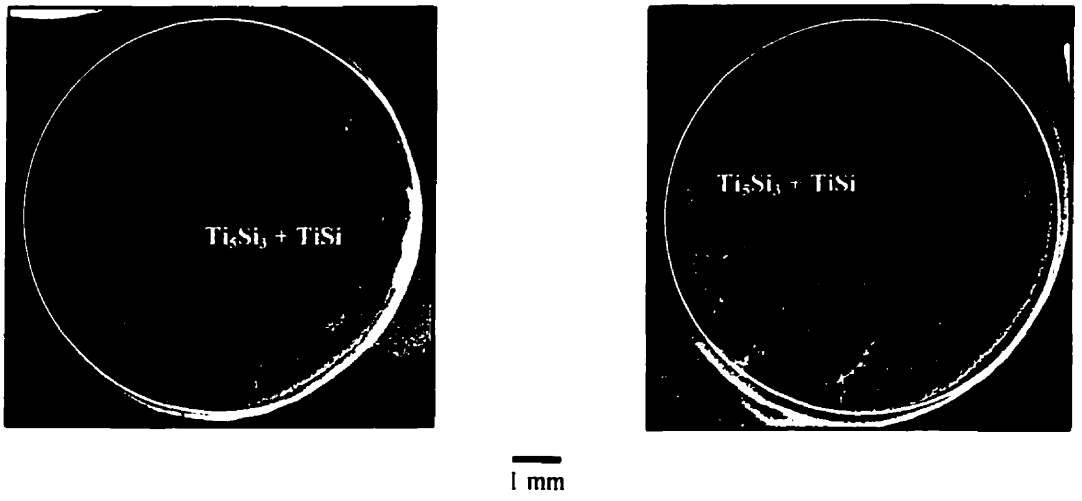

Figure 6.19. Fractograph of Si_3N_4/Ti/Si_3N_4 samples after four-point bending test.

The microhardness of the materials and compounds of the interface were obtained and the results, in ***kg/mm²***, are showed in Table 6.3:

Table 6.3. Vickers Hardness in kg/mm²

β-Si_3N_4	TiN	Ti_5Si_3	TiSi	α-Ti
1754 ± 150	------	976 ± 86	------	1542 ± 125

Unfortunately the value corresponding to TiN could not be obtained due to the thinness of this interlayer. The errors correspond to plus or minus one standard deviation based on 15 tests. The large errors in the measurements reflect the scatter in the data probably resulting from overlapping of phases and surface defects such as scratches and voids. The results for the Si_3N_4 are in good agreement with the starting samples of Si_3N_4, however the result corresponding to Ti is very high compared with the value measured on the starting Ti, (254 ± 35 kg/mm^2).

...Chapter 7:

Discussion

The objective of this chapter is to analyze and discuss the results presented in the previous two chapters. Initially, an examination of the thermodynamic predictions is made in order to establish the accuracy of the current data with other sources. This is followed by an analysis and explanation of the results obtained by hot pressing and interfacial characterization of Si_3N_4/Ti samples. Finally, a mechanism for the interface formation is proposed and a correlation between the mechanical strength of the joint and interfacial growth behavior is presented.

7.1. Interpretation of Joining Behavior

The thermodynamics evaluation of the Si_3N_4/Ti system carried out using F*A*C*T predicts that during the hot-pressing of Si_3N_4/Ti samples carried out in a vacuum (20 Pa)

between 1200°C and 1500°C. Ti_5Si_3 and TiN form according to the following reaction:

$$Si_3N_4 + 9\ Ti = Ti_5Si_3 + 4\ TiN \qquad (7.1)$$

and is thermodynamically more favorable than any other reaction above 1100°C (Figure 5.2). Similar results have been found in thermodynamic analyses carried out for Si-N-Ti system by other authors [40, 107] using different sources of data. In an experimental study Suganuma et al.[108] found TiN and Ti_5Si_3 at the Ti and Si_3N_4 interfaces, respectively, when Si_3N_4/Ti samples were hot-isostatically pressed under a pressure of 100 MPa in vacuum at 1200°C. Because diffusion is the dominating mechanism in solid state joining, silicide transformations may or may not be observed depending on the joining parameters, especially bonding temperature and time. These parameters affect the concentration of diffusing Si at the interface, and therefore, the nature of the resulting silicide. A similar thermodynamic analysis can be made based on the cross-section of the Ti-Si-N phase diagram. Figure 7.1 shows the 1000°C isothermal section of the Ti-Si-N phase diagram [109]. The authors of the diagram in Figure 2.20 [79] state that the tie-lines in their diagram are the same over the range 700°-1000°C, however in Figure 7.1 Ti_2N does not occur.

In a ternary cross-section of a phase diagram, the interface between two materials is represented by a straight line connecting the two components. Everytime the interface intercepts a tie line, a reaction occurs and the corresponding products are the compounds found at the end of the corresponding tie-line and within the compatibility triangle. In this situation the lever rule applies, and it can be used to estimate the relative amounts of each compound. The Si_3N_4/Ti interface intercepts the tie-lines in the points labeled by *(a)*, *(b)*, and

(c), in Figure 7.1. At the extremities of those tie-lines are Ti_5Si_3 and TiN, TiSi and TiN, and $TiSi_2$ and TiN respectively. Thus, the sequence of events proposed by the following equations confirms the observations from the phase diagram.

$$Si_3N_4 + 9\ Ti = Ti_5Si_3 + 4\ TiN \qquad (7.2)$$

$$Si_3N_4 + 7\ Ti = 3\ TiSi + 4\ TiN \qquad (7.3)$$

$$Si_3N_4 + 11/2\ Ti = 3/2\ TiSi_2 + 4\ TiN \qquad (7.4)$$

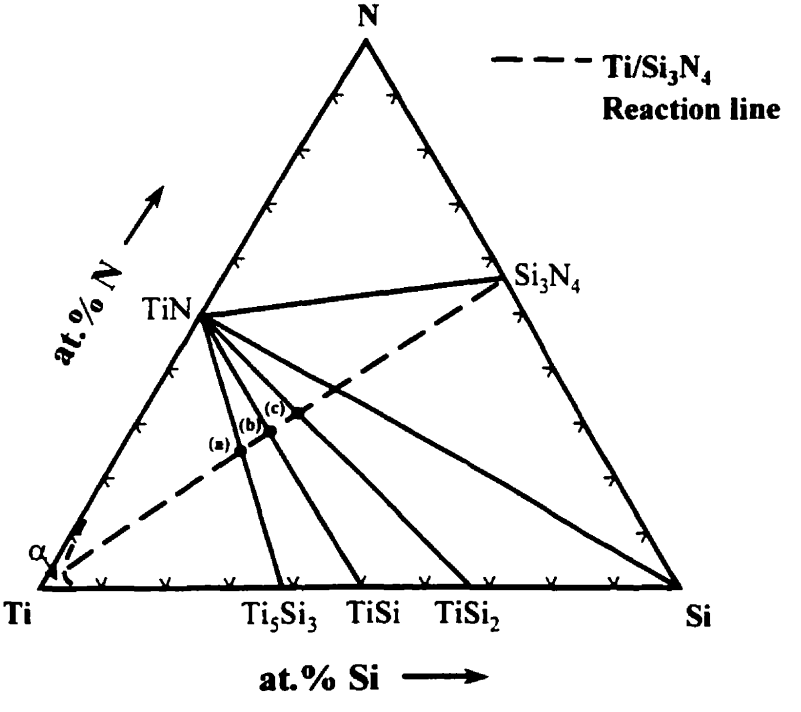

Figure 7.1. Section through the ternary Ti-Si-N phase diagram at 1000°C [109].

The relative concentration of each compound can be calculated from equations *(7.2)*, *(7.3)*, and *(7.4)*, or by the lever rule applied to the tie-lines on Figure 7.1. The products of the reaction expressed by *(7.2)* correspond to Ti_5Si_3 and TiN in a wt.% ratio of 1 to 0.76. This result corresponds to the first reaction between Si_3N_4 and Ti, labeled *(a)*, in Figure 7.1 where the wt.% ratio of Ti_5Si_3 to TiN was calculated to be 1 to 0.73. Subsequently, the interface intercepts a tie-line labeled *(b)*, containing TiSi and TiN in a wt.% ratio of 1 to 1.12. This reaction corresponds to equation *(7.3)*, where the wt.% ratio between TiSi and TiN is 1 to 1.09. In the case of the reaction expressed by *(7.4)*, this corresponds to the formation of $TiSi_2$ and TiN in a wt.% ratio of 1 to1.59. This result corresponds to the reaction between Si_3N_4 and Ti, labeled *(c)*, in Figure 7.1, where the wt.% ratio of $TiSi_2$ to TiN was calculated to be 1 to 1.60. On the other hand, we have to observe that according to the Ti-Si phase diagram (Figure 2.19) liquid can be easily formed at joining temperatures of 1330°C and higher, and precipitation of Ti-silicide would occur when the amount of dissolved Si in the eutectic liquid is sufficient to stabilize the solid phase at the particular temperature of joining. As a consequence, the interface growth rate can be affected drastically due to liquid formation.

In the present work, joining temperature and time were the main parameters studied. The first step in creating an interface is to achieve intimate contact, and subsequently bonding can occur. The driving force for the formation of an interface between materials is the free energy decrease of the system resulting from joining. In solid-state bonding, a mechanical load is applied to establish contact between the materials, however the formation of a continuous interface is mainly determined by the surface finish of the ceramic. Surface irregularities obstruct the formation of a continuous interface, because the metal cannot fill

sharp grooves, even if the plastic deformation is extremely large, interface pores can only be eliminated by transport of matter. The pressure applied to the hot-pressed sample was limited to values between 5 and 20 MPa, since this is in the range of the compressive yield strength of Ti in this temperature range. However no clear effect of the pressure in the bonding of Si_3N_4/Ti was observed. Since joining of Si_3N_4 to Ti occurred at relatively high temperature and Ti-Si liquid formation occurred during the process, this promoted an interfacial reaction and bonding between the materials.

Successful joining of Si_3N_4 to Ti occurred in samples hot-pressed at temperatures greater than 1400°C, (see Table 5.1 and 6.1). Liquid formation can occur at the start of joining, by the interaction of the Si with Ti (at 1330°C and higher) until the amount of Si is enough to stabilize a solid Ti_5Si_3 phase. As a result, the interface growth rate could be fast at the initial stage of the interface formation, contributing to the greater thickness of the reaction layer. On the other hand, liquid would not be formed in samples hot-pressed at temperatures lower than 1330°C, and as a consequence the diffusion rates are lower, due to the absence of liquid, and longer times are necessary to form a joint interface.

Joints are formed through a reactive interface on the Ti side of the sample as a result of diffusion of N and Si and can be explained since diffusion is more difficult in ceramics than in metals [110]. The essential difference between metals and ceramics lies in the nature of the bond type in a ceramic since they are either ionic, covalent or for the majority, iono-covalent. In all cases the cohesion energies are much higher for ceramics than for metals. The nature of these bonds increases the melting point, hardness and brittleness and, consequently decreases the plasticity. In ceramic due to their high melting

point, the number of points defects is generally much less than in metals at the same temperature. That implies very low diffusion coefficients, in comparison to diffusion coefficients measured in metals. Moreover, the nature of the chemical bond of ceramics gives rise to stronger bonding than in metals.

The reaction rates became significant at 1400°C and 1500°C, mainly because diffusion is a thermally activated mechanism and liquid was present during joining. The interfaces consisted of one layer with three intermixed phases. Ti_5Si_3 growths inside the Ti and the formation of TiSi occurred as a consequence of rapid transformation of Ti_5Si_3, which indicates considerable decomposition of Si_3N_4, and an abundant supply of Si, as was anticipated as a result of the thermodynamic analysis of the Ti-Si-N system. On the other hand TiN remains within the interface adjacent to Si_3N_4. Starting from the fact that Si has larger atomic radius (1.18 Å) than N (0.71 Å) one would expect N to diffuse faster than Si and this is contrary to the present observations. However, as can be observed on Figure 7.2a [111, 112] the activation energy for the diffusion of Si in Ti (23.82 kJ/mol) is lower than the corresponding values for the diffusion of N in Ti (141.51 kJ/mol). This indicates that upon joining of Si_3N_4 to Ti, Si would diffuse faster into Ti than N. It has been suggested that in the case of reaction diffusion of nonmetals in transition metals, the rate is determined not by the size of the atom of the diffusing nonmetal species, but by its ionization potential, which characterize the ability of the nonmetal atom to give up its valence electrons in the formation of a common electron group with the atoms of the metal. The lower the ionization potential of the nonmetal species, the easier (lower activation energy), is the reaction and diffusion into the transition metal. Following this argument Si

would be expected to diffuse more rapidly into Ti than N, as a result of its lower ionization potential compared to that of N. Figure 7.2b shows that the ionization potential of Si is 8.14 eV and that of N is 14.51 eV. However, the high affinity of Ti for Si and N resulted in immediate formation of a liquid phase, followed by the precipitation of silicides, initially Ti_5Si_3 and TiN, thus preventing Si from diffusing extensively into the Ti.

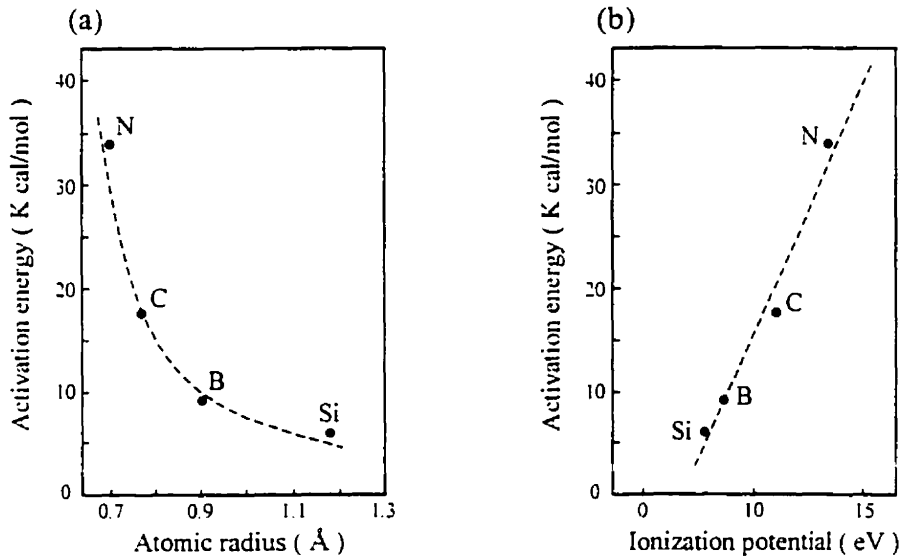

Figure 7.2. Relationships of the activation energies for the diffusion of Si, B, C, and N in Ti, as a function of the (a) atomic radius and (b) ionization potential of the nonmetal species [111, 112].

TiN was identified from the X-ray diffraction analysis of the fracture surfaces (Figure 5.9). A quantitative overview of the different components in the interface was obtained by WDS line analysis using EPMA. This method also resulted in a profile for

oxygen, and consequently, it was possible to establish the presence of oxide phases. These results (illustrated in Figure 5.11) show that Ti was not detected in the Si_3N_4 confirming no Ti diffusion into the ceramic. The presence of high levels of Al, Y, and O in zone (B) would suggest the segregation of the sintering aids to the interface due to the decomposition of Si_3N_4. The latter is most likely to be an amorphous alumino-silicate, since no additional crystalline phases were detected at the interface by the X-ray diffraction analysis (Figure 5.9). The lattice parameters of the different compounds observed at the interface of the Si_3N_4/Ti were also calculated. The results (Table 7.1) showed values of the lattice parameters, for TiSi, Ti_5Si_3, and TiN phases, which are in good agreement with the values reported in the literature for these compounds [112, 113].

7.2. Interface Depth Analysis

As Si_3N_4/Ti interfaces are characterized by a change in composition with sample depth, it is useful to know the effective depth of penetration of X-rays for each compound. X-ray analysis carried out by continuously removing material from the Ti surface for a sample hot-pressed at 1400°C for 90 minutes (Figure 6.4) showed Ti_5Si_3, TiN, and TiSi at the interface. The decrease of the Ti_5Si_3 peaks and increase of TiSi peaks after grinding of materials is attributed to the different degree of penetration of the X-rays into the interface. Figure 7.3 [114] shows the fraction, Gx, of the total diffracted intensity contributed by a surface layer of (a) 5 μm and (b) 10 μm of thickness as a function of 2θ for the different compounds of the Si_3N_4/Ti reaction products.

Table 7.1. Comparison between observed and reported values of the lattice parameters of the compounds forming the interface [112, 113].

Phase	Structure	Lattice Parameters, Å (measure)	Lattice Parameters, Å (literature)
β-Si_3N_4	Hex.	a = 7.678, c = 2.881	a = 7.606, c = 2.909
TiN	Cub.	a = 4.247	a = 4.249
Ti_5Si_3	Hex.	a = 7.437, c = 5.141	a = 7.465, c = 5.162
TiSi	Orthor.	a = 6.405, b = 3.630, c = 5.040	a = 6.544, b = 3.638, c = 4.997
α-Ti	Hex.	a = 2.598, c = 4.970	a = 2.950, c = 4.686

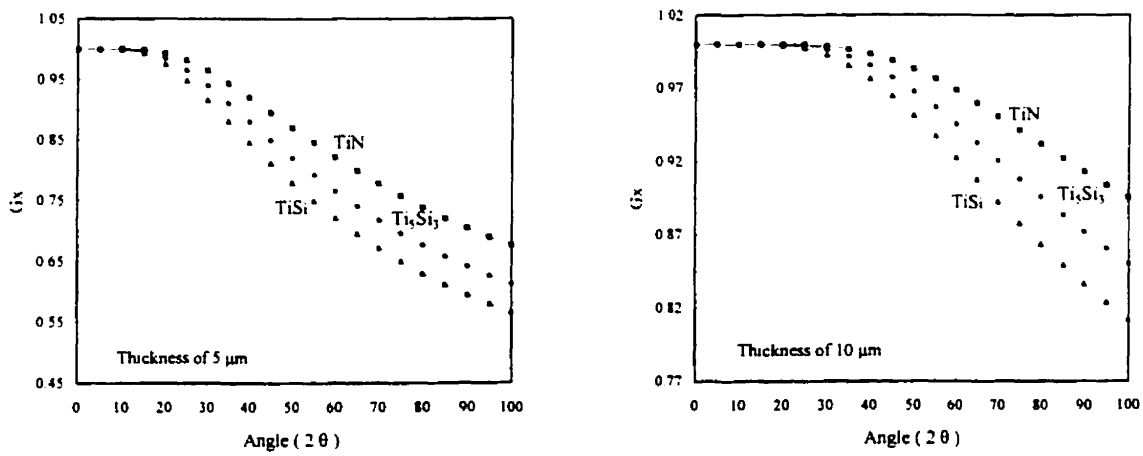

Figure 7.3. Fraction, Gx, of the total diffracted intensity contributed by a layer of (a) 5 μm and (b) 10 μm for the different interface compounds [114].

It can be seen that the information obtained from the diffraction pattern increase or is more clear when the thickness of the layer increases. It was noted that for all three compounds, TiN, Ti_5Si_3, and TiSi, 95% of the X-ray patterns analyzed originated from a layer of about 10 μm, which explains the difficulty in obtaining a clear TiSi spectra. The variation of *Gx* with the angle also accounts for the predominance of TiSi peaks at high diffraction angles. The Ti-Si phase diagram (Figure 2.19) shows the transformation of Ti_5Si_3 to Ti_5Si_4, however there was no evidence of this phase in the X-ray spectra obtained at different depths within the Ti fracture surface.

7.3. Interface Thermal Cracking

Several thermal cracks can be observed within the reaction layer, mainly in the Ti_5Si_3 region (Figure 6.3), which could be attributed to a decrease in volume in relation to the volume of the metal, Ti, during the solidification shrinkage and to the thermal expansion mismatch due to the difference in coefficient of thermal expansion of the interface compounds and the starting materials, Ti and Si_3N_4. When cracking occurs perpendicular to the interface it is characteristic of the mismatch in the thermal expansion properties of the joining materials (Figure 2.23). On the other hand, cracking that occurs parallel to the interface is related to the contraction corresponding to phase transformation. Because of the brittle nature of Ti_5Si_3, cracking resulted and is due to the volume contraction upon cooling.

In addition, the interface showed Ti_5Si_3 in contact with TiSi and Ti, on one side, and TiN on the other (Figure 6.2). From the coefficient of thermal expansion of these phases (Table 2.3 and 4.2), the CTE mismatch $\Delta\alpha$ between TiN and Ti_5Si_3 is 1.65 x 10^{-6} $°C^{-1}$, between Ti_5Si_3 and TiSi is 2.2 x 10^{-6} $°C^{-1}$, and between Ti_5Si_3 and Ti is 2.36 x 10^{-6} $°C^{-1}$. These differences in thermal expansion coefficients associated with the brittle nature of each phase was the main factor that contributed to the formation of cracks in the silicides.

7.4. Joining Mechanisms

Comparing the results of bonding for hot-pressed Si_3N_4/Ti (Table 5.1), and Si_3N_4/Ti/Si_3N_4 samples (Table 6.1), some variations can be observed. In both cases, bonding was not observed in samples hot-pressed for temperature lower than 1400°C. At 1300°C, for example, even for holding times up to six hours, strength of the bonded interface was insufficient to establish a reliable mechanical joint between the ceramic and the metal. The formation of a liquid phase when the samples were hot-pressed at temperatures of 1330°C and higher, improved the joining, mainly because it increased the initial area of contact between the materials and because the diffusion coefficients are higher in the liquid than in the solid for the same species. As a consequence, longer times were necessary when the samples were hot-pressed at temperatures lower than 1330°C, where a solid-state reaction takes place.

Si_3N_4 was successfully joined to Ti for temperatures higher than 1400°C. However the strength of the joint observed in the Si_3N_4/Ti/Si_3N_4 sandwich samples was higher than the single Si_3N_4/Ti samples. In the latter case, some samples debonded during cooling or during sample preparation. Several reasons for this difference are possible. One reason could be attributed to thermal expansion mismatch produced by the difference in thickness of the Ti metal as well as the configuration of the hot-pressed samples. Thermal expansion mismatch usually induces tensile stresses in the ceramic adjacent to the interface that promote failure of the joint, the stresses decrease in magnitude as the relative metal thickness decreases so that thin metal layers can be used to reduce thermal expansion mismatch [115]. This could result in the development of differential residual stresses in the interface, which would be higher in Si_3N_4/Ti than that in Si_3N_4/Ti/Si_3N_4 joints, however absolute values are difficult to calculate.

Therefore, the sequence of reaction within a Si_3N_4/Ti interface can be summarized as follows: when Ti comes in contact with Si_3N_4, it decomposes into Si and TiN, however the interaction of Ti with Si produces liquid, when the joining temperature is higher than 1330°C, followed by precipitation of Ti_5Si_3 as the liquid saturates with Si. The next step in the reaction should be the formation of Ti_5Si_4, as reported for experiments on siliconizing of Ti [116], however no evidence of this phase was found and the addition of Si resulted in the transformation of Ti_5Si_3 into TiSi. There was no evidence of gas bubble formation at the interface.

7.5. Interface Growth and Surface Roughness

The main process parameters in diffusion bonding are temperature and time. Temperature is, however, the most important one due to the fact that in thermally activated processes, a small change in temperature can result in a large change in process kinetics compared with other parameters.

The growth behavior of the Si_3N_4/Ti interfaces as a function of time can be observed in Figure 6.6. These results suggest that diffusion of Si and N into Ti was immediately followed by reaction, which contributed to the growth of the interfaces. The interfaces grew in a parabolic fashion, which is characteristic of processes of reactive diffusion through an interface that is growing. As diffusion mechanisms are thermally activated processes, increasing the temperature from 1200°C to 1500°C resulted in substantial mass transport across the interface and faster growth of the reaction zones. Temperature increases interaction across a metal/ceramic interface by increasing the mobility of atoms and also the mobility of dislocations in the metal during bonding. Since the mobility of dislocations increases with temperature, then the pressure required for bonding decreases with increasing temperature [117]. On the other hand, the initial interaction of Ti with Si results in a liquid formation, on the surface of the Ti contributing to the fast grow rate of the interface when the samples are hot-pressed at temperatures of 1330°C and higher. This contrasts with samples hot-pressed at temperatures lower than 1330°C where liquid formation would not occur and longer times for bonding were necessary. Therefore, an increase in joining temperature should generally enhance bonding

or increase the reaction layer of a metal/ceramic interface for a given pressure and time.

The effect of the surface roughness on interface growth of the reaction products as a function of holding time is shown in the plot of the average thickness of the interface obtained for unpolished $Si_3N_4/Ti/Si_3N_4$ samples hot-pressed at 1500°C and shown in Figure 6.11. As for polished samples the interface grew in a parabolic fashion. Comparing the results of the interface formation as a function of temperature using both polished and unpolished materials (Figure 6.12), it can be observed that there is a difference in the absolute values of the interface thickness of hot-pressed samples, which is lower for unpolished materials than for polished samples, because of the difference in the initial area of contact. For both polished and unpolished samples, the thickness of the interfaces is an exponential function of the joining temperature.

Since bonding mainly occurs within the interface, the results show that surface roughness plays an important role in the diffusion bonding processes, especially when the samples were hot-pressed at temperatures lower than 1330°C. For a rough surface, deformation of the metal differs greatly from the case of a polished surface. In general, asperities prevent large-scale plastic deformation at the surface because the metal is anchored between the asperities. This greatly limits the development of metal/ceramic contact and adversely affects the strength of the interface [51]. The initial surface contact of polished and unpolished specimens during diffusion joining is schematically shown in Figure 7.4 [118].

In the case of high surface roughness (Figure 7.4b) atomic diffusion across the interface can occur in region I where as no mass transport occurs across the gap in region

II. Therefore surface diffusion, or plastic deformation or creep must occur within the interface in order to promote effective joining. On the other hand, if the specimen surfaces are well prepared with very low roughness (Figure 7.4a) the local contact area increases. However, for the case of bonding samples at temperatures higher than 1330°C, where a eutectic liquid formation occurs within the interface, the effect of surface roughness is reduced due to the liquid penetrating the voids and increasing the contact area.

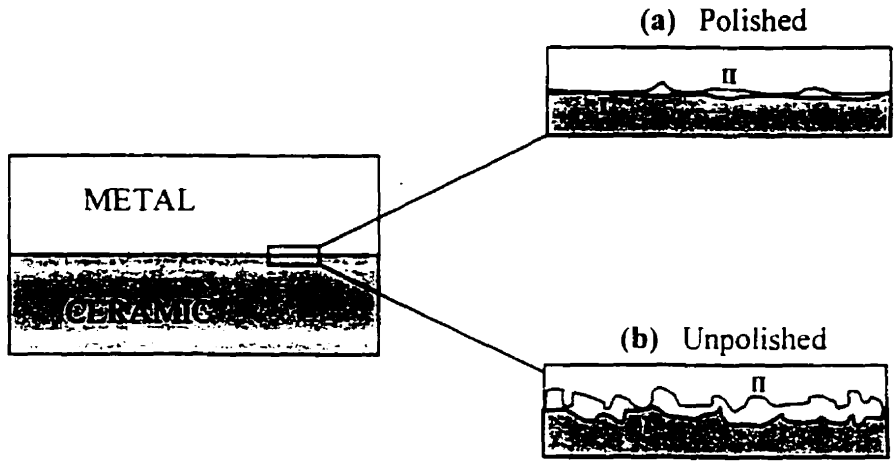

Figure 7.4. Schematic representation of the state of surface contact in polished and unpolished samples.

Comparing the microstructural evolution of $Si_3N_4/Ti/Si_3N_4$ interfaces after joining, using polished and unpolished samples, indicated that the same sequence of events occurred in both cases. However, in order to obtain successful joining of Si_3N_4 to Ti using

unpolished samples, higher temperatures and longer times were required to obtain the same microstructures compared to polished samples. However the same reaction products were observed in both cases. This clearly indicates that diffusion bonding is accelerated not only by a surface free of contamination, but also intimate contact between the matching materials.

7.5.1. Interface Growth Kinetics

The activation energy, Q, for the formation of Si_3N_4/Ti interfaces was calculated from the slope of the Arrhenius curves obtained for vacuum conditions in polished and unpolished samples as shown in Figure 6.7 and 6.13 respectively. In the case of polished samples an activation energy of 72 ± 11 kJ/mol was obtained, associated with samples hot-pressed involving liquid formation, and a higher value of 123 ± 18 kJ/mol was obtained associated with the solid-state reaction. Hot pressing using unpolished samples did not result in a significant change in the value of the activation energy of 90 ± 10 kJ/mol associated with the liquid formation mechanism, and a value of 158 ± 22 kJ/mol was obtained in the case of a solid-state reaction mechanism. One difference between the curves for polished and unpolished samples was a slight shift of the frequency factor, (pre-exponential term K_0), to a lower value for the samples hot-pressed using unpolished samples, which accounts for the thinner interfaces compared to the specimens produced with polished materials. It can be observed that, within experimental error, the corresponding values for the activation energy for unpolished and polished samples are

essentially the same. The lower activation energy obtained in samples hot-pressed at high temperature (>1330°C) compared with samples hot-pressed at lower temperatures (<1330°C), is associated with the formation of a liquid phase and as a consequence an increase in the diffusion coefficient.

The values of the activation energy in the case of solid-state reaction mechanism are of the same order of magnitude of previousiy results reported (146 ± 30 kJ/mol) for a diffusion bonding system using Ti interlayer, in the AlN/Ti/AlN system joined in the range of 1050°C to 1200°C [119]. The interpretation of activation energies is a controversial topic. While some researchers have reported that the resulting value of activation energy depends solely on the dominating diffusion mechanism [52], others have reported that the activation energy of atomic diffusion for the diffusion bonding process depends not only on the atomic species, but also on the environment [64]. Furthermore, it has been suggested that the activation energy for the formation of interfaces can be obtained by simply summing the energy terms corresponding to the decomposition of the ceramic, and those associated with diffusion of the atomic species. Comparing the activation energy for the formation of Si_3N_4/Ti interfaces produced in the solid-state (123 ± 18 kJ/mol for polished and 158 ± 22 kJ/mol for unpolished) with the activation energy for the solid-state diffusion of N into Ti (141.51 kJ/mol), it can be noted that the values are similar. This would suggest that the value of activation energy depends on the dominating diffusion mechanism, in this particular system. However a more complete assessment would require the values of the activation energy for the diffusion of N through Ti_5Si_3 and Si through TiN, which are not available in the literature.

Hot-pressing using polished and unpolished samples did not result in a significant change in the value of the activation energy, indicating that the activation energy is associated with the diffusion mechanism, which remains the same in both samples. Therefore, the activation energy for the formation of interface is directly related to the slowest diffusion process. Nevertheless, the difference in the starting surface contact area affected the extent of reaction/diffusion but not the value of the activation energy for the formation of those interfaces.

7.6. Interpretation of Joint Strength

The effect of a reaction layer on the interface strength depends on a number of factors such as the mechanical properties of the reaction layer, its thickness and morphology, the strength of the interfacial bond and the mode of loading at the interface. Reactions formed at metal/ceramic interfaces include solid solutions, amorphous and crystalline phases. Each of these reaction products forms a different type of interface between the metal and ceramic and the relative efficiency of these various types of reaction products on the strength of metal/ceramic interfaces is not fully understood. However, most reaction layers are brittle and therefore potentially detrimental to the interface properties. Although the concentration of residual stresses in joints is a function of the joining temperature, the thickness of the reaction zone may dominate in the final strength. To verify this assumption, plots of modulus of rupture, MOR, as a function of time for

sandwich $Si_3N_4/Ti/Si_3N_4$ samples hot-pressed at 1500°C and different bonding temperatures are shown in Figures 6.16 and 6.17, respectively. Excellent joint strength for samples hot-pressed at 1500°C after 45 minutes is noted, reaching values of greater than 100 MPa, even for holding time of up to three hours. A schematic correlation between joint strength and interfacial microstructure for $Si_3N_4/Ti/Si_3N_4$ samples hot-pressed at 1500°C is shown in Figure 6.18. Samples hot-pressed for two hours at different bonding temperatures indicate an acceptable joint strength even at 1450°C, however the joint strength was somewhat lower for samples hot-pressed at 1400°C and 1550°C, where the average joint strength was about 60 MPa.

Reaction products are generally brittle and as the thickness of these phases increases, the joint strength, at first rises and then reaches a maximum at a certain thickness and then decreases as the interface continues to grow. Therefore, the reaction layer thickness must be controlled to enhance joint strength. An indication that the amount of reaction and consequently the thickness of the reaction zone drastically affected the joint strength of Si_3N_4/Ti joints is illustrated in Figure 7.5, which shows the relationship between the joint strength as a function of the reaction products thickness for samples hot-pressed at 1500°C.

It is clear that the amount of interfacial reaction played a major role in determining the final mechanical properties of the joints. Furthermore, the nature of the reaction products may also have influenced the mechanical properties of the joints. The mechanical properties of a metal/ceramic interface depend upon many factors such as the elastic

properties of the metal and ceramic, the thickness of the metal layer, the specimen geometry and the mode of loading. In addition, residual stresses due to elastic and thermal mismatch are associated with most metal/ceramic interfaces.

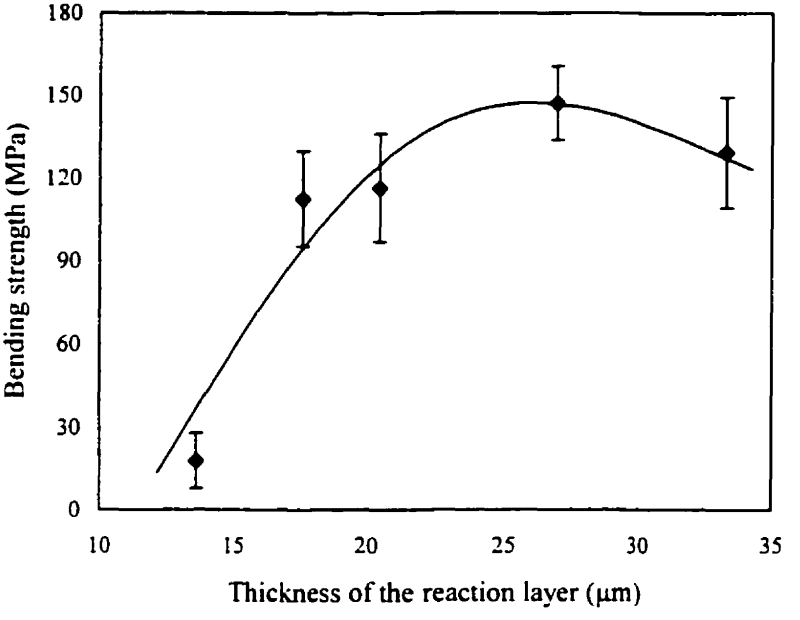

Figure 7.5. Change of joint strength with reaction layer thickness for Si_3N_4/Ti/Si_3N_4 joints hot-pressed at 1500°C.

In summary, the choice of suitable conditions to prepare ceramic/metal/ceramic joints, requires a knowledge about the mechanism of reaction between the materials and the evolution of the interface. For the case of hot-pressed Si_3N_4/Ti/Si_3N_4 diffusion samples, strong bonding was obtained for the joining conditions of 1450°C for 120 minutes, and

1500°C for times greater than 45 minutes with a resulting average bend strength of higher than 100 MPa. The maximum value of 147 MPa was obtained for samples hot-pressed at 1500°C and 120 minutes. This strength is of the same order as the bending strength reported for diffusion bonding of Si_3N_4/Si_3N_4 joints using a ZrO_2 interlayer made at 1550°C and 60 minutes (175 MPa) [52], and higher than that reported for brazing of Si_3N_4 to different metals, i.e. Mo/Si_3N_4 joints brazed with Cu-5%Cr alloy reports 120 MPa [34].

Fractography of the joints showed the same mode of fracture and is illustrated in Figure 6.19. Fracture originated and mainly propagated through the Si_3N_4/reaction interface zone and passed into the Ti metal to the other side of reaction zone/Si_3N_4 interface. The fracture surface was mainly on the titanium silicide side of the Si_3N_4/reaction zone interface and probably initiated at the edge of the sample. Edges and corners are a major source of failure for metal/ceramic interfaces when there is a mismatch in either the thermal expansion or elastic modulus of the metal and ceramic [120]. When a metal has either a larger thermal expansion coefficient or a lower modulus than the ceramic or both (which is often the case), the unconstrained metal develops a smaller lateral expansion at the interface than the ceramic. In order to maintain continuity at the interface, the metal must be uniformly extended by the application of edge forces. Surface forces which are equal in magnitude but opposite in sign must then be applied to the metal in the bonded state to achieve a stress-free conditions at the surface and this introduces large normal and shear stresses near the edge of the metal/ceramic joint [115]. A mismatch in modulus generates interfacial tensile stresses at the edge and thus always enhances the propensity to fracture.

7.7.1. Microhardness

Table 7.2 shows a comparison between the observed and reported microhardness values for the compounds in the interface. For non-reactive systems, the interface is formed by the development of van del Waals forces or it consists of very thin diffusion layers. In such cases, joint strength is primarily a function of the fraction of bonded surface [70]. However, reactive systems such as Si_3N_4/Ti, develop reaction zones which may be detrimental to the strength of the joints.

Table 7.2. Comparison between observed and reported values of the microhardness of the compounds in the interface.

Phase	Microhardness kg/mm^2 (measured)	Microhardness kg/mm^2 (liter.)
β-Si_3N_4	1754 ± 150	1800
TiN	——	2050
Ti_5Si_3	976 ± 86	986
TiSi	——	1039
α-Ti	1542 ± 125	175

It can be seen that the microhardess measured for β-Si_3N_4 and Ti_5Si_3 are in good agreement with the values reported in the literature, however the microhardness measured

in the case of Ti is very high compared with the values reported in the literature. This can be associated with the content of interstitial alloying elements, (as N_2 and O_2) in the Ti. The solubility of N_2 in Ti is very high and during the joining process the interaction of Ti with N_2 could result in the formation of TiN and in the dissolution of N_2 in Ti increasing the final microhardness of Ti. On the other hand, some oxidation of the Ti could occur during the joining experiments increasing the content of dissolved O_2 in Ti. Figure 7.6 shows the effect of interstitial element content on strength of Ti. It can be seen that the strength of Ti increases significantly with interstitial N_2 and O_2 content.

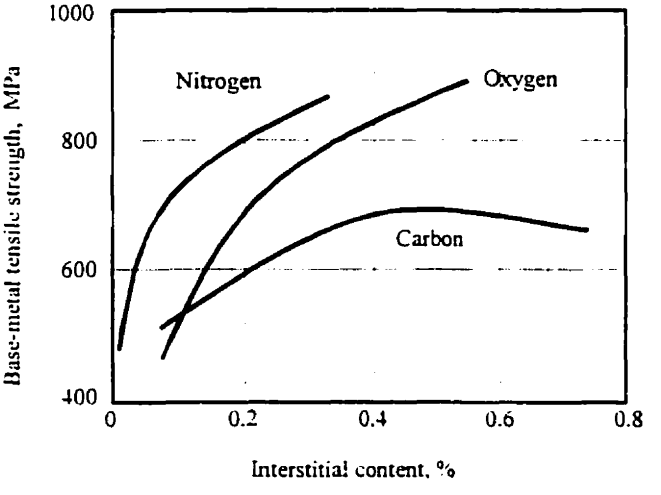

Figure 7.6. Effect of interstitial element content on strength of Ti [23, 25].

Silicides have relatively low values of physical properties, compared with nitrides. The microhardness of silicides is much less than the microhardness of nitrides. These

differences are due to the difference in the nature of the silicides, on the one hand, and nitrides on the other. As is well known, the silicides are typical substitutional phases, the substitution of the metal atoms, Ti in the present case, ($r_{(Ti)}$ = 1.32 Å) by the smaller Si atoms ($r_{(Si)}$ = 1.18 Å) facilitates shear deformation, affecting in a decisive manner the hardness and melting point of the silicides. On the other hand, nitrides are structurally interstitial types of phases, and in such structures, shear deformation is difficult, affecting the hardness of the nitride [121].

Chapter 8:

Conclusions

This chapter presents the conclusions that have been drawn from a series of Si_3N_4/Ti and Si_3N_4/Ti/Si_3N_4 diffusion samples hot-pressed using different experimental parameters such as, joining temperature, time, and pressure, as well as surface roughness of the joint materials. Conclusions drawn from the characterization and mechanical evaluation of the corresponding ceramic/metal interfaces of the joints are also presented.

8.1. Conclusions on Si_3N_4/Ti Joints

From the results obtained during hot-pressing of Si_3N_4/Ti samples, the following conclusions can be drawn:

- Ti could not be bonded to Si_3N_4 when hot-pressed at temperatures lower than 1400°C

for the different holding times studied; the samples always peeled apart at the interface resulting in two fracture surfaces.

- Successful joining of Si_3N_4 to Ti occurred at temperatures higher than 1400°C by the formation of a reactive interface on the metal side of the joint.

- In general, the phases present at the interfaces can be predicted on the basis of thermodynamic considerations, however some differences between the thermodynamic analysis performed on the Si-N-Ti system and the experimental observations are found.

- At temperatures higher than 1330°C, liquid formation occurred by the interaction of Si with Ti and the high affinity of Ti for Si resulted in the rapid formation of silicides, initially Ti_5Si_3. The diffusion of N into Ti resulted in TiN formation.

- Results obtained from X-ray diffraction on Si_3N_4 and Ti fracture surfaces confirmed the presence of Ti_5Si_3, TiSi and TiN at the joint interface. Lattice parameters values obtained for these phases are in good agreement with those reported in the literature.

8.2. Conclusions on $Si_3N_4/Ti/Si_3N_4$ Joints

On the basis of the results obtained during hot-pressing of $Si_3N_4/Ti/Si_3N_4$ sandwich samples, the following conclusions can be drawn:

- Eutectic liquid formation plays an important role in promoting bond and interface formation between Si_3N_4 and Ti samples hot-pressed at temperatures higher than 1330°C. On the other hand, liquid was not formed in samples hot-pressed at temperatures lower than 1330°C, and consequently very long times (> 9 hours) were necessary to form an interface.

- There was no evidence of the transformation of Ti_5Si_3 to Ti_5Si_4 in the X-ray spectrum obtained at different depths within the Ti fracture surface for samples hot-pressed at 1400°C and 90 minutes.

- The interfacial growth rate thickness of the reaction layers follows a parabolic rate law for both polished and unpolished materials and for both samples bonded at temperatures above and below 1330°C.

- The surface roughness of the starting materials is an important factor affecting the extent of the interface growth. For similar joining conditions, hot-pressing of samples using unpolished materials produced thinner interfaces than polished samples.

- The activation energy for the formation of Si_3N_4/Ti interfaces was not affected significantly by the surface roughness of the materials. In the case of hot-pressed samples involving liquid formation, activation energies of 72 ± 11 kJ/mol and 90 ± 10 kJ/mol were obtained for polished and unpolished samples, respectively. Higher activation energies, 123 ± 18 kJ/mol for polished and 158 ± 22 kJ/mol for unpolished samples, were obtained in the case of hot-pressed samples involving solid-state reaction.

- The amount of reaction between Si_3N_4 and Ti was an important factor in the mechanical reliability of the joints. Initially, the bend strength of Si_3N_4/Ti/Si_3N_4 joints produced at 1500°C increased with holding time to a maximum average value of 147 MPa, obtained for samples hot-pressed for 120 minutes. Increasing the joining time further caused a decrease of the joint strength.

- Bending tests performed on Si_3N_4/Ti/Si_3N_4 joints hot-pressed at different joining temperatures confirmed that there is an intimate relationship between the thickness of the interface and joint strength. Excessive growth of the reaction layer decreased joint strength, however strong bonding was obtained for joining conditions of 1450°C for 120 minutes, and 1500°C for times greater than 45 minutes, with an average bend strength of greater than 100 MPa.

Contribution to Original Knowledge

The present thesis has addressed several important aspects of the diffusion bonding of Si_3N_4 to Ti for the first time. Through the investigation of the critical process parameters involved in the application of Ti-foil for the joining of Si_3N_4 to Si_3N_4, a thorough description of the diffusion bonding technique as applied to these materials was developed.

The following are the most important contributions to original knowledge achieved in this study:

- Microstructural evolution of the interfaces of diffusion samples was studied as a function of joining parameters including temperature, time, and surfaces roughness, and the results were correlated with the thermodynamic behavior of the system.

- Crystal structure of the different reaction products was studied by successive X-ray diffraction analyses of the interface as well as the distribution of atomic species across the interface was investigated by EPMA.

- The surface roughness of the joining materials was measured by the atomic force microscope technique (AFM), for the first time and a relationship between sample preparation and interface growth behaviour of the resulting interfacial reaction was established.

- The activation energies for the interface formation of hot-pressed samples were calculated in both ranges of temperatures, lower and higher than 1330°C, using both polished and unpolished materials, establishing that the activation energy is associated with the diffusion/reaction mechanisms, which remains the same in both samples.

- Evaluation of joint quality and strength was measured as a function of experimental parameters. Optimization of the joint strength was investigated, assessing the optimum joining conditions in terms of holding time and temperature under which strong $Si_3N_4/Ti/Si_3N_4$ joints could form.

References

1. Engineered Materials Handbook, ***"Ceramics and Glasses"***, Vol. 4, ASM International, Materials Park, USA, 1991.

2. D.W. Richerson, Modern Ceramic Engineering, 2nd Edition, Marcel Dekker, New York, USA, 1992.

3. A.P. Tomsia, ***"Ceramic/metal joining for structures and materials"***, J. Phys. IV, Vol. 3, Nov. 1993, p. 1317-1326.

4. N.D. Tinsley, J. Huddleston, and M.R. Lacey, ***"The reduction of residual stress generated in metal-ceramic joining"***, Mater. Manuf. Proc., Vol. 13, No. 4, 1998, p. 491-504.

5. D. Tréheux, P. Lourdin, V. Guipont, and D. Juvé, ***"Mechanical behaviour of metal-ceramic bonds"***, J. Phys. III, Vol. 4, Oct. 1994, p. 1883-1898.

6. S.D. Peteves and M.G. Nicholas, ***"Evaluation of brazed silicon nitride joints: Microstructure and mechanical properties"***, J. Am. Ceram. Soc., Vol. 79, No. 6, 1996, p. 1553-1562.

7. M. Ueki, Y. Sato, and K. Fukuda, ***"Practical application of silicon nitride ceramics for sliding parts of rotary engine"***, Key Eng. Mater., Vol. 89-91, 1994, p. 725-730.

8. A.G. Foley, ***"Ceramic joining applications in gas turbines"***, Industrial Ceramics, Vol. 19, 1999, p. 193-195.

9. N.L. Loh and Y.L. Wu, ***"Diffusion bonding of ceramics to metals"***, Mater. Manuf. Proc., Vol. 8, No. 2, 1993, p. 159-181.

10. K. Suganuma, ***"Joining non-oxide ceramics"***, Eng. Mater. Handbook, Vol. 4, 1991, p. 523-531.

11. L.M. Sheppard, ***"Hot new applications for ceramics"***, Adv. Mater. Process, Vol. 11, Sept. 1985, p. 39-43.

12. Kirk-Othmer, Ceramic Encyclopedia of Chemical Technology, 3rd edit., Vol. 5, New York, Wiley, 1979.

13. R.A.L. Drew, ***"Silicon nitride and sialon ceramics–A review"***, Canadian Metallurgical Quarterly, Vol 27, No. 1, 1988, p. 59-64.

14. M.M. Julian and G.V. Gibbs, ***"Bonding in silicon nitrides"***, J. Phys. Chem., Vol. 89, No. 25, 1985, p. 5476-5480.

15. G. Ziegler, J. Heinrich, G. Wotting, ***"Review–Relationships between processing, microstructure and properties of dense and reaction-bonded silicon nitride"***, J. Mater. Sci., Vol. 22, 1987, p. 3041-3086.

16. H.M. Jennings, ***"Review on reactions between silicon and nitrogen –Part 1 Mechanisms"***, J. Mater. Sci., Vol. 18, 1983, p. 951-967.

17. J. Weiss and W.A. Kaysser, ***"Liquid phase sintering"***, Progress in Nitrogen Ceramics, M. Nijhoff Pub., Boston, USA, 1983, p. 169-186.

18. G. Ziegler, ***"Thermo-mechanical properties of silicon nitride and their dependence on microstructure"***, Mater. Sci. Forum, Vol. 47, 1989, p. 162-203.

19. G. Ziegler, J. Heinrich, and G. Wotting, ***"Relationships between processing, microstructure and properties of dense and reaction-bonded silicon nitride"***, J. Mater. Sci., Vol. 22, No. 9, 1987, p. 3041-3086.

20. N.L. Hecht, D.E. McCullum and G.A. Graves, ***"Investigation of selected silicon nitride and silicon carbide ceramics"***, Ceram. Eng. Sci. Proc., Vol. 9, No. 9-10, 1988, p. 1313-1332.

21. C. Chatfield, T. Ekstrom and M. Mikus, ***"Microstructural investigation of alpha-beta yttrium sialon materials"***, J. Mater. Sci., Vol. 21, 1986, p. 2297-2307.

22. E. Tani, S. Umebayashi, K. Kishi, K. Kobayashi, and M. Nishiyima, ***"Gas-pressure sintering of Si_3N_4 with concurrent addition of Al_2O_3 and 5 wt% rare earth oxide: high fracture toughness Si_3N_4 with fiber-like structure"***, Am. Ceram. Soc. Bull., Vol. 65, No. 9, 1986, p. 1311-1315.

23. M.J. Donachie, Jr., Titanium –A Technical Guide, ASM International, Metals Park, USA, 1988.

24. R.R. Boyer, ***"Titanium and titanium alloys"***, Metals Handbook 9th Edition, Vol. 9, 1985, p. 458-461.

25. R.R. Boyer, G. Welsh, E.W. Collings, ***"Titanium alloys"***, Materials Properties Handbook, ASM International, 1994.

26. R.E. Loehman, Ed., Characterization of Ceramics, Managing Ed. L.E. Fitzpatrick, Boston, Butterworth-Heinemann, Greenwich, Manning, 1993.

27. M.L Santella, ***"A review of techniques for joining advanced ceramics"***, Ceramic Bulletin, Vol. 71, No. 6, 1992, p. 947-954.

28. R.E. Loehman, A.P. Tomsia, ***"Joining of ceramics"***, Ceramic Bulletin, Vol. 67, No. 2, 1988, p. 375-380.

29. G. Elssner and G. Petzow, ***"Metal/ceramic joining"***, ISIJ International, Vol. 30, No. 12, 1990, p. 1011-1032.

30. M.G. Nicholas, D.A. Mortimer, ***"Ceramic/metal joining for structural applications"***, Mat. Sci. Tech., Vol. 1, Sep. 1985, p. 657-665.

31. R.E. Loehman, A.P. Tomsia, J.A. Pask, and S.M. Johnson, ***"Bonding mechanisms in silicon nitride brazing"***, J. Am. Ceram. Soc., Vol. 73, No. 3, 1990, p. 552-558.

32. M.G. Nicholas, Joining Processes–Introduction to Brazing and Diffusion Bonding, Kluwer Academic Publishers, Boston, 1998.

33. M.G. Nicholas, ***"Joining Structural Ceramics"***, Designing Interfaces for Technological Applications, (S.D. Peteves, Ed.) Elsevier Appli. Sci., Amsterdam, 1989, p. 49-76.

34. T. Okamoto, ***"Interfacial structure of metal-ceramic joints"***, ISIJ International Vol. 30, No. 12, 1990, p. 1033-1034.

35. J.M. Howe, ***"Bonding, structure and properties of metal/ceramic interfaces"***, Mater. Res. Soc. Symp. Proc., Vol. 314, 1993, p. 27-37.

36. K. Suganuma, T. Okamoto, and M. Koizumi, and M. Shimada, ***"Method for preventing thermal expansion mismatch effect in ceramic-metal joining"***, J. Mater. Sci. lett., Vol. 4, 1985, p. 648-650.

37. D.V. Dunford and A. Wisbey, ***"Diffusion bonding of advanced aerospace metallics"***, Mater. Res. Soc. Symp. Proc., Vol. 314, 1993, p. 39-50.

38. S.D. Peteves, G. Ceccone, M. Paulasto, V. Stamos, and P. Yvon, ***"Joining silicon nitride to itself and to metals"***, JOM, January 1996, p. 48-52.

39. M.R. Locatelli, B.J. Dalgleish, K. Nakashima, A.P. Tomsia and A.M. Glaeser, ***"New approaches to joining ceramics for high-temperature applications"***, Ceramics Intern., Vol. 23, 1997, p. 313-322.

40. M.G. Nicholas, Joining of Ceramics, Advanced Ceramic Reviews – Institute of Ceramics, Chapman and Hall, New York, 1990.

41. S. Elliot, I.A. Bucklow, and E.R. Wallach, ***"An examination of diffusion bonded interfaces in a mild steel"***, J. Mater. Sci., Vol. 15, 1980, p. 2823-2833.

42. E.A. Almond, A.M. Cottenden, and M.G. Gee, ***"Metallurgy of interfaces in hardmetal/metal diffusion bonds"***, Metals Sci., Vol. 17, 1983, p. 153-158.

43. I.-W. Chen and A.S. Argon, ***"Diffusive growth of grain-boundary cavities"***, Acta Metall., Vol. 29, 1981, p. 1759-1768.

44. A.C.F. Cocks and M.F. Ashby, ***"Creep fracture by coupled power-law creep and diffusion under multiaxial stress"***, Metals Sci., Vol. 16, 1982, p. 465-474.

45. B. Derby and E.R. Wallach, ***"Diffusion bonds in iron and low-alloy steel"***, J. Mater. Sci., Vol. 19, 1984, p. 3149-3158.

46. A. Hill and E.R. Wallach, ***"Modelling solid-state diffusion bonding"***, Acta Metall., Vol. 37, No. 9, 1989, p. 2425-2437.

47. K. Burger and M. Ruhle, ***"Material transport mechanisms during the diffusion bonding of Nb to Al_2O_3"***, Ultramicroscopy, Vol. 9, No. 1-4, May 1989, p. 88-97.

48. B. Derby and E.R. Wallach, ***"Theoretical model for diffusion bonding"***, Metal Sci., Vol. 16, Jan. 1982, p. 49-56.

49. J. Pilling, D.W. Livesey, J.B. Hawkyard, and N. Ridley, ***"Solid state bonding in superplastic Ti-6Al-4V"***, Metal Sci., Vol. 18, Mar. 1984, p. 117-122.

50. B. Derby and E.R. Wallach, ***"Diffusion bonding: development of theoretical model"***, Metal Sci., Vol. 18, Sep. 1984, p. 427-431.

51. B. Derby, ***"The influence of surface roughness on interface formation in metal/ceramic diffusion bonds"***, in Ceramic Microstructures '86: Role of Interfaces, Eds. J.A. Pask and A.G. Evans, Plenum, New York, 1986, p. 319-28.

52. O.M. Akselsen, ***"Diffusion bonding of ceramics"***, J. Mater. Sci., Vol. 27, No. 3, 1992, p. 569-579.

53. M. Naka, M. Kubo, and I. Okamoto, ***"Wettability of silicon by aluminium, copper and silver"***, J. Mater. Sci. Lett., Vol. 6, 1987, p. 965-966.

54. A.E. Martinelli, Diffusion Bonding of Silicon Carbide and Silicon Nitride to Molybdenum, McGill University, Thesis, 1996.

55. M.G. Nicholas and R.M. Crispin, ***"Diffusion bonding stainless steel to alumina using aluminium interlayers"***, J. Mater. Sci., Vol. 17, 1982, p. 3347-3360.

56. A.E. Martinelli and R.A.L. Drew, ***"Microstructural and mechanical strength of diffusion bonded silicon nitride-molybdenum joints"***, J. Europ. Ceram. Soc., Vol. 19, No. 12, 1999, p. 2173-2181.

57. M.M. Schwartz, Ceramic Joining, ASM international, materials Park, USA, 1990.

58. P. Lourdin and D. Juvé, ***"Reliability of Ni/Al_2O_3 junctions made by solid state bonding"***, Mater. Sci. Forum, Vol.126-128, 1993, p. 711-714.

59. A.E. Martinelli, R.A.L. Drew, and R. Berriche, ***"Correlation between the strength of SiC-Mo diffusion couples and mechanical properties of the interfacial reaction products"***, J. Mat. Sci. Lett., Vol. 15, No. 5, 1996, p. 307-310.

60. K. Suganuma, T. Okamoto and M. Koizumi, and M. Shimada, ***"Joining of silicon nitride to silicon nitride and to invar alloy using an aluminium interlayer"***, J. Mater. Sci., Vol. 22, 1987, p. 1359-1364.

61. D. Treheux, P. Lourdin, B. Mbongo, D. Juve, ***"Metal/ceramic solid state bonding: mechanisms and mechanics"***, Scripta Metall. Et Mater., Vol. 31, No. 8, 1994, p. 1055-1060.

62. S.D. Peteves and M.G. Nicholas, ***"Materials factors affecting joining of silicon nitride ceramics"***, Metal Ceramic Joining, Edited by P. Kumar and V.A. Greenhut, The Minerals, Metals & Mater. Soc., 1991, p. 43-65.

63. K. Suganuma, ***"Recent advances in joining technology of ceramics to metals"***, ISIJ International, Vol. 30, No. 12, 1990, p. 1046-1058.

64. B.T.J. Stoop and G. Den Ouden, ***"Diffusion bonding of silicon nitride to austenitic stainless steel without interlayer"***, Metall. Trans. A, Vol. 24A, August 1993, p. 1835-1843.

65. A.E. Martinelli and R.A.L. Drew, ***"Microstructural development during diffusion bonding of α-silicon carbide to molybdenum"***, Mater. Sci. Eng., A191, 1995, p. 239-247.

66. Y. Ishida, J.Y. Wang, and T. Suga, ***"Structural features to relax thermal stress at metal/ceramic joined interface"***, ISIJ International, Vol. 30, No. 12, 1990, p. 1041-1045.

67. J.M. Howe, Interfaces in Materials, J. Wiley & Sons Inc., New York, USA, 1997.

68. B. Derby, ***"The formation of metal/ceramic interfaces by diffusion bonding"***, Acta Scr. Metall. Proc. Ser., Vol. 4, 1990, p. 161-167.

69. J.T. Klomp and J. Vrugt, ***"Interfaces between metals and ceramics"***, Mater. Science Res., Vol. 14, 1981, p. 97-105.

70. J.M. Howe, ***"Bonding, structure and properties of metal/ceramic interfaces: Part 1 chemical bonding, chemical reaction, and interfacial structure"***, Intern. Mater. Rev., Vol. 38, No. 5, 1993, p. 233-256.

71. T. Wagner, R. Kirchheim, and M. Ruhle, ***"Chemical reactions at metal/ceramic interfaces during diffusion bonding"***, Acta Metall. Mater., Vol. 43, No. 3, 1995, p. 1053-1063.

72. D.A. Porter and K.E. Easterling, Phase Transformations in Metals and Alloys. Second Edition, Chapman and Hall, 1992.

73. J.T. Klomp, ***"Ceramic-metal interactions"***, Mat. Res. Soc. Symp. Proc., Vol. 40, Pittsburgh, USA, 1985, 381-391.

74. A.P. Tomsia and R.E. Loehman, ***"Reactions and microstructure at selected ceramic/metal interfaces"***, Materials and Manufacturing Processes, Vol. 9, No. 3, 1994, p. 547-561.

75. B.J. Dalgleish, E. Saiz, A.P. Tomsia, R.M. Cannon and R.O. Ritchie, ***"Interface formation and strength in ceramic/metal systems"***, Scripta Metallurgia et Materialia, Vol. 31, No. 8, 1994, p. 1109-1114.

76. M. Gautier and J.P. Duraud, ***"Formation of metal-ceramic interfaces: a surface science approach"***, J. Phys. III France, Vol. 4, 1994, p. 1779-1794.

77. H. Baker, Alloy Phase Diagrams, ASM Handbook Vol. 3, ASM International, Materials Park, Ohio, USA, 1992.

78. H.O. Pierson, Handbook of Refractory Carbides and Nitrides- Properties, characteristic, processing and applications, Noyes Publication, Westwood, New Jersey, U.S.A., 1996.

79. R. Beyers, R. Sinclair, and M.E. Thomas, ***"Phase equilibria in thin-film metallizations"***, J. Vac. Sci. Technol. B, Vol. 2, No. 4, Oct.-Dec. 1984, p. 781-784.

80. D. Brandon and W.D. Kaplan, Joining Processes –An Introduction, John Wiley and Sons, New York, 1997.

81. K. Suganuma, T. Okamoto, and M. Koizumi, ***"Effect of interlayers in ceramic-metal joints with thermal expansion mismatches"***, Communications of the American Ceramic Society, December 1984, p. c-256-257.

82. K. Suganuma, ***"Reliability factors in ceramic/metal joining"***, Mat. Res. Soc. Symp. Proc., Vol. 314, 1993, p. 51-60.

83. K. Suganuma, T. Okamoto, M. Shimada, and M. Koizumi, ***"New method for solid/state bonding between ceramic and metals"***, Communications of the American Ceramic Society, July, 1983, p. c-117-118.

84. R.F. Pabst and G. Elssner, ***"Adherence properties of metal to ceramic joints"***, J. Mat. Sci., Vol. 15, 1980, p. 188-196.

85. J.D. Cawley, ***"Introduction to ceramic-metal joining"***, Metal Ceramic Joining, Edited by P. Kumar and V.A. Greenhut, The Minerals, Metals and Materials Society, 1991, p. 3-11.

86. T. Tanaka, H. Morimoto, and H. Homma, ***"Joining of ceramics to metals"***, Nippon Steel Technical Report, No. 37, April, 1988, p. 31-38.

87. G.R. Van Houten, ***"A survey of ceramic to metal bonding"***, Ceramic Bulletin, Vol. 38, No. 6, 1959, p. 301-305.

88. K. Suganuma, T. Okamoto, and K. Kamachi, ***"Influence of shape and size on residual stress in ceramic/metal joining"***, J. Mater. Sci., Vol. 22, 1987, p. 2702-2706.

89. R.M. Anderson, ***"Testing advanced ceramics"***, Advan. Mater. Proc., Vol. 3, 1989, p.31-36.

90. H. Mizuhara, E. Huebel and T. Oyama, ***"High-reliability joining of ceramic to metal"***, Ceramic Bulletin, Vol. 68, No. 9, 1989, p. 1591-1599.

91. M. Turwitt Mülheim, ***"Bending test for active brazed metal/ceramic joints–A round Robin"***, CFI – Ceramic Forum Intern., Vol. 71, No. 7, 1994, p. 406-411.

92. W.-C. Lee, ***"Strength of Si_3N_4/Ni-Cr-Fe alloy joints with test methods: shear, tension, three-point and four-point bending"***, J. Mater. Sci., Vol.32, 1997, p. 6657-6660.

93. G.D. Quinn and R. Morrell, ***"Design data for engineering ceramics: A review of the flexure test"***, J. Am. Ceram. Soc., Vol. 74, No. 9, 1991, p. 2037-2066.

94. G. Cam, K-H. Bohm, J. Mullauer, and M. Kocak, ***"The fracture behavior of diffusion bonding duplex gamma TiAl"***, JOM, Nov., 1996, p. 66-68.

95. G.D. Quinn, ***"Strength and proof testing"***, Engineered Materials Handbook, Vol. 4, USA, 1991, p. 585-598.

96. J. Emsley, The Key to the Elements, Clarendom Press, Oxford, UK, 1991.

97. D. W. Richerson, Modern Ceramic Engineering, Second Edition, Revised and Expanded, New York, USA, 1992.

98. M.G. Bassin, Statics and Strength of Materials, Gregg Division, McGraw Hill, New York, USA, 1988.

99. ***"Supplier's Data"***, Ceradyne Inc. Costa Mesa, CA, USA, 1997.

100. ***"Supplier's Data"***, Johnson & Matthey, Toronto, Canada, 1997.

101. E.W. Collings, The Physical Metallurgy of Titanium Alloys, American Society for Metals, Metals Park, OH, USA, 1984.

102. C.W. Bale, A.D. Pelton and W.T. Thompson, ***"F*A*C*T 2.1 –User manual"***, Ecole Polytechnique de Montréal / Royal Military College, Canada, July 1996.

103. ***"Supplier's Data"***, Speer Canada Inc., Montreal, Canada, 1993.

104. C.J. Chen, Introduction to Scanning Tunneling Microscopy, Oxford University Press, Oxford, 1993.

105. K.L. Mittal and A. Pizzi, Adhesion Promotion Techniques (Technological Applications), Marcel Dekker, Inc., New York, 1999.

106. A.T. Hubbard, The Handbook of Surface Imaging and Visualization, CRC Press, New York, 1995.

107. H. QiLiang, C. Juan, P. Wei, C. Jian, and L. Jie, ***"In situ processing of TiN/Si_3N_4 composites by Ti-Si_3N_4 solid state reaction"***, Mat. Lett., Vol. 31, 1997, p. 221-225.

108. K. Suganuma, T. Okamoto, M. Shimada, M. Koizumi, and M. Koizumi, ***"Joining Si_3N_4 to type 405 steel with soft metal interlayers"***, Mater. Sci. Technol., Vol. 2, 1986, p. 1156-1161.

109. P. Rogl and J.C. Schuster, ***"Phase Diagrams of Ternary Boron Nitride and Silicon Nitride System"***, Monograph Series on Alloy Phase Diagrams, ASM International, Materials Park, OH, 1992, p. 198-202.

110. B. Lesage, ***"Some aspects of diffusion in ceramics"***, J. Phys. III, Vol. 4, 1994, p. 1833-1850.

111. G.V. Samsonov, P. Epik, W.A. Gibeaut, E.S. Bartlett and D.H. Leeds, Coating of High-Temperature Materials, Ed. H.H. Hausner, Plenum Press, New York, 1966.

112. G.V. Samsonov and I.M. Vinitskii, Handbook of Refractory Compounds, Plenum, New York, 1980.

113. P. Villars and L.D. Calvert, Pearson's Handbook of Crystallographic Data for Intermetallic Phases, 2nd Edn., American Society for Materials, Materials Park, Ohio, USA, 1991.

114. B.D. Cullity, Elements of X-ray diffraction, Addison-Wesley, Reading, USA, 1956.

115. T.S. Oh, R.M. Cannon, and R.O. Ritchie, ***"Subcritical crack growth along ceramic/metal interfaces"***, J. Am. Ceram. Soc., Vol. 70, No. 12, 1987, C352-355.

116. B. Cockeram and G. Wang, ***"The influence of multi-layered kinetics on the selection of primary phase during the diffusion-controlled growth of titanium silicide layers"***, Thin Solid Films, Vol. 269, 1995, p. 57-63.

117. B. Gibbesch and G. Elssner, ***"Ultra high vacuum diffusion bonded Nb-Al_2O_3 and Cu-Al_2O_3 joints – The role of welding temperature and sputter cleaning"***, Acta Metall. Mater., Vol. 40, Suppl., 1992, p. S59-S66.

118. H. Guo, E. Steinhauer and J.-J. Chene, ***"Solid state diffusion bonding for structural joining with similar and dissimilar materials"***, Welding in the World, Vol. 37, No. 3, 1996, p. 107-113.

119. M.H. El-Sayed, M. Naka and J.C. Schuster, ***"Interfacial structure and reaction mechanism of AlN/Ti joints"***, J. Mater. Sci., Vol. 32, 1997, p. 2715-2731.

120. H.C. Cao, M.D. Thouless and A.G. Evans, ***"Residual stresses and cracking in brittle solids bonded with a thin ductile layer"***, Acta Metall., Vol. 36, No 8, 1988, p. 2037-2046.

121. A.A. Kodentsov, J.K. Kivilahti, and F.J.J. Van Loo, ***"The formation of nitride phases during diffusion bonding of Ni-Cr alloys with Si_3N_4-ceramic"***, High Temp. Mat. Sci., Vol. 34, 1995, p. 137-153.